INVESTIGATION OF STRESS RELAXATION IN THICK-WALLED CYLINDERS SUBJECT TO RADIAL THERMAL LOADING

A Thesis submitted for the award of Doctor of Philosophy in Engineering at the University of London.

by

K.G. TORR

Mechanical Engineering Department
Imperial College
London S.W.7.

February 1974

ABSTRACT

Several computer codes have been developed which predict the stress and strain history in a component subjected to any prescribed loading sequence, taking account of plastic and creep strains. One such code, CREEPA, has been developed at Imperial College to perform a one-dimensional analysis of a thick-walled cylindrical component under axi-symmetric loading, in a state of generalised plane strain. This code has been checked against earlier experimental and analytical solutions only for certain loading cases, and it is important that the code should calculate transient creep strains correctly if the life of a component is to be predicted reliably.

The object of the work described is to test experimentally the code predictions of transient creep in a thick-walled cylinder. This is done by measuring experimentally the residual stress pattern in a cylinder which has been subjected to a single steady load cycle during which stress redistribution due to creep is expected to occur, and compared with that predicted by the code.

For simplicity, the loading is obtained by inducing a radial heat flux in the wall of the cylinder by positioning an electrical resistance heater centrally in the bore of the cylinder within a specially built furnace. This is the only form of loading employed in the tests.

The selected test specimen is a cylinder of 75mm outside diameter, 25mm bore and 150mm length and the material used in these tests is Nimonic 80A extruded bar.

Measurement of the residual stress distribution is by the well known method due to Sachs. To reduce induced stresses on layer removal, a method by chemical milling has been developed in preference to lathe turning, and the resulting strain changes on the bore surface are measured by means of foil strain gauges.

The technique of residual stress measurement was verified by obtaining acceptable agreement in results from replicate specimens. Correlation between the residual stress pattern predicted by the computer code and the experimentally obtained values was found to be poor. Possible explanations are discussed and suggestions for further work are made.

NOTATION

σ_r	Radial stress
σ_θ	Circumferential stress
σ_z	Axial stress
τ	Shear stress
e_r	Total radial strain
e_θ	Total circumferential strain
e_z	Total axial strain
ε_{e_r}	Radial Elastic strain
ε_{c_r}	Radial Creep strain
ε_{T_r}	Radial Thermal strain
$\dot{\varepsilon}$	Strain rate
T	Temperature
r	Radius
$\alpha_{r,z}$	Coefficients of Thermal expansion
E	Youngs Modulus
ν	Poissons Ratio
λ	Axial surface strain in the bore due to the removal of an outer layer to radius r.
θ	Circumferential surface strain in the bore due to the removal of an outer layer to radius r.

LIST OF CONTENTS

		Page
TITLE		1
ABSTRACT		2
NOTATION		4
LIST OF CONTENTS		5
LIST OF ILLUSTRATIONS		7
CHAPTER 1 -	INTRODUCTION	8
CHAPTER 2 -	METHOD OF ANALYSIS	14
2.1	Governing Equations	14
2.2	Computational Procedure	16
2.3	Material Behaviour	19
2.3.1	Coefficient of Thermal Expansion	19
2.3.2	Elastic Constants	20
2.3.3	Creep Behaviour	21
2.4	Computer Results	29
CHAPTER 3 -	GENERATION OF TEST SPECIMENS	30
3.1	Furnace Design	30
3.1.1	Heater element	33
3.2	Specimen Form	35
3.3	Loading Cycle	37
3.4	Specimen Material	37
3.4.1	Structure of Nimonic 80A	38
3.4.2	Heat-Treatment of Nimonic 80A	39

Page

CHAPTER 4 - MEASUREMENT OF THE RESIDUAL STRESS PATTERN 41

4.1 Sach's Boring Method 41

4.2 Layer Removal Techniques 44

4.3 Chemical Milling 47

4.4 Method of Strain Measurement 50

4.5 Method of Bonding Strain Gauges 54

4.6 Strain Measuring Circuit 58

CHAPTER 5 - MEASURED RESIDUAL STRESSES 60

5.1 Experimental Results 60

5.2 Estimation of Errors 64

5.3 Calculation of Residual Stresses 72

CHAPTER 6 - DISCUSSION AND CONCLUSIONS 86

ACKNOWLEDGEMENTS 92

REFERENCES 93

APPENDIX 1 97

LIST OF ILLUSTRATIONS

		Page
1.	Residual stress distributions after 500 and 1000 hours as predicted by the computer code CREEPA.	28
2.	Layout of the stressing furnace.	31
3.	Layout of the chemical milling tank.	48
4.	Temperature controlled box and strain measuring equipment.	52
5.	Mandrel used for positioning strain gauges in the cylinder bore, and inspection 'periscope'.	56
6.	Schematic layout of strain measuring circuit.	59
7.	Load-strain graph for Young's Modulus determination in remnant cylindrical shell.	63
8.	Metallographic structure of specimen after 1000 hours in stressing furnace.	65
9.	Metallographic structure of specimen after 500 hours in stressing furnace.	66
10.	Graph of measured surface strains in five 500 hour specimens indicating confidence intervals.	75
11- 18.	Measured residual stress distributions in Specimens 1 to 8.	77-84
19.	Measured stress distribution of 500 hour specimens showing the estimated error bounds.	85

CHAPTER ONE

INTRODUCTION

Recent years have witnessed greatly increased demands on the design engineer as a result of the requirement for the development of larger and more complex structures requiring to be operated under more severe conditions. The fields of electrical power generation, aeronautics and chemical processing are but a few areas in which numerous typical examples can be found. With the vast amounts of money that stand to be lost when such plant is rendered idle through crucial component failure, it is understandable that a high degree of reliability is demanded and therefore this aspect of engineering design has received much attention.

The integrity of a structure or component during its lifespan is governed by the performance of the component material in the most highly stressed areas. The behavioural characteristics of the material, as obtained from basic material tests, are obvious essential requirements of an analysis which must give careful consideration to the geometrical features of the structure and also the type of loading to which it will be subjected during service. In many typical plant operating regimes, components operating at elevated temperatures and subjected to cyclically varying loads, undergo plastic deformation. The complex interaction of creep and fatigue effects under these conditions may lead to premature failure either by initiating and/or propagating cracks or by excessive cumulative deformation.

The problem facing the designer then, is to ensure that his structure has an adequate margin of safety against the loadings which will be imposed on it in operation, and to ensure that it will continue to give satisfactory service, free from cracking and excessive distortion over its whole working life. This has, of course, to be done within the constraints of time, money and available manufacturing techniques. The designer must therefore be able to perform a complicated stress analysis of the crucial areas where stress levels and strain ranges are highest, for the anticipated loading regime. Before the advent of modern computer programs, these problems were intractable for design calculations under a general state of stress, and emphasis was placed on the simplification of the problem. While this is still a useful and economical analysis tool in components which are not critically stressed, it is inadequate for more severe complex conditions.

Computer technology has made astonishing progress recently and in conjunction, an advanced state of development has been reached in sophisticated numerical techniques for the idealization and analysis of reasonably complex structures subject to time-varying loading schemes. This is well illustrated by the number of associated papers contributed at a recent International Conference on Structural Mechanics in Reactor Technology[1]. With adequate information apertaining to the material behaviour, a precise history of the conditions at every crucial point in the structure may thus be obtained. It is at this point, however, that complications arise. Progress in analytical methods has far outstripped our knowledge

of the material to be analysed, since these technical materials are so complex that the physical and metallurgical processes involved are at best only approximately understood. Very little information is available on the performance of component materials at high temperature under cyclic conditions. So although many computer codes have been developed which can deliver numbers, the theory on which they are based may be sufficiently different from the real material behaviour for the time, number of cycles and history of loading, that totally erroneous numbers result.

While a great deal of work has gone into the experimental measurement of creep in thick cylinders under steady loading conditions[3],[36]-[38], it appears that insufficient effort is currently being directed towards the verification of complex computer analyses for more realsitic non-steady loading. It was for this reason that this experimental project was instigated. The initial objective was to ascertain whether, by using standard uniaxial creep data and simple creep laws, a recently developed computer code*, was effective in predicting the time-varying state of stress in a cyclically loaded thick cylinder.

The interaction of creep and fatigue is usually studied by means of axial loads or combined torsion and axial load on a test specimen. At the start of this work, it was decided to study a representative component, namely a thick-walled cylinder, in which the material is in a state of multiaxial stress. The one-dimensional analysis of an axisymmetrically loaded, long thick cylinder is relatively simple but it still

---

*This is a simple finite difference code similar to the PITT code presently being used by the C.E.G.B. The basic theory of the analysis and method of solution is briefly described in Chapter Two.

serves as a searching test of the algorithms of the computer code and also saves computing time. Clearly, one essential requirement of the computer code, if it is to be of any use in predicting the stress/strain history of the material under cyclic loading conditions, is that is should correctly predict the stress redistribution due to creep, during any 'hold-time' in the load cycle. It was therefore decided to subject the component initially to a single load cycle during which there should be significant stress redistribution due to creep. The stress redistribution will manifest itself in a residual stress pattern on removal of the load. The computer code has the capability of predicting this residual stress pattern. A searching test of the computer code could then be made by comparing the predicted residual stress pattern with an experimentally measured stress pattern. Only if the programme can correctly predict this residual stress pattern (and therefore by implication the stress redistribution) can there be any hope that it will successfully predict cyclic stress/strain history. Even granted successful prediction of the stress relaxation in a single application of load, the prediction of stress/strain cycles under repeated or cyclic loading raises other questions which need to be answered. For example, to what extent does the material have a 'memory' of prior events and how can these be modelled in the code?

A large amount of experimental work has been performed in the area of residual stress determination.[17] Most of the work can be classified into three separate groups. These consist of the non-destructive methods of X-ray diffraction and ultrasonic methods and the destructive layer removal methods.

Clearly, non-destructive techniques of residual stress measurements would hold a great advantage over destructive methods in this particular application, as the whole history of the deformation induced during the loading regime could be determined by periodic inspection of the test specimen.

The X-ray diffraction technique has this advantage of leaving the specimen intact but it is quite costly by virtue of the specialized equipment required and can only be used to determine surface stresses at a point. It was therefore rejected as a potential method for this application.

A relatively recent innovation in the area of experimental residual stress determination is the ultrasonic technique. Due to the phenomenon of 'acousto-elasticity', which is analogous to photo-elasticity, the stress in the material can be detected by the measurement of the variation in the velocity of the ultrasonic waves. The techniques of absolute and differential velocity measurement, reviewed by Ratcliff[2] seem to be capable of detecting small stress changes. All of the measurements from these techniques, however, give a mean result for the regions traversed by the ultrasonic beam and do not necessarily apply to each individual region along the path length.

The most widely used technique in residual stress work is the layer removal procedure. This technique involves the removal of layers from a test specimen such that the stresses in each layer may then be determined by consequent dimensional changes in the remaining material. Major variations in the use of this technique lie in the manner in which the dimensional changes are determined, and in the method of layer removal. The major advantages of this technique stem from the fact that

it is generally easier to apply, does not require the expensive equipment of the other methods and it gives a complete picture of the residual stress field. The major disadvantage, of course, lies in its destruction of the test specimen.

It was therefore clear, that the layer removal technique was the only feasible method of residual stress measurement for this investigation. As a first stage in the experiment then, the technique in applying this method had to be developed so that residual stress measurements could be made accurately and consistently. The technique was verified to the extent that results could be replicated to an acceptable degree. The method was used to test the accuracy with which the code can predict a single load cycle. As described in later sections the code was found to predict the stress redistribution rather poorly. No time was available to verify possible explanations for this and to begin cyclic loading experiments. However, some suggestions are included concerning the possible development of the work in this direction.

CHAPTER TWO

THE ANALYSIS OF CYCLIC LOADING OF A LONG TUBE WITH CREEP AND THERMAL EFFECTS.

2.1 Governing Equations

The derivation of the governing equations for stress readjustment in the wall of a thick tube, together with appropriate boundary conditions are presented briefly in this section. Certain simplifying assumptions have been made in the analysis and these are mentioned at the appropriate stage.

For axisymmetric bodies of revolution, the equilibrium equations are (as usual):

$$\frac{\partial \sigma_r}{\partial r} + \frac{\partial \tau_{rz}}{\partial z} + \frac{\sigma_r - \sigma_\theta}{r} = 0 \qquad (1a)$$

$$\frac{\partial \tau_{rz}}{\partial r} + \frac{\partial \sigma_z}{\partial z} + \frac{\tau_{rz}}{r} = 0 \qquad (1b)$$

$$\frac{\partial \sigma_\theta}{\partial \theta} = 0 \qquad (1c)$$

Body forces are assumed to be zero.

Equilibrium of forces in the axial direction require that

$$\int 2\pi r \sigma_z \, dr = L_A \qquad (2)$$

where L_A is an applied axial force. This equation is valid for an 'open-ended' cylinder with a pressure difference across the wall in addition to the axial load, L_A.

A fundamental assumption is that the total strains consist of the sum of elastic, creep and thermal components.

$$e_r = \varepsilon_{e_r} + \varepsilon_{c_r} + \varepsilon_{T_r} \tag{3a}$$

$$e_\theta = \varepsilon_{e_\theta} + \varepsilon_{c_\theta} + \varepsilon_{T_\theta} \tag{3b}$$

$$e_z = \varepsilon_{e_z} + \varepsilon_{c_z} + \varepsilon_{T_z} \tag{3c}$$

Substituting expressions for the component strains in equations (3), the strain displacement expressions are:

$$e_r = s_{rr}\sigma_r + s_{r\theta}\sigma_\theta + s_{rz}\sigma_z + \varepsilon_{c_r} + \alpha_r T = \frac{\partial u}{\partial r} \tag{4a}$$

$$e_\theta = s_{r\theta}\sigma_r + s_{rr}\sigma_\theta + s_{rz}\sigma_z + \varepsilon_{c_\theta} + \alpha_r T = \frac{u}{r} \tag{4b}$$

$$e_z = s_{rz}\sigma_r + s_{rz}\sigma_\theta + s_{zz}\sigma_z + \varepsilon_{c_z} + \alpha_z T = \frac{\partial w}{\partial z} \tag{4c}$$

$$\gamma_{rz} = g_{rz}\tau_{rz} + \tau_{rz_c} = \frac{\partial u}{\partial z} + \frac{\partial w}{\partial r} \tag{4d}$$

where u and w are the radial and axial displacements respectively, g_{rz}, s_{rz}, .. etc, are elastic coefficients, and α_r, α_z are coefficients of thermal expansion.

With equations (4) written in the above form, allowance is made for possible anisotropy between the axial and transverse directions.

One further important assumption in the analysis made here is that of plane strain. The displacement w is therefore assumed constant and independent of radius, both $\frac{\partial w}{\partial r}$ and τ_{rz} become zero and the analysis thus becomes applicable only to regions away from the ends of the cylinder. This assumption simplifies the foregoing equations such that the simultaneous equations to be satisfied at any instant in the lifetime of the cylinder are reduced to the following four:-

Equation (1a) becomes

$$\frac{d\sigma_r}{dr} - \frac{1}{r}(\sigma_\theta - \sigma_r) = 0 \tag{5}$$

Combining equations (4a) and (4b)

$$\frac{d}{dr}\left[s_{r\theta}\sigma_r + s_{rr}\sigma_\theta + s_{rz}\sigma_z + \alpha_r T + \varepsilon_{c_\theta}\right] + \frac{1}{r}\left[(s_{r\theta} - s_{rr})(\sigma_r - \sigma_\theta) + \varepsilon_{c_\theta} - \varepsilon_{c_r}\right] = 0 \tag{6}$$

Equation (4c) is

$$e_z = s_{rz}(\sigma_r + \sigma_\theta) + s_{zz}\sigma_z + \alpha_z T + \varepsilon_{c_z} \tag{7}$$

Together with equation (2). For a tube with 'closed-ends' and axial load L_A, equation (2) becomes

$$2\pi\int r\,\sigma_z\,dr = \pi\left[r_i^2 p_i - r_o^2 p_o\right] + L_A \tag{8}$$

where p_i and p_o are the inner and outer pressures respectively.

The boundary conditions requiring specification are the internal and external pressures and the total axial load, each of which may be functions of time.

2.2 Computational Procedure

A finite difference method was used to solve equations (5),(6),(7) and (8). Expressing these equations in a combined forward and backward finite difference form, equation (5) becomes

$$2r_{n+1}\sigma_{r_{n+1}} - 2r_n\sigma_{r_n} - \Delta r\sigma_{\theta_{n+1}} - \Delta r\sigma_{\theta_n} = 0 \tag{9}$$

giving (N-1) equations for (N-1) intervals.

Similarly equation (6) becomes

$$\sigma_{r_n}\left\{s_{r\theta_n}(-2r_n + \Delta r) - \Delta r(s_{rr_n} + s_{r\theta_{n+1}})\right\}$$

$$+ \sigma_{r_{n+1}}\left\{s_{r\theta_{n+1}}(2r_{n+1} + \Delta r) - \Delta r(s_{rr_{n+1}} + s_{r\theta_n})\right\}$$

$$+ \sigma_{\theta_n}\left\{s_{rr_n}(-2r_n + \Delta r) - \Delta r(s_{r\theta_n} + s_{rr_{n+1}})\right\}$$

$$+ \sigma_{\theta_{n+1}}\left\{s_{rr_{n+1}}(2r_{n+1} + \Delta r) - \Delta r(s_{rr_n} + s_{r\theta_{n+1}})\right\}$$

$$+ \sigma_{z_n}\left\{s_{rz_n}(-2r_n) + s_{rz_{n+1}}(-\Delta r)\right\}$$

$$+ \sigma_{z_{n+1}}\left\{s_{rz_{n+1}}(2r_{n+1} + r_n) + s_{rz_n}(-r_{n+1})\right\}$$

$$= \varepsilon_{c_{\theta_{n+1}}}(-2r_{n+1}) + \varepsilon_{c_{\theta_n}}(2r_n) + \Delta r(\varepsilon_{c_{r_{n+1}}} + \varepsilon_{c_{r_n}})$$

$$+ T_n\left\{\alpha_{r_n}(2r_n - \Delta r) + \Delta r(\alpha_{r_n} + \alpha_{r_{n+1}})\right\}$$

$$+ T_{n+1}\left\{\alpha_{r_{n+1}}(-2r_{n+1} - \Delta r) + \Delta r(\alpha_{r_{n+1}} - \alpha_{r_n})\right\} \qquad (10)$$

This gives (N-1) equations for (N-1) intervals.

Equation (7) becomes

$$s_{rz_n}\sigma_{r_n} + s_{rz_n}\sigma_{\theta_n} + s_{zz_n}\sigma_{z_n} + e_z = -\alpha_{z_n}T_n - \varepsilon_{c_{z_n}} \qquad (11)$$

giving N equations for (N-1) intervals.

If Simpsons Rule is applied to equation (8), using seven nodal points, it becomes[10]:

$$r_1\sigma_{z_1} + 5r_2\sigma_{z_2} + r_3\sigma_{z_3} + 6r_4\sigma_{z_4} + 5r_6\sigma_{z_6} + r_7\sigma_{z_7}$$

$$= -\frac{1}{\Delta r}\frac{5}{3}\left[r_1^2\sigma_{r_1} - r_7^2\sigma_{r_7}\right] \qquad (12)$$

Equations (9) - (12) give a total of (3N-1) equations for the (3N-2) unknown stresses at the nodal points, and one unknown strain, e_z, which can all be combined into matrix form as

$$[A]\{y\} = \{B\}$$

The solution vector

$$\{y\} = (\sigma_{r_2}, \ldots \sigma_{r_{N-1}}, \sigma_{\theta_1}, \ldots \sigma_{\theta_N}, \sigma_{z_1}, \ldots \sigma_{z_N}, e_z)$$

is found from the relation

$$\{y\} = [A]^{-1}\{B\}$$

The stresses calculated thus at the start of the period of constant load are used as first estimates of the stresses at the end of the first time-step, which is a data input, and from these the creep strain increments for the time-step are estimated by assuming

$$\delta\varepsilon_{c_{r,\theta,z}} = \left[\frac{\partial \varepsilon_{c_{r,\theta,z}}}{\partial t}\right]_{t_{mean}} . \delta t$$

The stress system at the end of the time-step is then re-computed with the estimated (non-zero) creep strains. Improved estimates of the creep strain increments are calculated from the mean of the initial and estimated final stress system for the time-step. The procedure is repeated with the improved estimates of the creep strain increments until a convergence criterion is satisfied.

The size of the next time-step is determined by multiplying the first time-step by an optional constant ratio (greater than one) and the sequence of iterative calculations repeated

for each incremented time-step until the end of that period of constant load ends. The load parameters for the next loading period are read and the whole process repeated.

The residual stresses are computed simply by including constant room temperature conditions for a final short time interval, in the complete loading cycle.

2.3 Material Behaviour

The various relevant aspects of the behaviour of the constituent material of the cylindrical component, are represented in several subroutines. The dependancy of the material behaviour on such variables as time, stress, temperature, etc, is thus not restricted to any one assumed scheme, and the particular characteristics of any material behaviour can be appropriately described in the subroutines. In this particular project, the component material was the nickel-chromium superalloy Nimonic 80A and the relationships in the sections following are pertinent to this material.

2.3.1 Coefficient of Thermal Expansion

The mean coefficient of linear thermal expansion for the fully heat-treated material over various temperature ranges is given in the table below. This data, supplied by the manufacturers,[39] is typical for the material and is subject to approximately $\pm$ 5% variation due to compositional change within the release specification, processing history, and/or the heat-treatment condition.

Mean coefficient of thermal expansion (millionths per ^{o}C)

20 to 100°C	20 to 200°C	20 to 300°C	20 to 400°C	20 to 500°C	20 to 600°C	20 to 700°C	20 to 800°C	20 to 900°C
11.1	12.5	13.2	13.7	14.1	14.8	15.5	16.3	17.4

In the temperature range 500-900°C, which contains the region applicable to this particular investigation, the linear relation

$$\alpha_T = 7.25\times10^{-9}T + 10.5\times10^{-6}$$

gives a reasonable approximation to the measured thermal coefficients. Since no information to the contrary is available, it has been assumed that

$$\alpha_r = \alpha_\theta = \alpha_z = \alpha$$

2.3.2 Elastic Constants

As mentioned in section 2.2, allowance is made in the program for possible anisotropy between axial and transverse directions. In this event, the elastic constants of equations (4) are

$$s_{rr} = \frac{1}{E_1} \qquad s_{r\theta} = -\frac{\nu_1}{E_1}$$

$$s_{zz} = \frac{1}{E_2} \qquad s_{rz} = -\frac{\nu_2}{E_2}$$

where $E_1 = E_r = E_\theta$ $\qquad \nu_1 = \nu_{\theta r} = \nu_{r\theta}$

$E_2 = E_z$ $\qquad \nu_2 = \nu_{z\theta} = \nu_{zr}$

The elastic moduli are also temperature dependent and a suitable governing relation must be included in the subroutine.

In the case of Nimonic 80A, information concerning the modulus data in the axial and transverse directions for extruded material is not available, and again the assumption of isotropy has been made in the computer analysis. The values of dynamic Young's Modulus published by the manufacturers[39] and given in the table below were determined on fully heat-treated cylindrical specimens vibrated in a flexural mode.

These determinations were made at very low stress levels and are slightly higher than the corresponding static Young's Moduli. The difference between the static and dynamic moduli is approximately 0.2% at room temperature increasing to about 1% at 1000°C. For extruded material, the value of Young's Modulus is about 20% lower than that for other forms and is affected by subsequent processing and the heat-treatment procedure before testing. If a three stage heat-treatment is applied - this involves a 24 hour soak at 850°C between the normal solution and precipitation stages - the measured values of dynamic Young's modulus approach those of the material in a cold - rolled condition. These values are shown in the table below and were used in the analysis.

Dynamic Young's Modulus ($kg/mm^2 \times 10^{-3}$) (Ref 39)

400 °C	500 °C	600 °C	700 °C	800 °C	900 °C
20.1	19.5	18.7	17.9	16.9	15.6

For the temperature range 500-800°C, the linear relation

$$E_T = -9(T - 500) + 19.6 \times 10^3$$

provides a good estimate of the measured values in the table and was included in the subroutine in this form.

The slight increase in the value of the elastic Poisson's Ratio for Nimonic 80A with rising temperature has been ignored and a constant value of 0.3 was employed in all the calculations.

2.3.3 Creep Behaviour

Creep behaviour is described in empirical terms and

comprehensive results from creep tests of materials are usually only available for tests at constant stress and temperature under uniaxial tensile conditions. In studies involving a changing pattern of multiaxial stresses, it is necessary to augment the data by using certain hypotheses in order to permit firstly, estimates of behaviour under changing uniaxial conditions, and secondly, predictions of behaviour under multiaxial stress situations. Hypotheses frequently used are reproduced here for completeness.

Two common hypotheses used for variable uniaxial stress conditions have been incorporated in this investigation, namely the 'time hardening' and 'strain-hardening' relations. According to the 'time hardening' hypothesis, the creep strain rate depends only upon the current values of time, temperature and stress, and in the 'strain hardening' hypothesis, the creep strain rate is a function of stress, temperature and accumulated strain.

A commutative form of the general creep function is usually found to be a reasonable approximation, and the creep strain rates can be expressed as

$$\frac{d\varepsilon_c}{dt} = F_1(\sigma)\ \frac{dF_2(t)}{dt}\ F_3(T) \qquad \text{Time Hardening}$$

$$= F_1(\sigma)\ \dot{F}_2(t)\ F_3(T)$$

and

$$\frac{d\varepsilon_c}{dt} = G_1(\sigma)\ G_2(\varepsilon_c)\ G_3(T) \qquad \text{Strain Hardening}$$

The equations which refer to uniaxial tensile data can be extended to multiaxial situations by postulating equivalent

stresses (σ^*) and equivalent creep strain (ε_c^*) so that

$$\frac{d\varepsilon_c^*}{dt} = F_1(\sigma^*)\ \dot{F}_2(t)\ F_3(T)$$

and

$$\frac{d\varepsilon_c^*}{dt} = G_1(\sigma^*)\ G_2(\varepsilon_c^*)\ G_3(T)$$

σ^* and ε_c^* can be defined in terms of the principal stresses and principal strains by the von Mises equivalent stress and strain relations.*

$$\sigma^* = \frac{1}{\sqrt{2}}\sqrt{\left[(\sigma_1-\sigma_2)^2 + (\sigma_2-\sigma_3)^2 + (\sigma_3-\sigma_1)^2\right]}$$

and

$$\varepsilon_c^* = \frac{\sqrt{2}}{3}\sqrt{\left[(\varepsilon_1-\varepsilon_2)^2 + (\varepsilon_2-\varepsilon_3)^2 + (\varepsilon_3-\varepsilon_1)^2\right]}$$

The manner in which the deformation under multiaxial conditions is distributed between the three coordinate directions is governed by a flow rule. If a Levy-von Mises flow rule is combined with the condition of constant volume, the creep strain rate components for the time-hardening relation may be stated in the form

$$\dot{\varepsilon}_r = \frac{F_1(\sigma^*)}{\sigma^*}\ \dot{F}_2(t)\ F_3(T)\ (\sigma_r - \tfrac{1}{2}\sigma_\theta - \tfrac{1}{2}\sigma_z)$$

$$\dot{\varepsilon}_\theta = \frac{F_1(\sigma^*)}{\sigma^*}\ \dot{F}_2(t)\ F_3(T)\ (\sigma_\theta - \tfrac{1}{2}\sigma_r - \tfrac{1}{2}\sigma_z)$$

$$\dot{\varepsilon}_z = \frac{F_1(\sigma^*)}{\sigma^*}\ \dot{F}_2(t)\ F_3(T)\ (\sigma_z - \tfrac{1}{2}\sigma_r - \tfrac{1}{2}\sigma_\theta)$$

---

*The results of investigations in the field of creep of metallic materials under multiaxial stress systems have indicated that the von Mises criterion is valid for the creep deformation of isotropic materials. Taira and Ohtani [3] claim however that this may not be the best criterion for the prediction of creep rupture life, and the maximum principal stress criterion is superior in some cases.

For the strain-hardening hypothesis these assumptions result in the creep strain relations

$$\dot{\varepsilon}_r = \frac{F_1(\sigma^*)}{\sigma^*} \dot{F}_2(\tau)\ F_3(T)\ (\sigma_r - \tfrac{1}{2}\sigma_\theta - \tfrac{1}{2}\sigma_z)$$

$$\dot{\varepsilon}_\theta = \frac{F_1(\sigma^*)}{\sigma^*} \dot{F}_2(\tau)\ F_3(T)\ (\sigma_\theta - \tfrac{1}{2}\sigma_r - \tfrac{1}{2}\sigma_z)$$

$$\dot{\varepsilon}_z = \frac{F_1(\sigma^*)}{\sigma^*} \dot{F}_2(\tau)\ F_c(T)\ (\sigma_z - \tfrac{1}{2}\sigma_\theta - \tfrac{1}{2}\sigma_r)$$

where τ is given by the equation

$$F_2(\tau) = \frac{\varepsilon^*}{F_1(\sigma^*)\ F_3(T)}$$

For Nimonic 80A, an empirical expression for the uni-axial creep curves was assumed to be of the form

$$\varepsilon_c = \varepsilon_o \left(\frac{\sigma}{\sigma_o}\right)^n \left(\frac{t}{t_o}\right)^p \left(\frac{T}{T_o}\right)^q$$

From the data supplied by the manufacturers[39] and others,[40] the values of the constants and indices n,p,q, were calculated to be

$\varepsilon_o = 0.001$ $\qquad$ $p = 0.36$

$\sigma_o = 15.75$ $\qquad$ $q = 21$

$t_o = 100$ $\qquad$ $n = 8.28 - 6\times10^{-3}T$

$T_o = 1088$

for σ in kg_f/mm^2, t in hours and T in ^oK.

An alternative empirical expression for representing the observed creep strain behaviour of Nimonic 80A, for a wide range of times, stresses and temperatures, has been proposed by Clarke[5]. This is based on fitting a hyperbola to the results of log (creep strain) versus log (time) of the general form.

$$l.\ln^2\left(\frac{t}{\tau}\right) + m.\ln^2\left(\frac{\varepsilon}{\lambda}\right) + n.\ln\left(\frac{t}{\tau}\right)\ln\left(\frac{\varepsilon}{\lambda}\right) = A^2$$

The stress (σ) and temperature (τ) variation in the creep strain results within the normal experimental range, are represented by

$$\lambda = \exp\left\{B + C.\sigma\right\}$$

and

$$\tau = \exp\left\{D + E.\sigma\right\}$$

where B and C are constants, but D and E are temperature-dependent.

The parameters l,m,n and A are obtained simply from the geometry of the fitted hyperbola.

The calculation of strain rates from the creep formulae, using stress, temperature, and either the time- or the strain-hardening hypothesis, is achieved by the relation

$$\frac{d\varepsilon}{dt} = -\frac{2.lx + ny}{2.my + nx} \cdot \frac{\varepsilon}{t}$$

where $x = \ln\left(\frac{t}{\tau}\right)$

and $y = \ln\left(\frac{\varepsilon}{\lambda}\right)$

Inherent in the above analysis is the assumption that the material is isotropic. This is an unlikely assumption

in the case of polycrystalline metals which undergo hot- and cold-working processes during component manufacture. This results in a 'preferred' grain orientation, and consequent variation in mechanical properties relative to the direction of working. Creep properties, in particular, are highly structure sensitive. The degree of anisotropy resulting from the lattice distortion left in the hot-worked material might be expected to depend on the temperature at which the hot-working is concluded. In the case of Nimonic 80A, the anisotropy might be expected to be less for an extrusion process, where the hot-working is effectively carried out within a very narrow range of temperature (around 1200^{o}C), than in a hammer-forging or rolling process, where the hot-working proceeds over a wider range of temperature. Subsequent heat-treatment processes which permit annealing of the lattice would therefore reduce the anisotropy, particularly if a high solution temperature is involved. Betteridge[4] claims that his experience has shown that the heat-treatments normally applied to the Nimonic alloys, involving solution-treatment at 1080^{o}C or higher, are sufficient to restore all hot-worked material to an essentially common condition.

Experimental data for Nimonic 80A bar that has been extruded only is rather scant, and the assumption of isotropy used in the analysis reported here, is supported only by the findings of Betteridge. He concluded from a limited check by experiments on a few specimens after normal heat-treatment, that there is no significant difference between creep properties in the longitudinal and transverse directions of extrusion.

Provision may be made for anisotropy in the analysis, if it is assumed that the material is orthotropic, (i.e. it

has three mutually perpendicular axes of symmetry), and that incompressibility holds true. If the principal axes of stress coincide with the principal axes of anisotropy so also will the principal axes of strain increment coincide with the stress axes. A yield criterion is then chosen such that it reduces to the Von Mises law for small degrees of anisotropy, Finnie and Heller[6] proposed:

$$\sigma^* = \frac{1}{\sqrt{2}}\sqrt{\left[F(\sigma_r-\sigma_\theta)^2 + G(\sigma_\theta-\sigma_z)^2 + H(\sigma_z-\sigma_r)^2 + 6L\tau_{r\theta}^2 + 6M\tau_{rz}^2 + 6N\tau_{\theta z}^2\right]}$$

where F,G,H,L,M and N are assumed to be constants which characterize a given state of anisotropy. It is further assumed that the strain rates depend only on some function of σ^*,

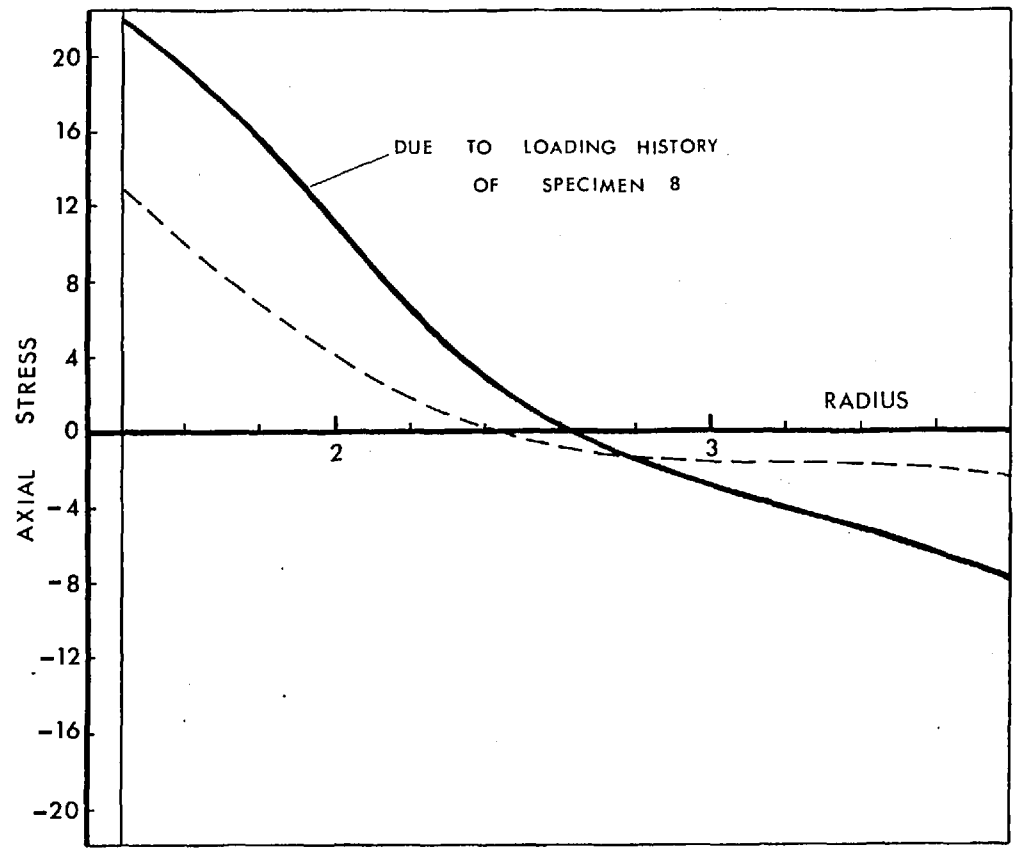
$$\text{i.e.} \quad \dot{\varepsilon}_r = \frac{\partial\sigma^*}{\partial\sigma_r}\dot{\varepsilon}^*$$

and two similar equations. Finnie and Heller [6] employ a relation $\dot{\varepsilon}^* = B\sigma^{*n}$ to obtain

$$\dot{\varepsilon}_r = \frac{1}{2}B\sigma^{*n-1}\left[F(\sigma_r-\sigma_\theta) - H(\sigma_z-\sigma_r)\right] ,$$

and two similar equations.

The point is made here, that the analysis in the computer code is not limited to isotropic materials, provided that the constants of anisotropy are known. These however, are not usually known , except possibly for very simple cases, and therefore, as Penny and Marriott[7] point out, the usefulness of this analysis is in establishing whether the bounds of



Computed Residual Stresses

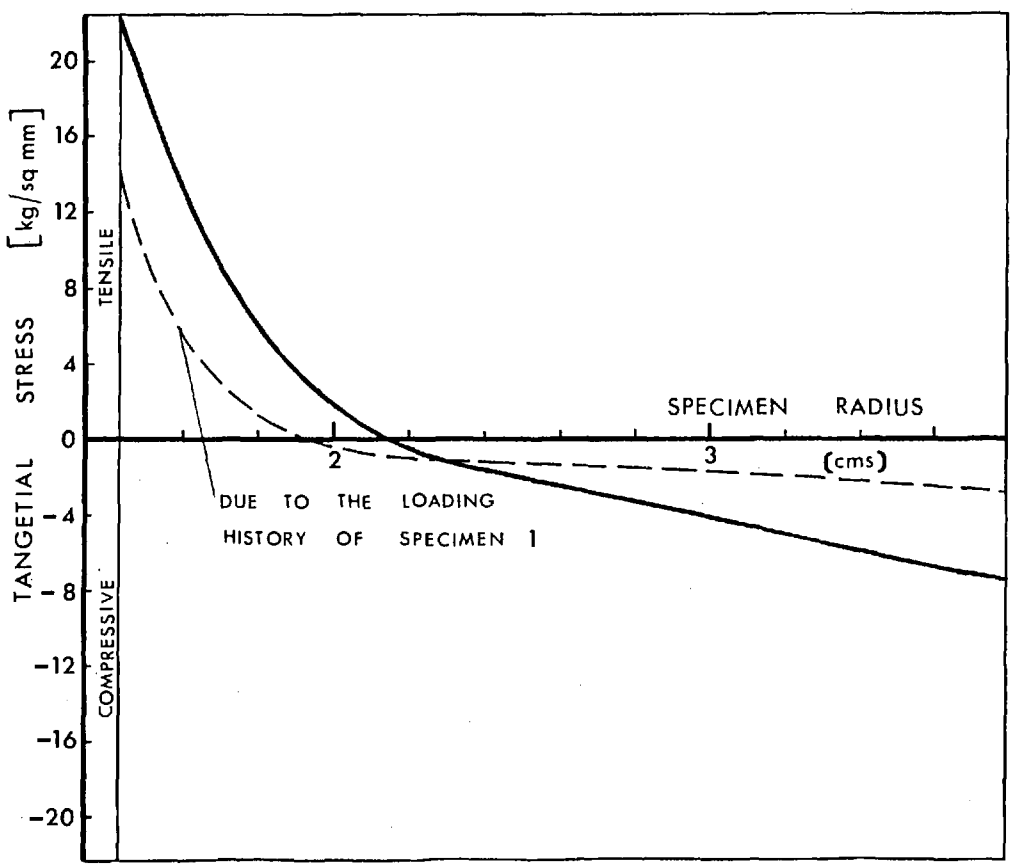
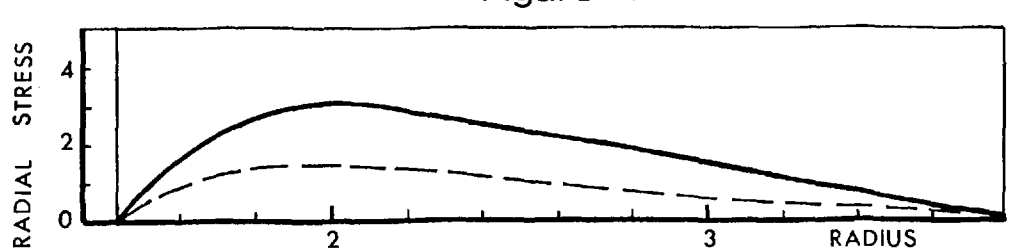
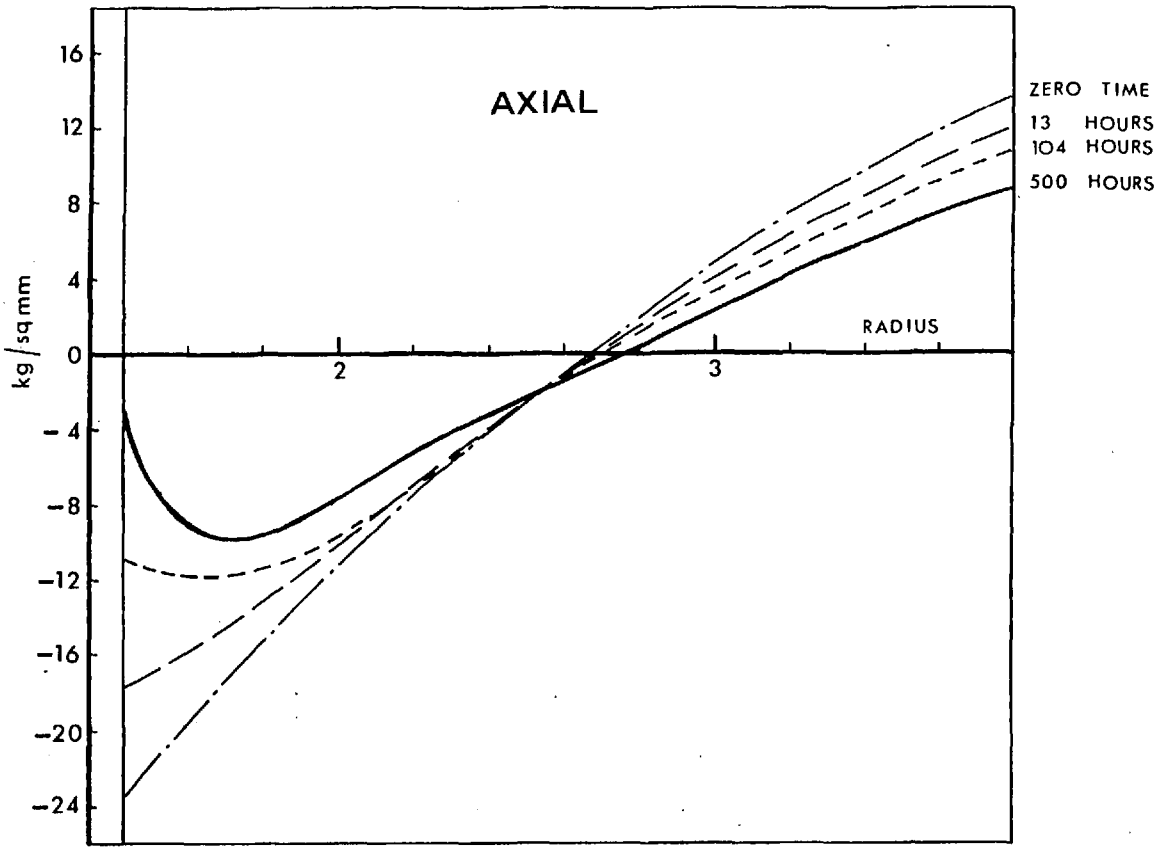
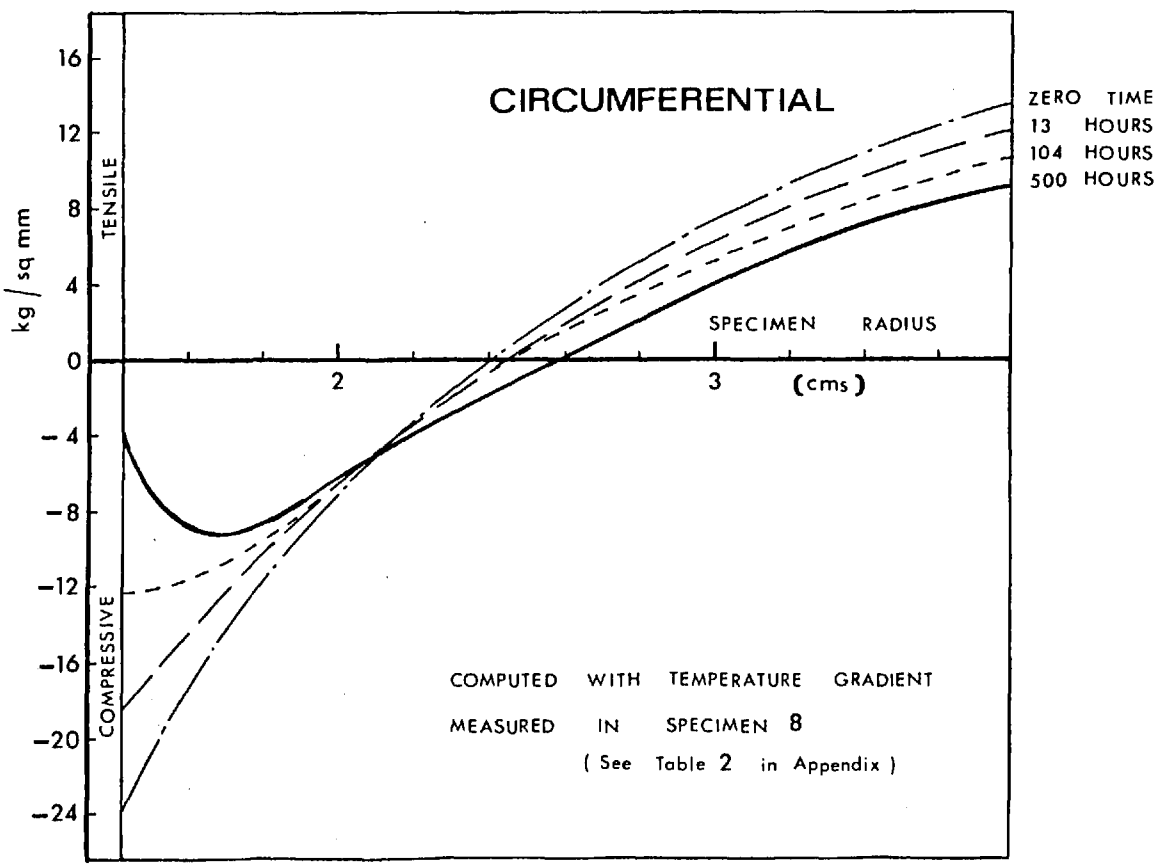


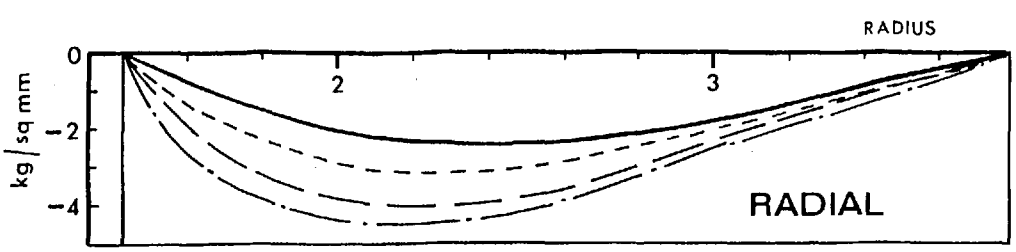
Figure 1





Computed Stresses at Various Time Intervals





anisotropy expected are likely to have any significant effect on the component response.

2.4 Computer Results

In a study performed by Spoelstra[8] the performance of the computer program CREEPA, using the above method of analysis, was evaluated by comparing the computed solutions with those of the illustrative examples quoted for some other codes[9], [10], as well as the elastic Lamé solution and Bailey's[11] steady-state solution. In each case the solutions were found to concur.

Using the material behaviour stated* in the previous section, the CREEPA code, was used to predict the residual stress pattern in a cylinder of Nimonic 80A, with dimensions as given in the next chapter, after having been subjected purely to a constant radial temperature gradient for periods of 1000 and 500 hours. These predicted residual stress distributions are illustrated in Fig 1.

---

*Both the time-hardening and strain-hardening relations were used in the computations, but little difference in the final residual stress values were obtained . Therefore, in Fig. 1 only the results obtained from the time-hardening relation have been illustrated.

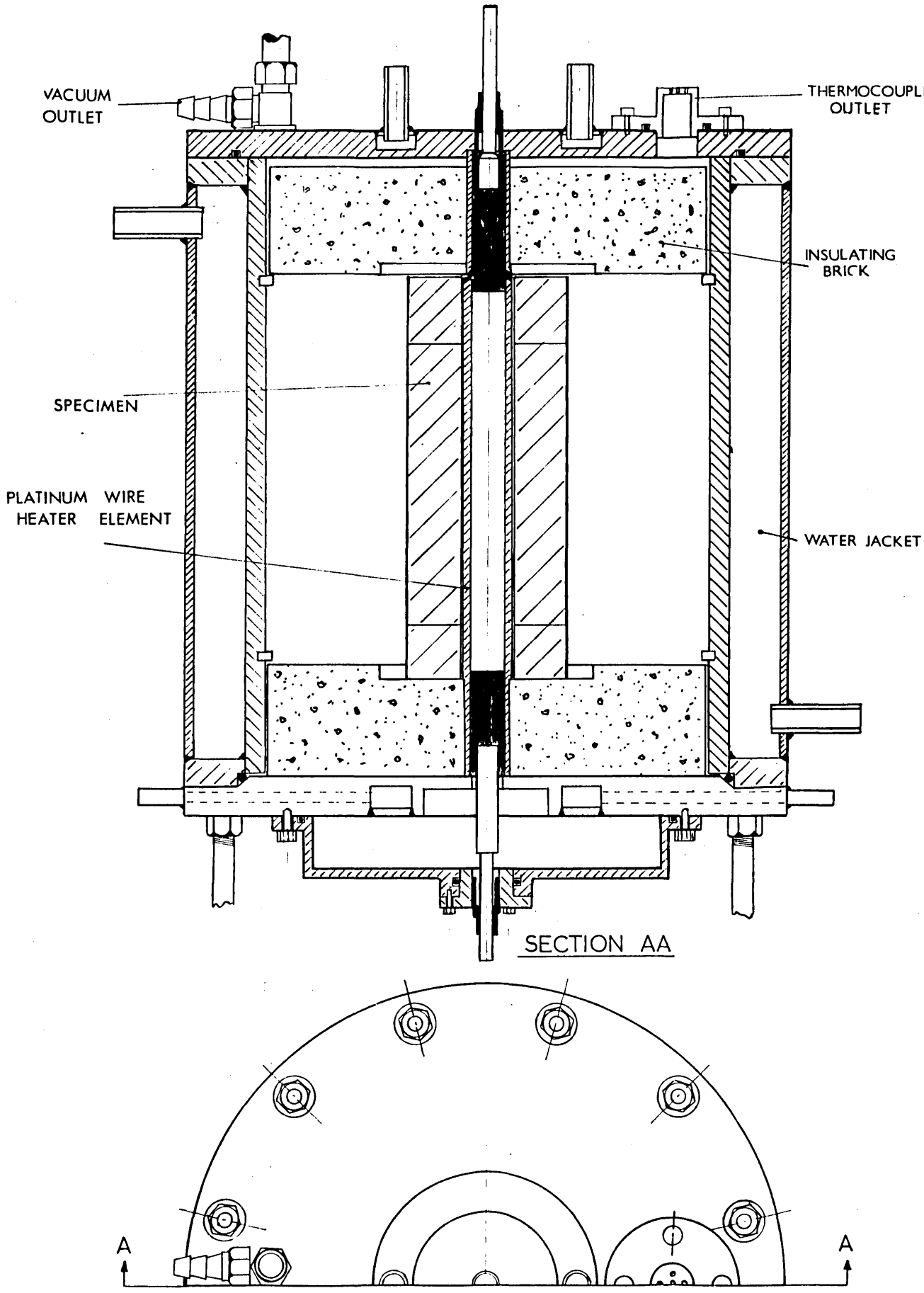
CHAPTER THREE

GENERATION OF TEST SPECIMENS

3.1 FURNACE DESIGN.

A special furnace was designed so that a complex axisymmetric load could be applied to a thick cylinder by means of a uniform radial temperature gradient, the heat transfer being purely by radiation. The furnace, illustrated in Fig 2 , was fabricated from mild steel being 285 mm in diameter and 320 mm high and supported vertically on three legs. A water jacket was incorporated in the wall of the furnace to act as a heat sink, and small water channels on top and bottom kept the electrical heater terminals cool. The specimen cylinder was located centrally within the furnace vessel with an electric resistance heater concentric with the bore of the cylinder. Insulating bricks in the top and the bottom of the furnace served to minimize the axial heat flow from the specimen. The inner wall surface of the vessel was given a matt-black finish to improve its absorbtivity.

The continuous operation of a Metrovac rotary vacuum pump ensured a constant partial vacuum of approximately 0.2 mm Hg inside the furnace, which was found to be necessary to elimate axial temperature variations resulting from circulation by natural convection of the air in the vessel. O-rings formed air-tight joints between the top and bottom lids and the vessel wall flanges, while p.t.f.e. seals prevented leakage at the heater feeder terminals and the thermocouple wires.



Layout of Stressing Furnace

Figure 2

A constant flow of cooling water gravitated from a large tank and was routed through the vessel via 12 mm diameter plastic tubing, and then led away to a drain. Thermometers at the inlet and outlet registered the temperature rise of the cooling water on its passage through the vessel. In the possible event of the water supply being stopped, two safety features were incorporated to shut off the power to the heater. A micro-switch, operated by a float valve when the water level in the tank dropped sufficiently, would de-energise a relay and cut off the electrical supply. As a back-up, a thermostat, positioned on top of the furnace could also de-energise the relay if the local temperature exceeded $55^{o}C$.

Voltage fluctuations in the 240 volt single phase power supply were controlled to within 1.2 volts by a Berco continuous voltage stabilizer unit. A Variac autotransformer, used for raising and lowering the power to the heater, received its 60 volt supply from a 3.6kVA fixed-winding step-down transformer. When the power was raised to produce optimum loading conditions in the specimen, the Variac was seen to be operating at its maximum rated current of 40 amps. It was discovered that after a few days of continuous operation at this maximum current level, the carbon brushes and the windings on which they were positioned began to deteriorate, producing large fluctuations in the applied voltage to the heater. To overcome this, two isolator switches were built into the circuit to enable the Variac to be switched out of the circuit once full operating conditions were reached. The heater was then supplied

directly across the step-down transformer. By adjusting the output voltage from the stabilizer unit, a condition could be reached where the output voltage from the transformer matched that of the Variac which gave the maximum heat flux for the desired inner wall temperature of 815°C. An ammeter in the circuit and voltmeter enabled the continuous power supply to be monitored.

The radial temperature gradient in the cylindrical specimen was measured by five chromel-alumel Thermocoax* thermocouples which were inserted in axial holes (1 mm dia) in the top of the specimen. These thermocouples were led vertically through the top insulating brick and out through the top furnace lid, and connected with chromel or alumel wires to the cold junction and selector switches. A Honeywell multipoint chart-recorder provided a continuous record of the temperatures. A Pye potentiometer test-set was also connected into the circuit to provide temperature indications on start-up and cool-down and to act as a check on the chart-recorder readings. Good correlation between these two measuring devices and a digital voltmeter verified the reliability of the recorder. A Thermos flask containing melting ice provided the cold junction for the thermocouples.

3.1.1 HEATER ELEMENT.

During the early stages of the test program, some difficulty was encountered in developing a heater which was capable of continuous operation under specified conditions for a number of identical test specimens. Initially,

*Trade name

several attempts were made at fabricating the heater by winding 15 swg Kanthal Al wire on an alumina former and embedding the coils in sufficient alumina cement to provide electrical insulation and mechanical support at high temperature. These, however, showed signs of deterioration after only about 70 hours of continuous operation and it became obvious that the actual heater surface temperature (around 1500^{o}C) was a lot higher than had been predicted at the design stage, and that rapid oxidation of the Kanthal wire was giving rise to local failure.

A platinum-20% rhodium heater element was then constructed from 1 mm diameter wire wound on a fused-alumina former. Holes were drilled through the former at both ends to enable the eletrical connections to pass axially out through the ends of the furnace. Despite the high melting point and oxidation resistance of platinum, the windings had to be firmly and completely embedded in refractory material in order to obtain a satisfactory life. On the first platinum heater this was done simply by coating with an alumina cement mixed with water and although a vast improvement on the life of the Kanthal heaters, it failed prematurely after 500 hours. This failure was due to local vaporization of the platinum wire giving rise to a large increase in the local temperature and eventual melting at that point.

Subsequent heaters were coated with a uniform layer of Rockide 'A' alumina, applied by flame-spraying and were found to be completely successful. This process increased the diameter of the heater slightly and in order to accomodate it without touching anywhere, the specimen bore had to be

increased from 25 mm to 29 mm. To assist with the winding of the heater, a grooved alumina former was used. Additional strands of platinum wire, wound round the former at the end of the element winding, increased the cross-sectional area of the terminal wires thus reducing the temperature in this region. The ends of the heater tube were plugged with alumina cement to reduce the end-losses from the heater and so provide a more uniform temperature along its axis.

The heater was located centrally within the specimen bore by means of an accurately positioned cup at the bottom end, upon which the element rested, and by an alumina sleeve which fitted neatly over the top end of the former locating on the top of the end-cap bore.

3.2 SPECIMEN FORM

Due to the difficulty in drilling small (1 mm diameter) thermocouple holes in the top end of the Nimonic specimens, it was thought convenient to make use of a detachable end-cap in which the thermocouple holes were made and so avoid this time consuming operation on each specimen, as the only effective method was by spark-erosion. A second reason for having detachable end-caps was that the region in which an axial temperature gradient was likely to be present, due to heat flow out through the ends, could be removed at the end of the test, and so ensuring that the temperature distribution in the test specimen was longitudinally uniform. The end-caps were thus 35 mm long and were located concentrically with the specimen by means of two dowels.

The thermocouples were inserted in the holes in the top end-cap up to the top surface of the specimen. The temperatures registered by the thermocouples in these positions were taken as truly representative of the temperatures at the corresponding radii within the specimen, on the assumption that the surface emissivities of end-caps and cylinder were the same. This assumption was checked on one specimen, by extending each thermocouple hole 10 mm into the top of the specimen and performing an axial temperature survey by gradually withdrawing each thermocouple in turn. From a series of tests, it was concluded that axial heat flow in the region of the interface was small but that slight differences in the emissivity between the end-cap and cylinder surfaces could result in measured temperature differences of up to 20°C between the two. Tests have shown[12] that the emissivity of Nimonic 80A is strongly dependant on the temperature at which the oxide is formed, the thickness of the oxide layer as well as the roughness of the surface. Every effort was therefore made to duplicate the surface conditions of the end-caps and the specimen to reduce this discrepancy. On the last five specimens, two thermocouple holes were extended 10 mm into the specimen to provide a check.

The specimens, 75 mm in diameter and 150 mm long were made from stock extruded bar. The 29 mm bore was machined out in a lathe and finished by honing. Great care was taken to ensure that the bore was concentric with the outer surface and of uniform diameter. The outer surface of the bar as

received had been rough ground and no further machining was required. The end faces were turned square and finally ground flat before drilling and reaming the dowel holes.

3.3 LOADING CYCLE

The loading sequence applied to the specimens consisted of a single cycle in which the temperature was gradually raised until an inner wall temperature of 815^{o}C had been obtained, maintained at this level for an extended period, and then gradually lowered to a constant room temperature. The duration of the extended period was 1000 hours for the first three specimens, and 500 hours for the last five specimens.

During the steady loading period, the temperature at any point in the specimen was constant to within $\pm$1^{o}C - the fluctuations arising from small variations in the applied voltage. Care had to be taken, however, to ensure that no air leaks occurred in the furnace as variations in the vacuum conditions could give rise to temperature variations of 20^{o}C. In the early stages of the experiment, failure of the heater element prevented uninterrupted, steady conditions from being achieved. Further reference to this is made in Chapter 5.

3.4 SPECIMEN MATERIAL

As has been mentioned already, the material selected for the tests in this program was Nimonic 80A.*
One reason for this choice is that it is a material on which

*Regd Trade Mark.

a great deal of creep data is available. Another reason is that with the relatively low thermal conductivity of this material, a reasonably high radial temperature gradient could be established by purely radiative heat transfer, while maintaining the maximum wall temperature within the range covered by the creep data. Typically, a wall temperature difference of 75°C could be obtained with an inner wall temperature of 815°C. Computer studies indicated that considerable relaxation of the initial thermal stresses would occur after 1000 hours under these conditions.

3.4.1 STRUCTURE OF NIMONIC 80A

Nimonic 80A is a creep resistant 18% chromium-nickel base alloy. Additions of a few per cent of titanium and aluminium introduces the γ' phase (based on Ni_3Al) which confers precipitation hardening characteristics on the material. In addition to this major precipitation phase, smaller quantities of other phases, mainly carbides and nitrides, occur in the alloy and also have an important role in determining its creep-rupture behaviour. Chromium carbides are particularly noticeable in the alloys based on the nickel-chromium solid solution and occur in the form Cr_7C_3 or $Cr_{23}C_6$ depending on the temperature history of the metal component. Betteridge and Franklin[13] have proposed that some grain boundary precipitation of chromium carbide is essential in order to produce an area deficient in chromium in the vicinity of the grain boundaries and thereby produce ductile zones which allow the accomodation of grain boundary distortions without propogation of intergranular stress cracks.

3.4.2 HEAT-TREATMENT OF NIMONIC 80A

Heat-treatment is applied to this alloy in order to develop the full mechanical properties of which it is capable, and at the same time it serves to remove the effects of prior working operations. The usual heat-treatment consists of two stages, the first being the solution stage and the second being the precipitation stage, but in applications where greater creep ductility is desirable, an intermediate stage is included. Systematic studies of the effects of the different stages of heat-treatment on the creep properties of this alloy have been reported by Betteridge and Franklin[13] and others[14]-[16]. These studies have suggested that the solution treatment has two principal functions; first to dissolve the phases which are subsequently to be precipitated to produce hardening, and second, to anneal the matrix and remove the effect of prior working. The subsequent treatments are designed to produce optimum precipitation of the hardening γ' phase and are normally carried out at temperatures close to those expected in service. Betteridge and Franklin concluded that the material exhibits the greatest creep resistance with the ageing temperature slightly above the subsequent testing temperature.

The standard recommended heat-treatment is that calculated to give the best compromise between creep resistance, life and creep ductility for the particular temperature range in which the alloy is chiefly used. For most of the Nimonic alloys, this is the temperature range involved in their use in aircraft gas turbines. The standard heat-treatment for Nimonic 80A is:

8 hours at 1080°C, air cool

16 hours at 700°C, air cool.

Since the available creep data had been gathered from specimens that had received this standard heat-treatment, the same process was applied to the cylindrical specimens in this examination, prior to treatment in the 'stressing' furnace.

CHAPTER FOUR

MEASUREMENT OF THE RESIDUAL STRESS PATTERN

It is well known that a radial temperature gradient gives rise to a triaxial thermal stress field in a thick cylinder and that creep causes a redistribution of these stresses, the rate of which depends in a complicated way on the stress, temperature and the total local plastic strain. In order to gain further insight into this process of complex stress redistribution, it was proposed to measure the residual stress field present in the specimen cylinder after an extended period during which considerable redistribution had taken place. Residual stresses have been of interest for a long time and some of the many ingenious experimental techniques devised for their measurement are summarized in a review by Denton[17] . The symmetrical simplicity of a uniformly stressed round section attracted the attention of early investigators in residual stress work with the result that Sachs[18] developed a method of measuring residual stresses in simple sections, such as right cylinders and thin-walled tubes, which has been widely used. Other techniques for the measurement of residual stresses in thin tubes have been devised, eg. the bending deflection method, but these are unsuitable for thick cylinders, and so the Sachs method was chosen for this investigation.

4.1 SACHS' BORING METHOD

The technique involves the measurement of changes in

strain on the outer surface of a long tubular section, as thin layers of material are removed in successive stages from the bore. An inversion of this boring-out process is also used where material is removed from the outer surface and strain measurements made in the bore. The theory utilizes these dimensional changes to define the triaxial state of stress existing in the whole body. The stress equations for the case of layer removal from the outer surface of the cylinder are derived by Buhler[19] and are

$$\sigma_z = -E'\left[(A-A_o)\frac{d\Lambda}{dA} + \Lambda\right]$$

$$\sigma_\theta = -E'\left[(A-A_o)\frac{d\Theta}{dA} + \{(A-A_o)/2A\}\Theta\right]$$

$$\sigma_r = -E'\left[\{(A-A_o)/2A\}\Theta\right]$$

where $E' = E/(1-\nu^2)$; ν = Poisson's Ratio, E = Young's Modulus.

$A_o = \pi r_o^2$ r_o = bore radius

$A = \pi r^2$ r = current radius of cylinder

$\Lambda = [\lambda + \nu\theta]$

$\Theta = [\theta + \nu\lambda]$

λ = axial surface strain in the bore due to the removal of an outer layer to radius r

θ = circumferential surface strain in the bore due to the removal of an outer layer to radius r

A plot of the inner surface strain readings against the changing surface area can then be used to obtain the initial triaxial residual stress pattern in the specimen.

Buhler has demonstrated that with combined turning down and boring out, the complete determination of the residual stress pattern is possible. Where this is not feasible, the stress in the remaining portion of the specimen has to be obtained by extrapolation and in some cases large errors can result. Barker and Hardy[20] proposed a way of reducing this error by rewriting the above Sachs equations in the form

$$\sigma_z = -E' \frac{d}{dA}\left[(A-A_o)\,\Lambda \right]$$

$$\sigma_\theta = -(E'/2\pi) \frac{d}{dR}\left[\{(A-A_o)/R\}\theta \right]$$

$$\sigma_r = -E' \left[(A-A_o)/2A \right]\theta$$

The values of the functions $(A-A_o)\Lambda$ and $\left[(A-A_o)/R\right]\theta$ are zero at both the inner and outer surfaces, thus making the extrapolations to the surface more certain.

This alternative form has been used for the stress calculations in this investigation.

Implicit in Sachs' analysis are the following assumptions:

1) During layer-removal, a circular section is maintained with the inner and outer walls concentric and parallel.

2) The residual stresses are distributed with rotational symmetry about the axis of the cylinder.

3) The condition of plane strain exists in the region where the change in surface strain is measured.

4) The material is effectively isotropic and has a constant value of Young's modulus and Poisson's ratio.

5) The recovery of the residual stresses on layer removal is purely elastic.

Near the ends of a long cylinder, a different residual-stress distribution is to be expected - characterized by lower axial stresses - from that at mid-length, where for a sufficiently large ratio of length to diameter, the condition of plane strain is approached. Buhler[19], Hanke and Tiemann[21] and Kawagoe[22] have investigated the question of what the minimum length to diameter ratio ought

to be in order to avoid erroneous measurements due to the overlapping of the zones of influence of the cylinder ends. In all cases this was found to be 2.

Barker and Hardy pointed out a limitation in Sachs' analysis when yielding occurs on layer removal, which is manifested in the calculated stress values being above the yield stress. The residual stresses in the present investigation were not high enough to be affected by this phenomenon.

4.2 LAYER REMOVAL TECHNIQUES

As mentioned above, Sachs' method of residual stress measurement relies on the observation of changes of dimensions due to the relaxation of constraints which one part of the cylinder exerts on others. This is satisfactory provided the process of subdivision does not cause disturbances of significant magnitude. The problem of removing material with the minimum effect on the stress pattern is thus important.

Mechanical machining is a convenient method of material removal and has been used by many residual stress investigations. In most cases the presence of induced machining stresses is acknowledged and precautions have been taken to maintain a minimum and constant effect by taking light cuts, using sharp tools and maintaining a liberal supply of cutting fluid to the cutting face. The main justification for adopting mechanical means of removal has been that the results obtained in the past have been satisfactorily checked against the equilibrium conditions given by:

$$\int \sigma_z \, dA = o \ ,$$

$$\int \sigma_\theta \, dR = o \ ,$$

$\sigma_r = o$ at the inner and outer cylindrical surfaces,

and when $\frac{d\sigma}{dr} r = o \qquad \sigma_r = \sigma_{r_{max}} = \sigma_\theta$

It should be pointed out that Sachs' equations will satisfy these equilibrium conditions for any continuous functions Λ and Θ, the only condition being that both functions are initially zero. The equilibrium checks, therefore, only apply to the calculation of the stress components and cannot eliminate or expose errors made in measuring the surface strains.

Denton[17] states that if machining stresses are kept constant, a shift but not a gradient change in the Λ vs A and Θ vs A plots may be expected and the corresponding stress values may not suffer. Preliminary tests on several mild-steel specimens, identical in form to the Nimonic specimens and 'stressed' in the manner described in the previous chapter, indicated that despite attempts at minimizing machining stresses and by maintaining constant cutting conditions, these stresses were significantly large and fluctuated in value. Due to the fact that Nimonic 80A is a difficult material to machine, because of its strong tendency to work-harden, the induced machining stresses were not likely to be any less than those in the mild steel specimens, and therefore an alternative method of layer removal which would eliminate these machining stresses, was sought.

Spark-machining, electro-chemical machining and chemical milling were the obvious stress-free alternatives. Spark-machining is not an entirely stress-free process, and although it has been successfully used by Denton[17] in thin tube applications, it was not suitable for this particular application due to its low rate of removal. Much has been done recently to develop electrochemical machining in the aircraft world, and this would be an ideal process for this particular application as high rates of material removal are attainable, good dimensional control is possible and the process is stress free. It does however, require a large specialized plant and for this reason it had to be rejected in this investigation.

The only alternative to mechanical machining therefore, was chemical milling (or acid etching), and despite its attendant problems of gauge protection, dimensional control - arising from local variations in the reaction - and corrosive environment, it was justified as a way of eliminating one further possible source of significant error.* Chemical milling has, of course, been used in residual stress work before - indeed by Sachs[24] himself - but it has been confined to the analysis of thin tubes where the problem of dimensional control is less severe.

---

*The effect of machining stresses is well illustrated in Table 4 of the recorded strain readings in Appendix 1, as light machining was used occasionally to maintain specimen symmetry during the chemical milling operation. This is discussed further in the following section.

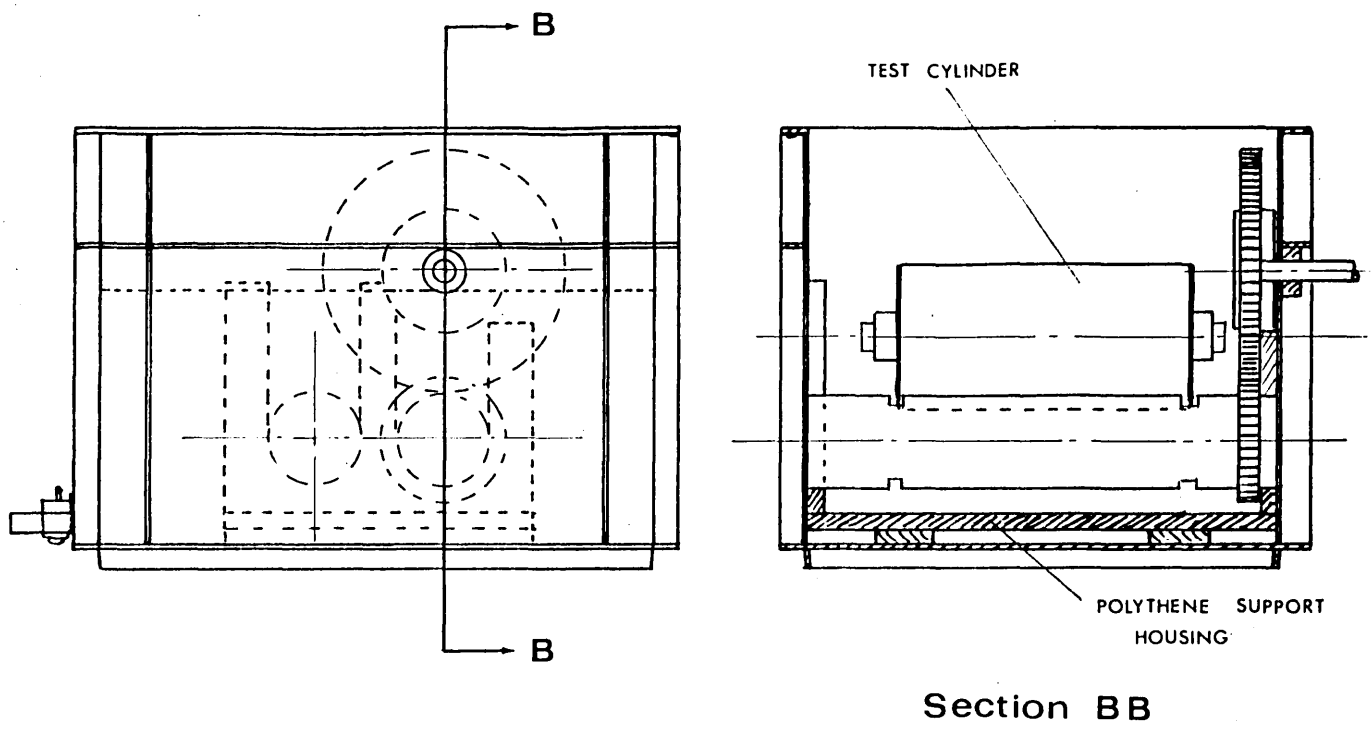
4.3 CHEMICAL MILLING

The main design requirements of the chemical milling equipment were to maintain a uniform removal of material from the outer surface of the specimen and to achieve this at a reasonable rate. It was also necessary for the specimen to be easily removable from the etching medium to enable the strain gauge readings to be recorded at regular intervals.

To meet with these requirements, a rectangular polypropylene container was modified to house two parallel polypropylene rollers, 60 mm in diameter, horizontally across its width. With the specimen simply resting on these rollers, each driven by a low speed motor, the specimen could be slowly rotated horizontally about its axis to produce a uniform reaction when completely submerged in the chemical reagent, and could also be easily removed. Some unsuccessful attempts with p.t.f.e. shaft seals resulted in the adoption of the system shown in Fig 3 where the drive to the rollers was transmitted by gears on the inside of the tank, with the drive-shafts passing through the tank wall above the level of the milling solution.

The rate at which metal is dissolved in the medium depended on the speed of the chemical reactions taking place on the surface of the metal and upon the speed with which the medium is supplied to the surface and the reaction products removed. The squeezing action on the milling solution between the cylinder and rollers was effective in performing this 'flushing' function.

The basis of a suitable chemical milling solution for Nimonic 80A was obtained by kind favour of Rolls-Royce, Bristol


B
B
TEST CYLINDER
POLYTHENE SUPPORT HOUSING
Section BB

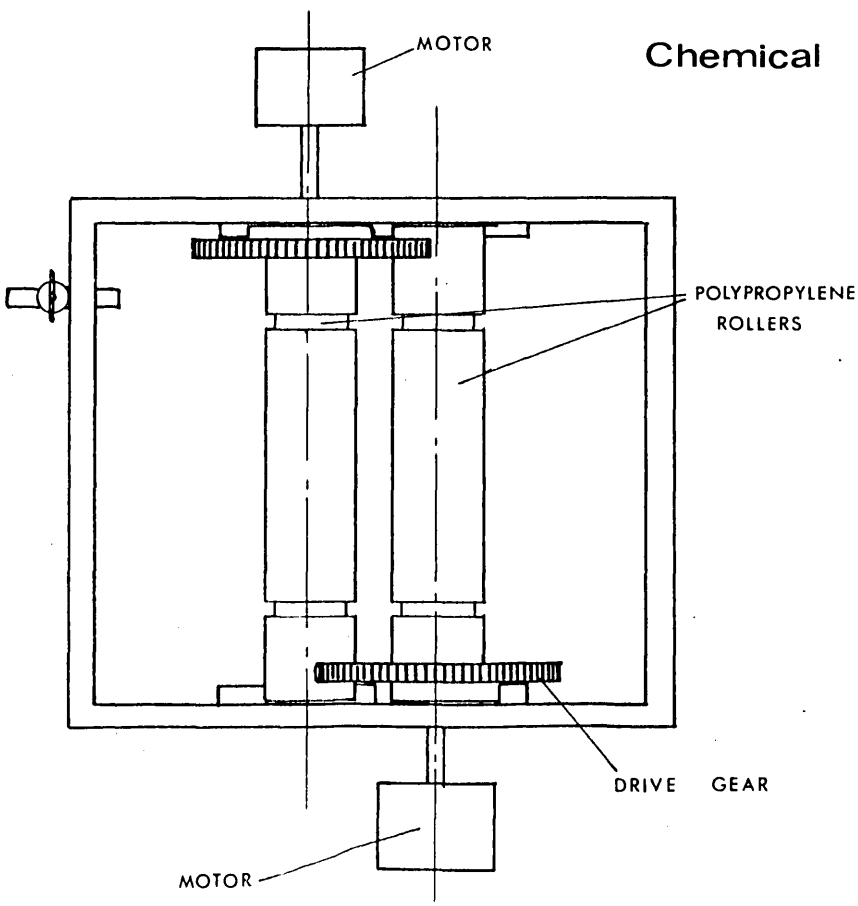

MOTOR
Chemical Milling Tank
POLYPROPYLENE ROLLERS
DRIVE GEAR
MOTOR

Figure 3

where it had been used for reducing turbine blades of Nimonic 105 after forging. The modified solution finally used for the chemical milling of the Nimonic 80A specimens was as follows:

12 parts Ferric Chloride solution

5 parts Nitric Acid

8 parts Hydrochloric Acid

2 parts Residue from previous batch solution.

The addition of some residue from the previous batch seemed to help in getting the reaction going with a fresh batch. The solution was most effective when used at 60°C and a large thermostatically controlled water-bath was used for heating the milling solution. The etchant was kept circulating through the milling tank by means of a small TEP*pump which had to be modified somewhat to prevent the magnetically driven impeller from dissolving in the solution.

Each end, and the entire bore of each specimen was coated with a thick layer of Turco*rubber to prevent attack by the acid. Special double-taper bungs of rubber and polythene were used to prevent the ingress of acid to the bore. These bungs also served to contain a sealed protective housing for the strain-gauge connectors in the event of acid leaking past the bungs. Shallow grooves were machined in the rollers to allow clearance for the rubber layer on each end as the metal was dissolved. This reduced the frequency of replacing the rubber resulting from acid getting under the layer as it was folded back by the roller. Small adjustable stops were positioned between the rollers to prevent the specimen from moving along the rollers.

*Regd. Trade Name.

It was found to be imperative to avoid any contamination of the surface of the specimen at any time between milling in order to prevent an uneven removal of material. Initially and again after each lathe machining operation the specimen was thoroughly degreased; and each time before commencing the milling operation, the specimen was immersed in concentrated hydrochloric acid for ten minutes. On removal from the hydrochloric acid and the milling solution, the specimen was washed in distilled water.

With this routine, dimensional control could be quite effectively maintained. There was, however, a tendency for the specimen to develop a slight barrel shape, and when the difference in the diameter between the centre and the ends was of the order of 0.5 mm, the cylinder was lightly machined in a lathe to restore its parallel and concentric form. This lathe operation was necessary only twice in the entire course of analysing a specimen. Eccentricity of the milled surface was found to be never greater than $\pm$ 0.2 mm.

If the concentration of the milling solution was maintained, a rate of removal of material of 0.012-0.025 mm per minute could be attained - approximately the same rate as machining in a lathe with a high-speed steel tool.

4.4 METHOD OF STRAIN MEASUREMENT

The most suitable method of measuring the changes in the surface strain in the bore is by means of resistance strain gauges. Extensometers and other mechanical methods have been used in past applications of Sachs' method but they are awkward and offer little advantage over strain gauges. Considerable advances have been made in the manufacture and

use of strain gauges and strain gauge cements, and this method of strain measurement has been used here. There are, however many pitfalls in using strain gauges and strict precautions are necessary for the attainment of reliable results.

One of the disadvantages of Sachs' technique is that the zero-strain reference point cannot be rechecked once layer-removal has commenced. It is thus necessary to keep the zero drift as small as possible, since all changes in the original zero will be interpreted as strain and added to the measurement caused by the release of residual stresses, causing large errors.

The major influence on the zero stability of a strain gauge installation is the temperature effect on the strain gauges and connection cables. The use of self-temperature-compensated strain gauges helped to compensate for the thermal expansion of the specimen material. Fig. 6 illustrates the 'quarter bridge' arrangement of each gauge circuit, in which a 3 lead wire system was employed to reduce the temperature effect on the leads. However, despite these precautions, significant variations in the strain gauge readings could still be detected, arising from fluctuating ambient conditions. This prompted the construction of a large insulated box, shown in Fig. 4 , wherein the temperature could be accurately controlled ($30^{o}\pm 0.1^{o}C$). With the entire measuring circuit and specimen inside this box, the temperature effect on the strain gauge stability could not be detected.

With d.c. bridge excitation, significant thermocouple potentials can be generated in strain gauge circuits when relatively small temperature differences occur between gauge

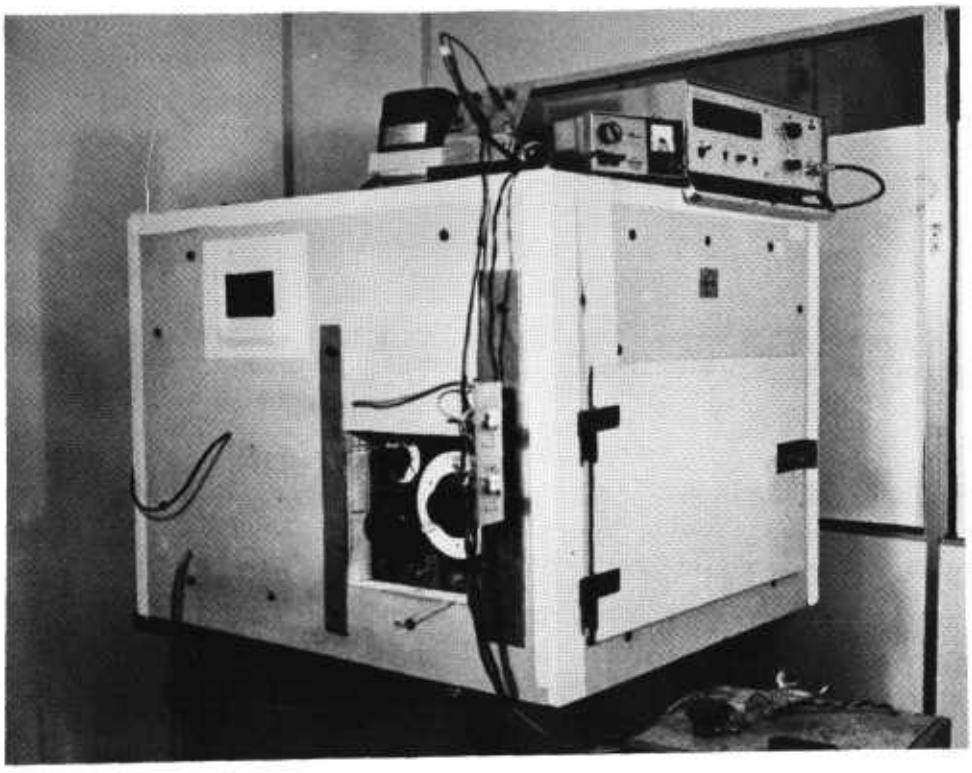
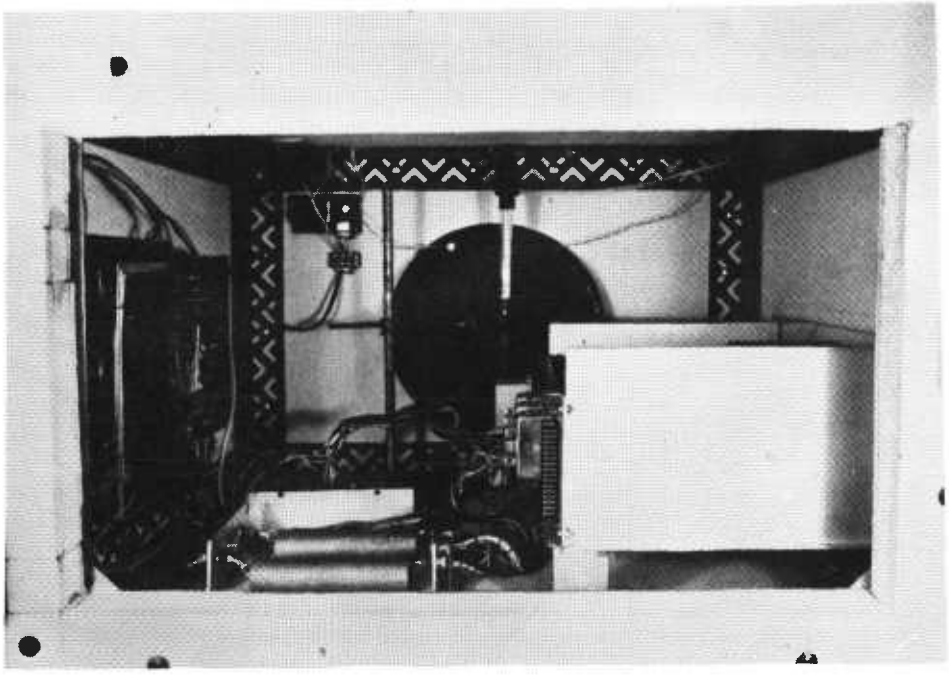


Figure 4



terminals, giving rise to zero shifts. These potentials may easily be detected by reversing the polarity of the supply voltage. With the measuring circuit enclosed in the temperature controlled box, no such effects could be detected.

In preliminary tests on mild steel specimens, some large variations in the zero were attributed to unsatisfactory performance of the gauge adhesive bond. It was therefore regarded to be of utmost importance to use a high quality cement exhibiting low hysteresis and zero instability effects- such as that used in transducers- and to ensure complete curing of the cement. A room-temperature- curing expoxy resin cement, requiring only a low temperature post-cure treatment, was found to be suitable for the gauge bonding technique employed. This is described in the next section.

In the case of layer removal from the outside of the cylinder, it is necessary for the strain gauges to be disconnected from the measuring circuit during this process. Clearly, variations in the contact resistance of the connectors used for this purpose, can give rise to large errors in the strain readings, and for this reason Bloomfield[25] found it necessary to manufacture his own silver-plated brass connecting plugs. As an alternative, two 14 pin Lemo* connectors were used for each specimen in this investigation. These are high-quality gold-plated pin connectors and used in a three-lead-wire system with the connection pins in opposite arms of the bridge circuit, they performed fairly satisfactorily: the changes of apparent strain arising from the variations in contact resistance were estimated at each

*Regd Trade Name.

strain reading by repeating the reading after unplugging and reconnecting several times, and found to be of the order of $\pm$ 5 microstrain. These connectors were rather vulnerable to the fumes generated by chemical milling method already described, and great care had to be taken in ensuring protection of the contacts.

4.5 METHOD OF BONDING STRAIN GAUGES

The precision of the strain readings may be influenced by variations in the location and consistency in the bonding of the strain gauges. The axial location at mid-length of the specimen was important due to the 'end effects' of the finite cylinder, and the alignment of gauges parallel to the cylinder axes was necessary to avoid a 'cosine' error.

Straight forward manipulation of the gauge to the required position in the bore by means of tweezers and dental mirror proved to be inaccurate, messy and quite unsatisfactory. A method proposed by Sweet and Weiner[26] in which the gauges were premoulded to the appropriate curvature was fairly successful, in that some readings were obtained, but since considerable effort was required to prepare the gauge in this form, location was not sufficiently precise and the glue-line could not be easily inspected after installation, this method was rejected.

Another technique was tested, in which a long thin card, equal in width to the bore circumference, was used to position the gauges in the specimen bore. Four rectangular apertures, each the size of the entire strain gauge and terminal tag, were cut in the card so that the gauges could

be evenly positioned on the bore surface at mid-length of the specimen. The gauges were stuck to the card with adhesive tape so that each of the gauge backing surfaces were exposed through the apertures in the card. The card was then rolled into a cylindrical shape, adhesive applied to the gauges and the card then inserted a pre-determined depth into the bore. An inflatable tube, similar to that suggested by Buhler[19] was used to hold the gauges firmly against the inner surface during curing. Several attempts were made with this technique before abandoning it due to regular occurrence of air bubbles trapped in the adhesive layer.

The technique finally adopted, was similar to a method devised at the C.E.G.B Berkley Laboratories, in which an inflatable rubber tube was 'sandwiched' between two halves of a mandrel of suitable diameter with the outer surfaces covered with a layer of Neoprene rubber. Two rubber bands held the whole assembly together. Alignment reference lines were marked on the mandrel with the aid of a special jig, so that with careful initial positioning of the gauges on the mandrel, accurate location of the gauges at the centre of the specimen bore could be achieved. As shown in Fig 5 , the strain gauges, with lead wires attached, were secured, bonding surface uppermost, to the mandrel by means of double-sided adhesive tape. The bonding adhesive was applied to the strain gauges and the whole assembly was inserted in the bore by the appropriate amount, taking care to ensure that the gauges retained the curvature of the mandrel to avoid air bubbles being trapped in the adhesive layer. The tube was then inflated to a pressure of 12½ psi and the adhesive

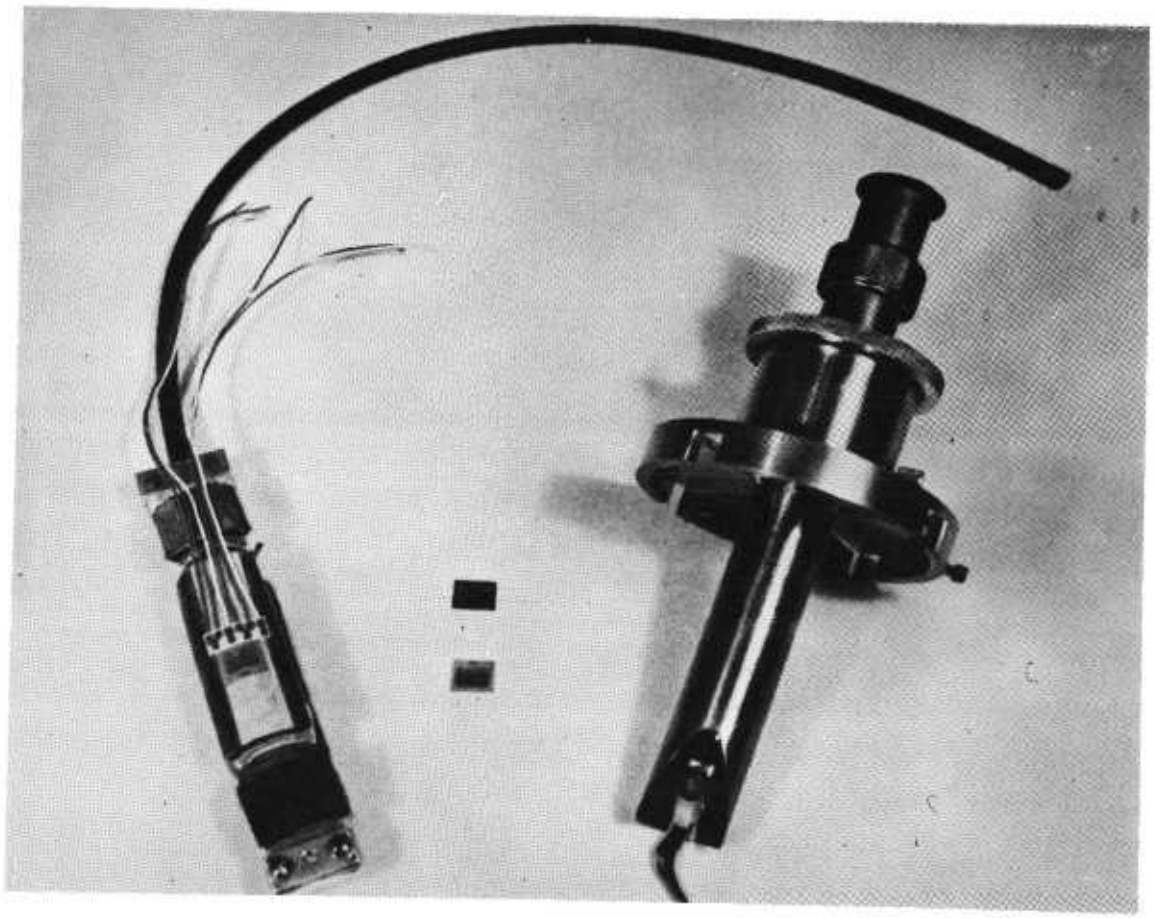


Figure 5

allowed to cure, after which the assembly was removed by deflating the tube and breaking the weak cellulose band of the adhesive tape. Two strain gauges were installed simultaneously by this method.

A special magnifying periscope was made to enable careful examination of each strain gauge installation, and if found unsatisfactory the gauge was scraped off and replaced. Measurement of the actual misalignment was found to be no greater than 5 degrees * and axial positioning at mid length was within 2 millimeters. A final check was made on the performance of the installed gauges before commencing with the layer removal by compressing the specimens axially, in a Dennison press, over the elastic strain range covered in the measurement of the residual stress pattern.

Two types of strain gauges were used in the tests, Micro-Measurements 90°Tee' Rosette, EA-06-125 TM-120, having a gauge length of 3.18 mm; and Kyowa 90° 'Tee' Rosette, KF-2-D1-11, with a gauge length of 2 mm. The layout of the terminal tags gave preference to the former type for this particular application.

Prior to bonding the gauges, the surface of the bore was scrupulously prepared, according to the gauge manufacturers

---

* The magnitude of the error due to misalignment, ϕ, may be estimated from the two-dimensional Mohr strain diagram .

$$\text{(measured)} \quad e = \tfrac{1}{2}(\varepsilon_1+\varepsilon_2) + \tfrac{1}{2}(\varepsilon_1-\varepsilon_2)\ \text{Cos}\ 2\phi$$

In this investigation, the axial and circumferential inner surface strains were both compressive and nearly equal in magnitude. The misalignment thus had to be of the order of 15 degrees to produce an error of 10 microstrain in the largest strain reading.

recommendations.[27] . The thick oxide layer which formed during the heat-treating process was removed by honing with a cast-iron plunger and grinding paste which produced an even but slightly roughened surface.

4.6 STRAIN MEASURING CIRCUIT

The arrangement of the strain measuring circuit is shown schematically in Fig 6.

A Tinsley slide-wire null-balancing Wheatstone bridge was used to measure the resistance changes of the strain gauges. This was built into the side of the temperature controlled box and operated from the outside. The out-of-balance condition was monitored on the accompanying galvonometer. With the relevant gauge-factor set, the strain could be read directly off the instrument. The calibration of the instrument was checked with precision resistors which simulated strain changes of 200 and 500 microstrain when fixed in parallel with a 120 Ohm resistor, the gauge factor being set at 2.00.

The initial bridge balance of each gauge circuit was attained by careful manipulation of the balancing potentiometers contained in a Solartron balancing unit.

Power to the measuring circuit was supplied by a stabilized d.c. voltage power-pack. The supply voltage was set at 2.000 volts and was constantly monitored on a Solartron digital voltmeter. The a.c. ripple arising from the rectification in the power-pack was less than one millivolt. Errors arising from gauge heating, earth leakage and impedance effects were thus kept to a minimum without seriously reducing the measuring sensitivity.

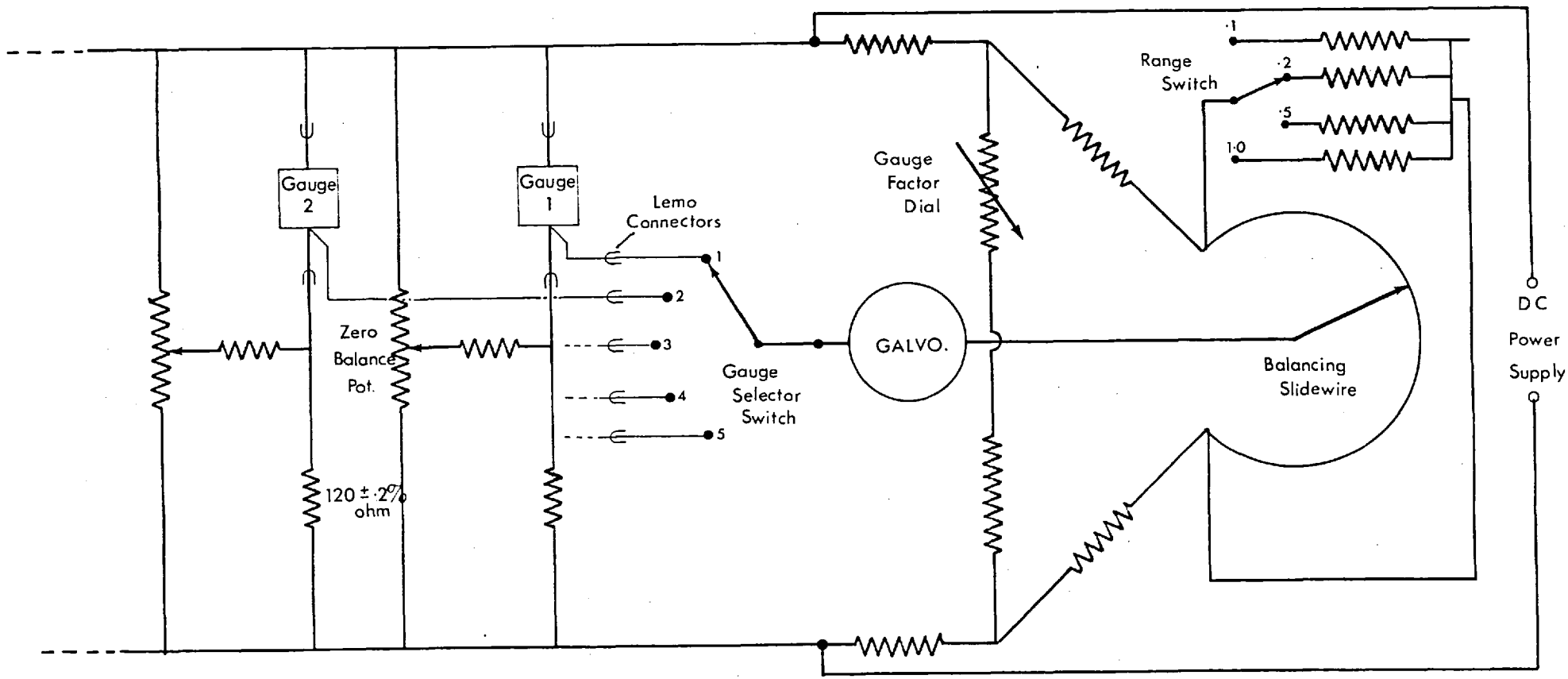

Gauge 2
Gauge 1
Lemo Connectors
Gauge Factor Dial
Range Switch
·1
·2
·5
1·0
Zero Balance Pot.
120 ± ·2% ohm
Gauge Selector Switch
GALVO.
Balancing Slidewire
DC Power Supply
1
2
3
4
5

Figure 6

CHAPTER FIVE

5.1 EXPERIMENTAL RESULTS

An account of the development of a suitable heater element and some of the difficulties encountered has been given in Chapter 3. These 'teething troubles' were not all eliminated before commencement of the testing program on the Nimonic specimens - indeed, they were only manifest once the long testing period was attempted ; with the consequence that replications of testing conditions for the first three specimens over the 1000 hour period was not achieved.

The first specimen was particularly affected by this malady, with two Kanthal heaters and the first platinum heater being used consecutively in the 1000 hour period. In the case of the Kanthal heaters, the deterioration was gradual before final failure with the result that the temperatures in the test specimen gradually drifted downwards for a considerable period before suddenly dropping on failure. The platinum heater failure was more sudden with indication of its imminence only being observed shortly before failure. A continuous record of the temperature history as measured by the five thermocouples was monitored and recorded on a chart recorder, but for illustrative purposes,the cycle history, as approximated by a series of step changes is presented in Table 1 in Appendix I.

During the loading cycle of Specimen 2, the performance of the Variac began to deteriorate from the oxidation of the carbon brushes through the continuous over heating induced by the high current being drawn by the heater element. The

Variac was successfully taken out of the circuit without interrupting the supply to the heater, but the slightly higher voltage then applied to the heater raised the temperature in the specimen by some 13 degrees. It was unfortunately not appreciated at that stage that adjustments to the applied voltage could be made through the voltage stabilizer unit, and the power was maintained at this higher level for the rest of the test period.

At the end of this test period, a switching arrangement was built into the heater circuit to facilitate isolation of the Variac once the desired test conditions had been reached. The temperatures recorded for this second specimen are shown in Table 2 in Appendix I.

The last heater element failure occurred 172 hours after steady temperature conditions had been reached in Specimen 3. Fortunately, this was only due to a poor contact at the electrical feeder terminal and was repairable. The recorded temperature distribution for this specimen is also given in Table 2 .

By this stage in the test programme, the heater 'teething troubles' had been eliminated and the reliable performance of the heater could at last be confidently assumed. In the three tests already completed, however, the desirable degree of replication had not been accomplished and due to the shortness of the remaining allotted time for the project, it was decided to reduce subsequent loading cycles to 500 hours. This enabled five more specimens to be tested under identical conditions, giving greater statistical significance to the measured residual stress pattern.

The extruded bar from which the first two specimens were made came from a different stock batch to that used to make up the other six specimens. Although hardness tests and metallographic examination showed that the bar as received had been heat-treated, all specimens, except the first two, were heat-treated again (as described in Chapter 3) after machining to the specified form. The hardness survey made of each specimen after the standard heat-treatment indicated that the metallurgical condition was similar and uniform. The values of hardness obtained were all within the range 290-370 HV specified for Nimonic 80A after the recommended heat-treatment.

There is some discrepancy in the values quoted by the manufacturers for Young's Modulus at room temperature for extruded bar, ranging from 18-22 x $10^3 kg/mm^2$. Since the measured surface strain changes are directly influenced by the elastic modulus, tension tests were performed on the remaining thin cylindrical shells of a few specimens to measure the elastic modulus of the material in an overaged condition. The cylindrical shells were lightly machined concentric with the bore and the middle 75 mm of each specimen was ground to a smaller diameter of 30.48 mm. Special jaws were made to enable the specimen to be accurately centralized in the Instron testing machine. These jaws were both fitted into universal joints to further eliminate bending stresses. The installed strain gauges in each specimen were used to record the resulting strain. The values of strain registered for various applied loads for two specimens are shown in Fig 7 , the value of Young's Modulus thus obtained was found

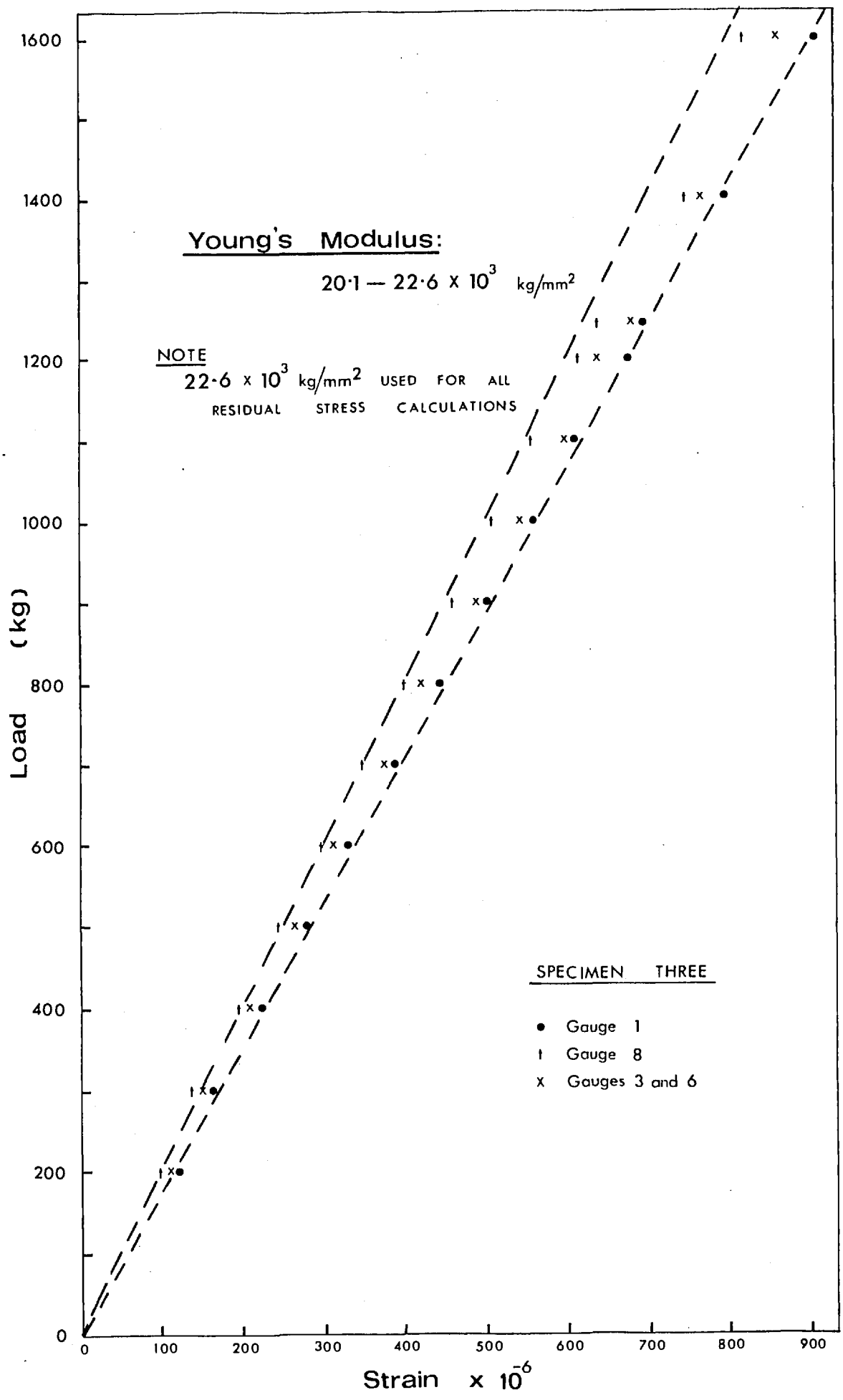

Young's Modulus:
20·1 — 22·6 X 10³ kg/mm²
NOTE
22·6 X 10³ kg/mm² USED FOR ALL RESIDUAL STRESS CALCULATIONS
SPECIMEN THREE
Gauge 1
Gauge 8
Gauges 3 and 6
Load (kg)
Strain x 10⁻⁶
0
200
400
600
800
1000
1200
1400
1600
0
100
200
300
400
500
600
700
800
900

Figure 7

to be within the range quoted by the manufacturers.

Microscopic examinations of samples cut from the remaining shells of each of the specimens confirmed the expected excess of intragranular γ' precipitate of the overaged condition. Figs 8 and 9 show typical structures and also indicate that the precipitation is not visibly greater in the specimens which had been heated for a much longer period.

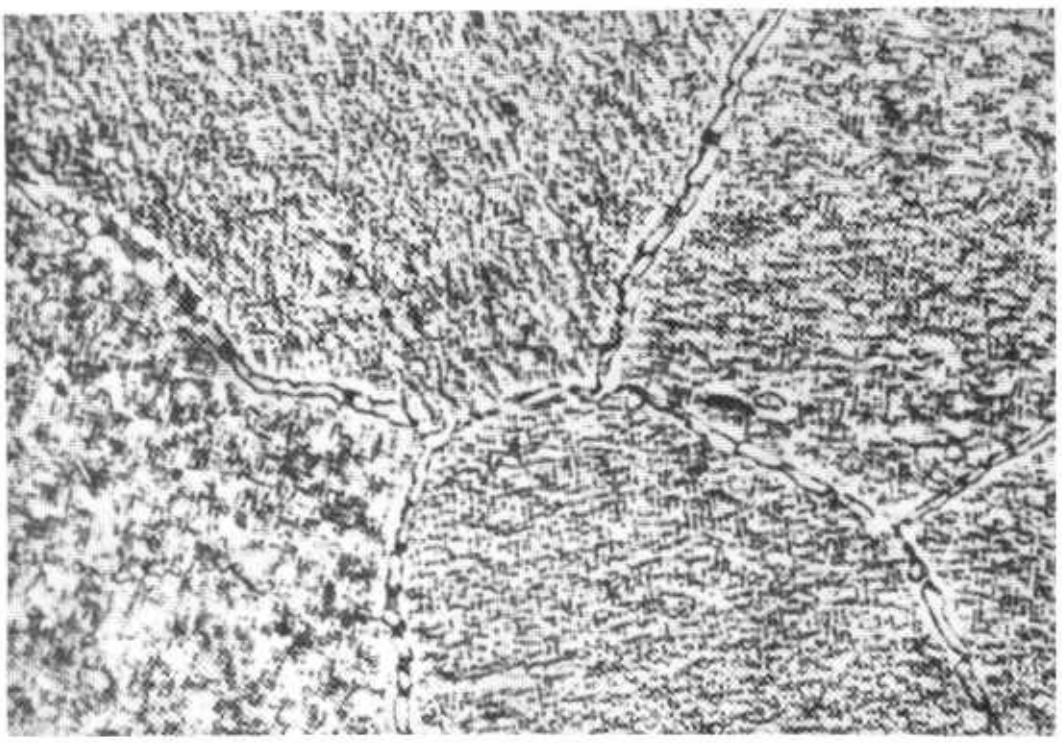
In order to test for anisotropy in the creep properties of the extruded bar from which the test cylinders were made, uniaxial creep test specimens were cut from the material in both the axial and transverse directions of extrusion. Unfortunately it was not possible to complete the creep tests on these specimens in time for inclusion in this thesis.

5.2 ESTIMATION OF ERRORS

The objective of this first stage of the experimental investigation has been the development of a reliable procedure for the measurement of the complex residual stress field present in a specified thick cylinder after stress redistribution has been allowed to take place during a loading period in which neither the stress nor strain has been constrained. For the method to be judged reliable, the results thus obtained ought to be both accurate and precise.* In the quest for accuracy, systematic errors and those associated

---

*A distinction is made between accuracy and precision. Accuracy is associated with the freedom from systematic error of a measurement, and precision with the random variation obtained in repeated tests.

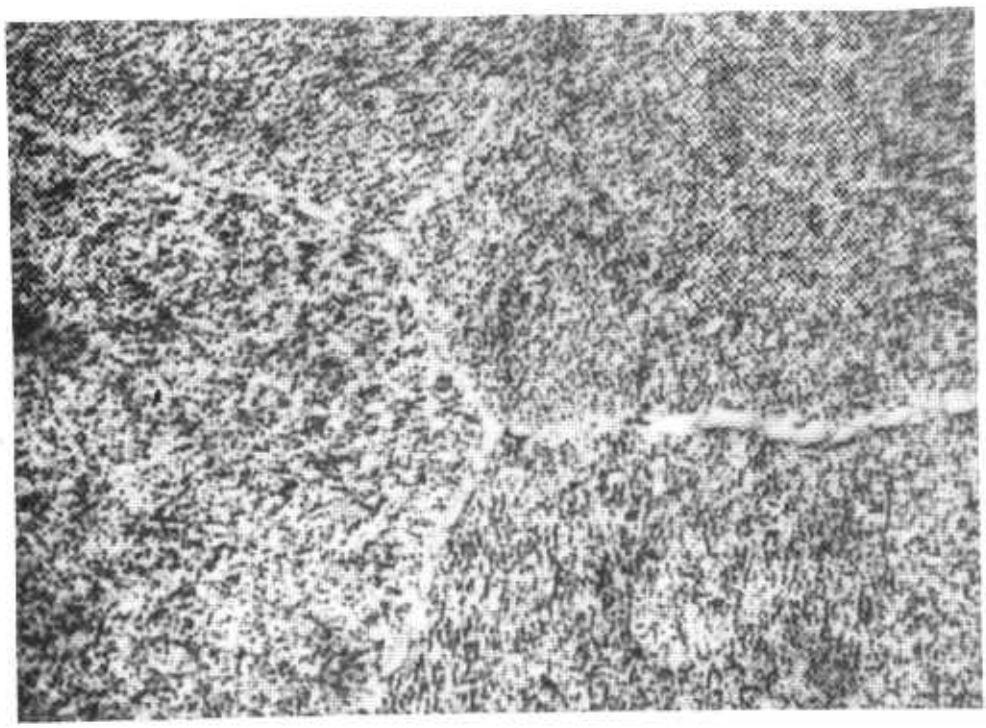


Specimen 3 – after 1000 hrs (x 2000)

Figure 8

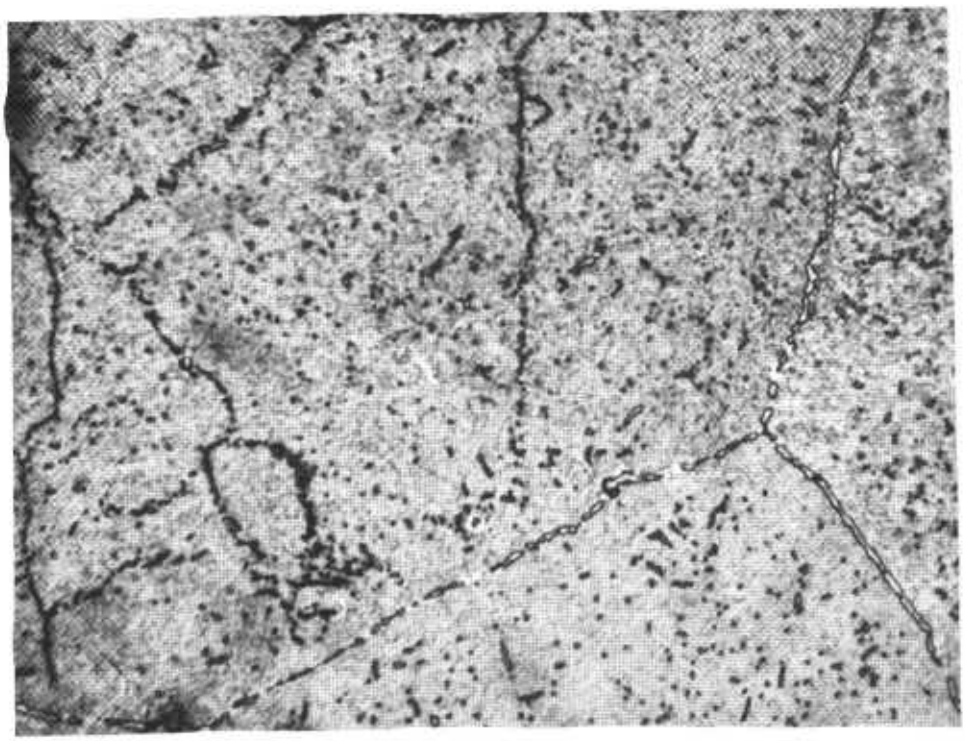


(x 400)



Specimen 7 – after 500 hrs (X 2000)

Figure 9



(X 800)

with assignable causes need to be eliminated from the experimental method. Several identical tests then performed under these conditions may usefully indicate the precision of the observed quantities.

The experimental procedure that has been developed has been described in detail in the proceeding chapters, but it is pertinent to this section to re-iterate the measures that were taken to eliminate systematic errors and those due to assignable causes, to ensure reliability. These may be divided into two main sections in accordance with Chapters 3 and 4.

1) Specimen Generation

a) Specimen

i) The assumption of parallel, axial symmetry in the test specimen was ensured by having each specimen made to close tolerances on the bore diameter, concentricity of the bore with the outer surface, and uniformity of bore diameter. A fine surface finish in the bore was achieved by final honing.

ii) Heat-treatment in accordance with the recommended two-stage procedure was designed to produce an initial suitable uniform metallurgical condition. It also served as a stress relieving measure after machining and a method of establishing a stable oxide film on the radiating cylindrical surfaces so as to improve the emissivity.

iii) Test specimens were manufactured from the same piece of extruded bar.

b) Stressing Cycle

i) To ensure axisymmetric stressing, the specimen was located centrally within the furnace with the uniform heater element positioned concentrically within the bore.

ii) The test temperature conditions were measured with the aid of chromel-alumel thermocouples, checked against each other and another standard. The calibration of the temperature recording equipment was proved against two different accurate instruments.

iii) The applied vacuum and the thermal gradient were constant throughout the loading programme. The duration of the testing period was the same for the last five specimens.

2) Residual Stress Measurement

a) Strain Measuring Equipment

i) The calibration of the strain scale of the Wheatstone bridge instrument was regularly checked at two measuring points with two standard resistances. Readings taken from strain gauges attached to a four-point bending beam concurred with the deflection measurements over all the instrument measuring ranges.

ii) The response of the strain gauge transducers assignable to temperature effects, were minimized by using self-temperature-compensating gauges and a three-lead wire system, all enclosed in a temperature controlled box. The bridge supply voltage was accurately maintained at a constant low value.

b) Strain Gauge Technique

i) The strain gauges were centrally located within the bore of the specimen and accurately aligned.

ii) The response of the bonded gauge was checked before commencing layer removal.

iii) The same surface preparation and bonding procedures were repeated for each specimen. The enviroment during strain gauge mounting was controlled in both temperature and humidity.

c) Layer Removal

i) A chemical milling technique was developed to avoid induced stresses on layer removal.

ii) The symmetrical form of the specimen was closely maintained throughout the chemical milling process.

d) Measurement Observation

i) Several readings of each strain measurement corresponding to a particular diameter were taken at different times to minimize the possibility of mistakes, and the readings averaged.

ii) The effect of variations in the contact resistance of the connectors in the strain gauge circuits was reduced by repeating the readings after each of several re-connections.

iii) Variation that might have occurred in the instrument slide-wire performance, was constantly monitored with an unbalanced quarter bridge circuit in which a fixed precision resistor was used in the place of a strain gauge.

One additional possible source of error, not mentioned in the above summary, has been investigated at length by Andrea[28] and Bergqvist[29] who claim that the usual 0.5% tolerance for the specified value of the gauge factor can be in error by a significant amount. This has not been accurately assessed in the present application but precautions have been taken with this in mind by using several pairs of strain gauges from different batches and taking the average of the readings. Both the lack of space and availability of suitable connectors restricted the number of gauges used on each specimen to four pairs, i.e. four axial gauges and four circumferential gauges. The differences in the gauge factor of the strain gauges arise mainly from manufacturing processes and extreme variations in enviromental conditions during storage prior to bonding, and during bonding. These enviromental conditions were closely controlled and these gauge factor variations have thus been included under the 'random' title.

After each layer removal operation, the specimen diameter was measured at several points around its central diameter with a micrometer. Measurements thus taken would correspond to the 'peak-to-peak' diameter of the roughened surface and would be slightly greater than the effective uniform surface diameter. This difference was estimated as being between 0.1 and 0.05mm on the diameter and since the strain change with decreasing radius was not great, the small error in the diameter reading was seen to be of little consequence. Therefore,in the analysis of the experimental results the values of the diameter were assumed to be precise.

Despite having taken all the above precautions, it cannot be claimed with certainty that all systematic error has been eliminated from the strain measurements. As already mentioned in Chapter 4, the zero-strain reference point cannot be re-checked in the Sachs method and therefore the occurrence of zero-drift cannot be disclaimed absolutely. However, confidence in the performance of the installed strain gauges can be drawn from their satisfactory performance before the commencement of layer removal on the cylinders and again from the tension tests performed on the thin residual shells, in which no signs of zero-drift could be detected on removal of the test load. Also, the measuring circuitry was unaltered, except for the zero potentiometers, for each of the specimens and drift in the readings could not be detected in the interval between making the initial zero adjustments and commencement of layer removal. On these, the only guidelines for assessing the significance of zero-drift, it is claimed that the systematic errors have been maintained at an insignificant level.

An assessment of the error bounds in the surface strain readings has therefore been made using fundamental statistical methods. Replication of a loading cycle has been achieved in the case of the last five specimens and the results obtained therefrom have been used to gauge the precision of the measurement technique. The standard deviation from the mean of the strain gauge readings from the five 500 hour specimens is shown in Fig 10. The measured surface strains for each of the specimens are given in Tables 3 to 10 in Appendix 1.

5.3 Calculation of Residual Stresses by Sach's Equations

In the method of residual stress determination as originally proposed by Sachs, curves of the two parameters

$$\Theta = [\theta + \nu\lambda]$$

$$\Lambda = [\lambda + \nu\theta]$$

against the current area were plotted from the measured values and the first derivatives of these parameters, required for the calculation of the axial and tangential stress components, were obtained graphically. This operation was subject to error due to the spread of measurements at each sampling point and therefore a numerical method of fitting the smooth regression curves was adopted. Due to their ease of evaluation and differentiation, polynomials of the general form

$$y_p(x) = \sum b_{pj} x^j$$

were used as the approximating functions. The degree of the polynomial also affords a convenient measure of smoothness. Using the least squares principle as a criterion for goodness of fit and the method of orthogonal polynomials*, the regression coefficients b_{pj} were calculated for polynomials up to seventh degree, with the aid of an established computer code[30]

---

*The fitted regression polynomial of degree k

$$y = a_o + a_1 x + \ldots\ldots + a_k x^k$$

can be rewritten in the form

$$y = a'_o + a'_1 f_1(x) + \ldots\ldots + a'_k f_k(x)$$

where $f_r(x)$ is a polynomial in x of degree r, and the constants a'_i depend on the values of a_i. It is possible to find a set of polynomials which satisfy the conditions

$$\sum w f_r(x) f_s(x) = o \quad (r \neq s), \text{ and } \sum f_r(x) = o$$

These orthogonal polynomials therfore greatly reduce the amount of computation in the least squares fitting. Also, by this method, estimates of the regression parameters are independent.

As a guide to judging the polynomial of lowest degree that fitted the data adequately, a statistical technique was adopted. This amounted to a significance test on the difference of the residual sum of squares

$$S_j = R_{j-1} - R_j$$

when a polynomial was increased from degree (j-1) to j. Statisticians have obtained the distribution for the ratio of two independant estimates of the variance of the same normal population. Since these are both estimates of the same quantity- the population variance- their ratio, called the 'variance ratio' and given the symbol F, is expected to be 'close' to unity. In order to see if the observed F-ratio is significantly large, it is compared with the upper percentage points of the F-distribution, given in standard tables. It can be shown[31] that S_j and $R_j/(n-j-1)$ are independent estimates of the residual variance, and that the ratio of these two quantities will follow on F-distribution with one and (n-j-1) degrees of freedom,

$$F_{1,(n-j-1)} = R_{j-1}/R_j$$

If a polynomial of degree j does fit the data better than a polynomial of degree (j-1), then R_j will be substantially less than R_{j-1} and the F-ratio may be significantly large. The F-test was performed after each sequential increase in the degree until two non-significant F-ratios at the 95% level were obtained. The regression coefficients of the polynomial with the last significant F-ratio were then used in the stress calculations. Although this test did provide a useful guide to judging the most suitable polynomial, it had to be used discretely as goodness of fit was not the only criterion to

be satisfied; the fitted function had also to be smooth and continuous.

The variation in the individual strain gauge readings, as indicated in Fig 10, increased as layers were successively removed from the outside of each specimen. It was necessary to take this variation in precision into account in the fitting of the curves by weighting the measurements appropriately. The weight of each point is usually taken as being inversely proportional to its variance, and this was not reliably obtainable from the four strain readings taken at each point. Therefore, as a scheme for calculating an appropriate weight for each fitted point, it was postulated that the percentage precision was constant - that is, for example, the standard deviation of λ_i was proportional to λ_i. The fact that this was not strictly true at points close to the initial zero value, was taken into account in applying the weights.

The weights used in finding the regression coefficients of the functions $[(A-A_o)/R]\theta$ and $(A-A_o)\lambda$ were found from the relations

$$w_i = B/\ \text{Variance}\left[\left(\frac{A_i-A_o}{R_i}\right)\ \theta_i\right]$$

$$= B/\left[\left(\frac{A_i-A_o}{R_i}\right)^2\ \text{Variance}\ \theta_i\right]$$

$$= B/\left[\left(\frac{A_i-A_o}{R_i}\right)^2\ \left\{\bar{\theta}_i^2+\nu^2\bar{\lambda}_i^2\right\}\right]$$

and $$w_i = C/\left[(A-A_o)^2\ \left\{\bar{\lambda}_i^2+\nu^2\bar{\theta}_i^2\right\}\right]$$

respectively. The constants B and C were chosen to provide

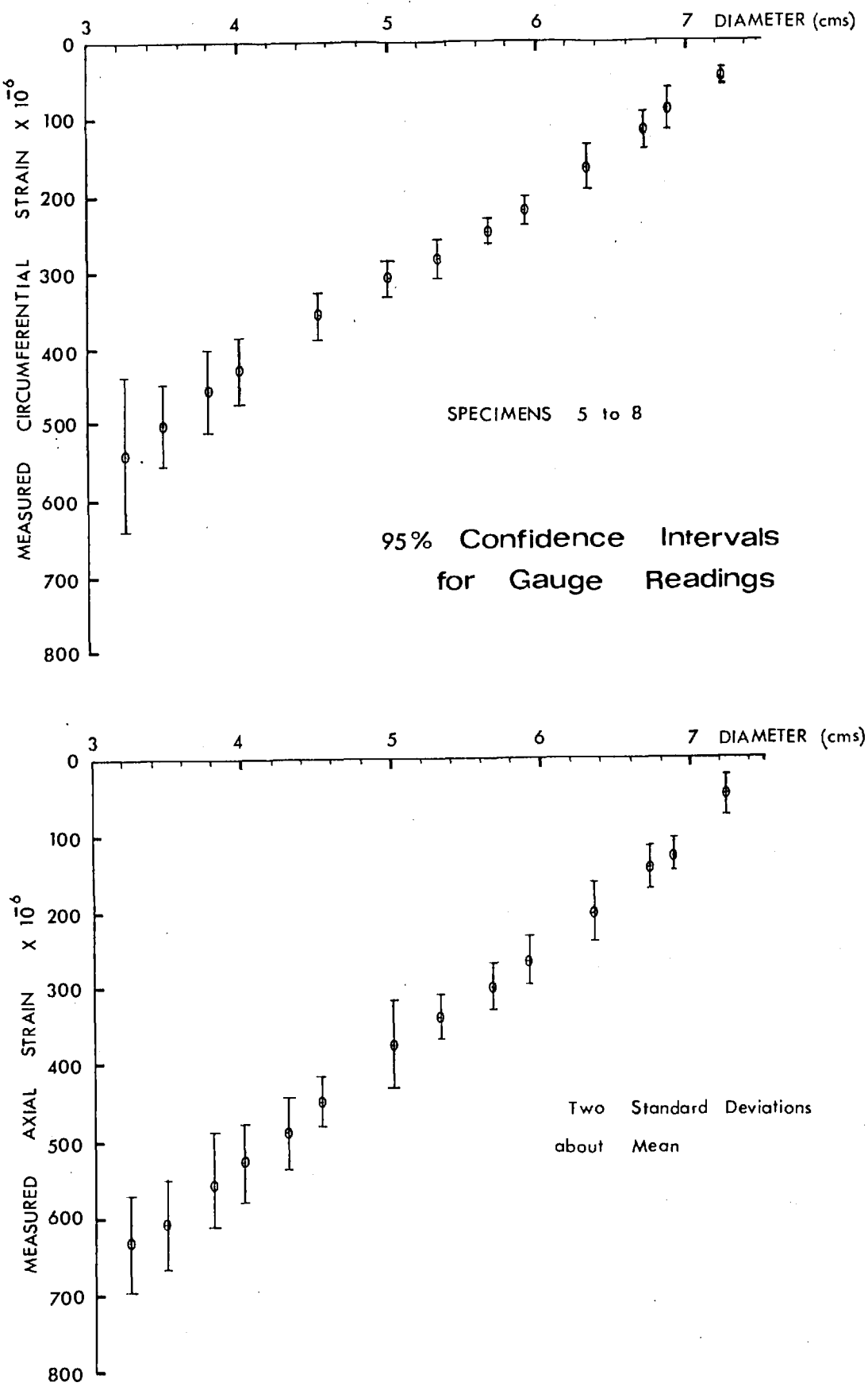
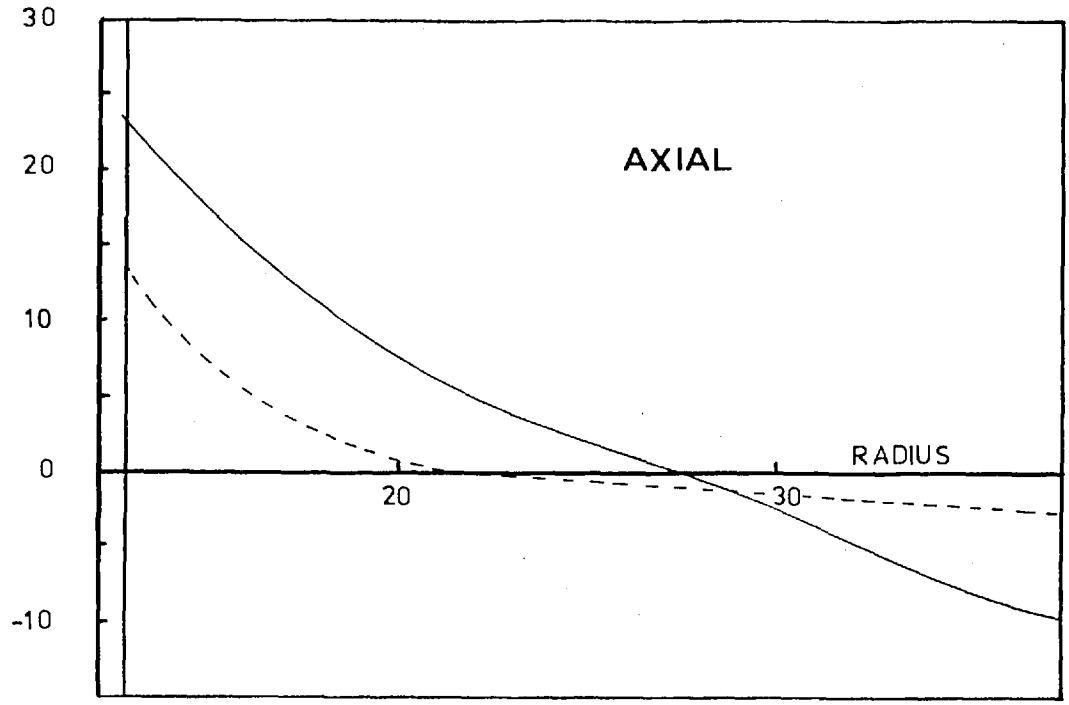

3
4
5
6
7 DIAMETER (cms)
0
100
200
300
400
500
600
700
800
MEASURED CIRCUMFERENTIAL STRAIN X 10⁻⁶
SPECIMENS 5 to 8
95% Confidence Intervals
for Gauge Readings
3
4
5
6
7 DIAMETER (cms)
0
100
200
300
400
500
600
700
800
MEASURED AXIAL STRAIN X 10⁻⁶
Two Standard Deviations
about Mean

Figure 10

convenient manageable values for the weights. In accordance with the extrapolation conditions, the points on the inner and outer surfaces were given weights of 1000 to force the curve through zero.

The coefficients of the appropriately chosen regression polynomial were used to calculate the residual stress components at points across the specimen wall by Sachs' equations in the form suggested by Barker and Hardy. The resulting residual stress distributions for each specimen are illustrated in Figs 11 to 18.

The calculation of the axial and tangential residual stress components involve first derivatives of the fitted functions and a meaningful error bound on the computed stress values is thus not readily found. Probable errors in the coefficients for the fitted functions could be used to calculate the extreme bounds of the differentiated polynomial, but these are likely to provide over-conservative estimates of the probable error in the slopes. An empirical approach to error estimation has therefore been adopted by superimposing the residual stress patterns of the five 500 hour specimens, as calculated by Sach's equations for a fixed value of Youngs Modulus, and an estimate made from the bounds of these curves. This is shown in Fig 19 , together with the predicted stress distributions.



Specimen 1

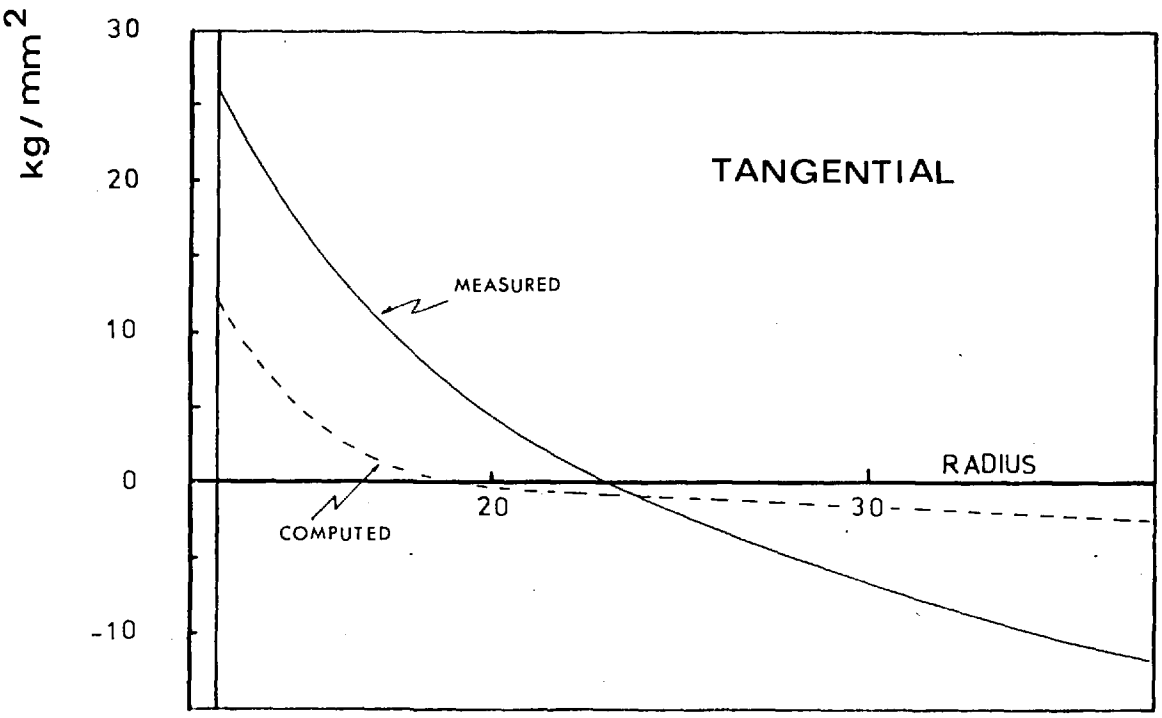
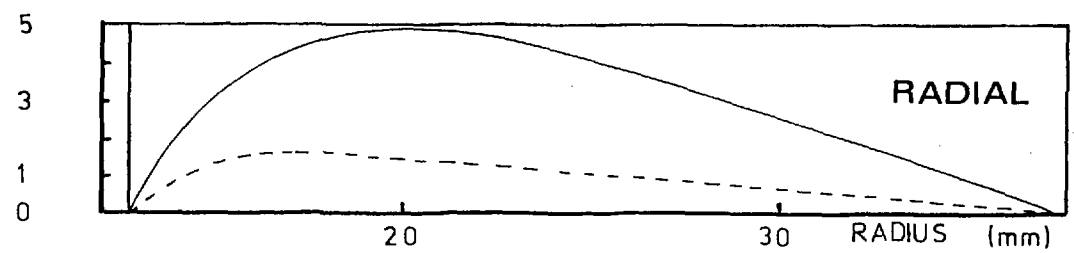
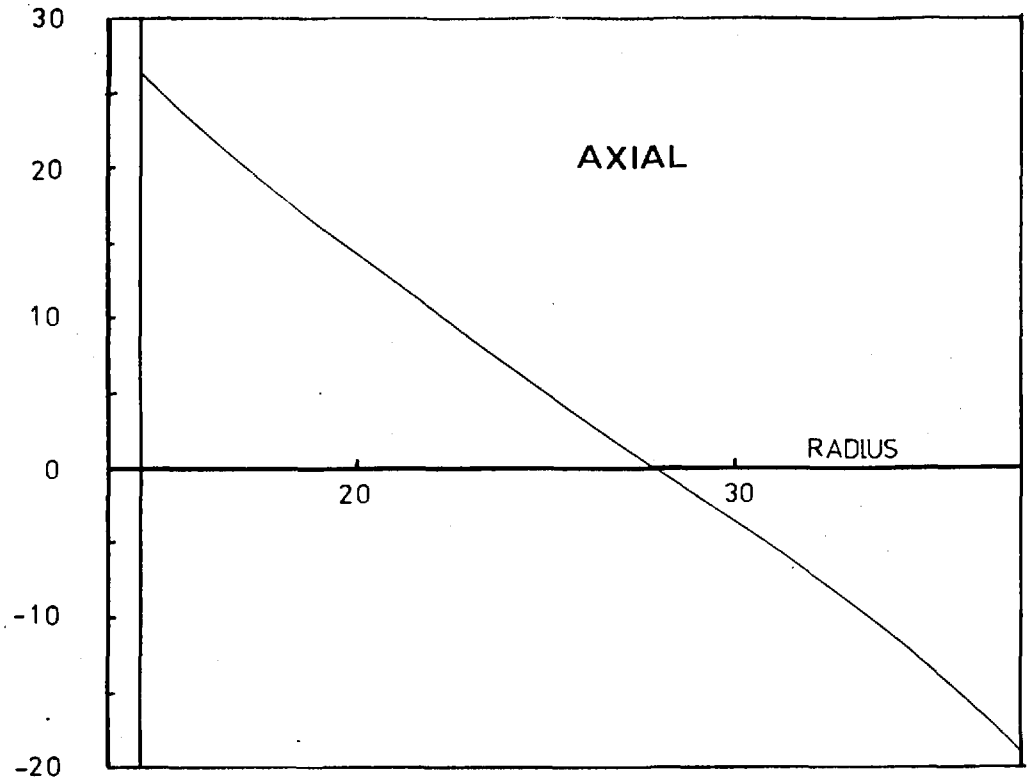


Figure 11



RESIDUAL STRESS



Specimen 2

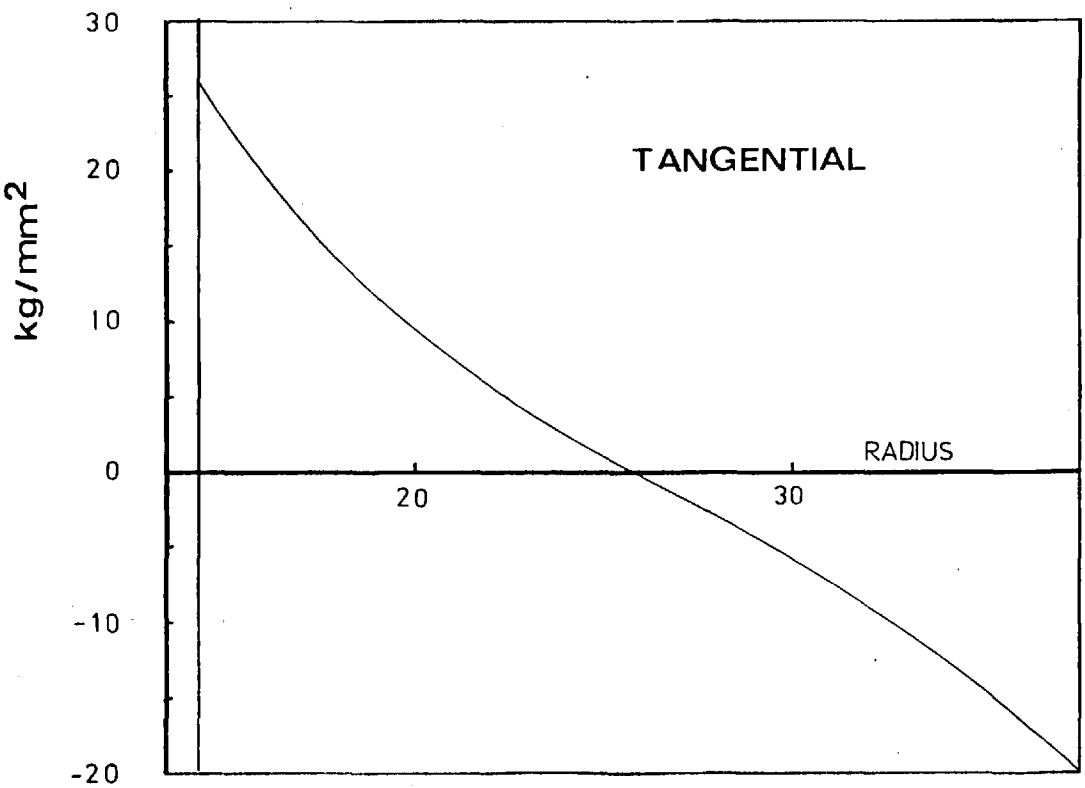
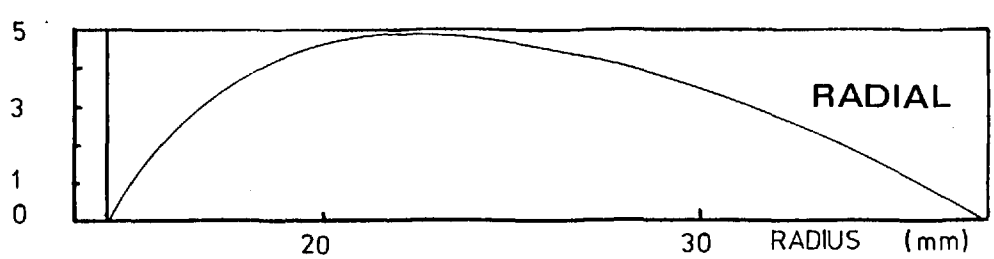
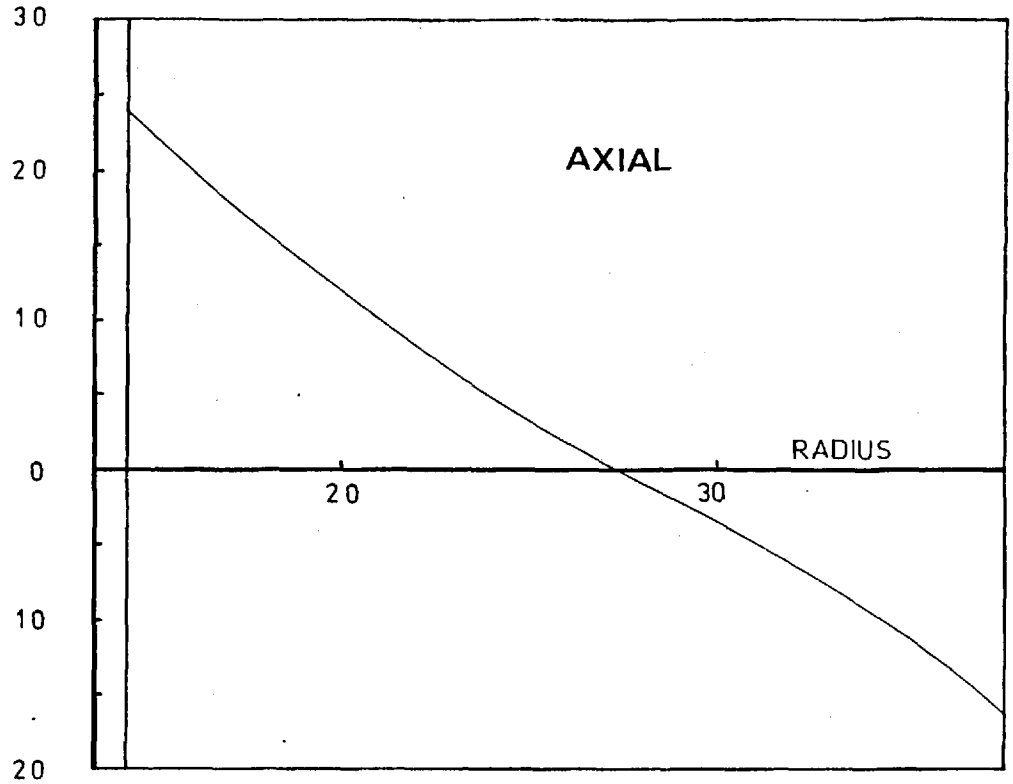


Figure 12



RESIDUAL STRESS



Specimen 3

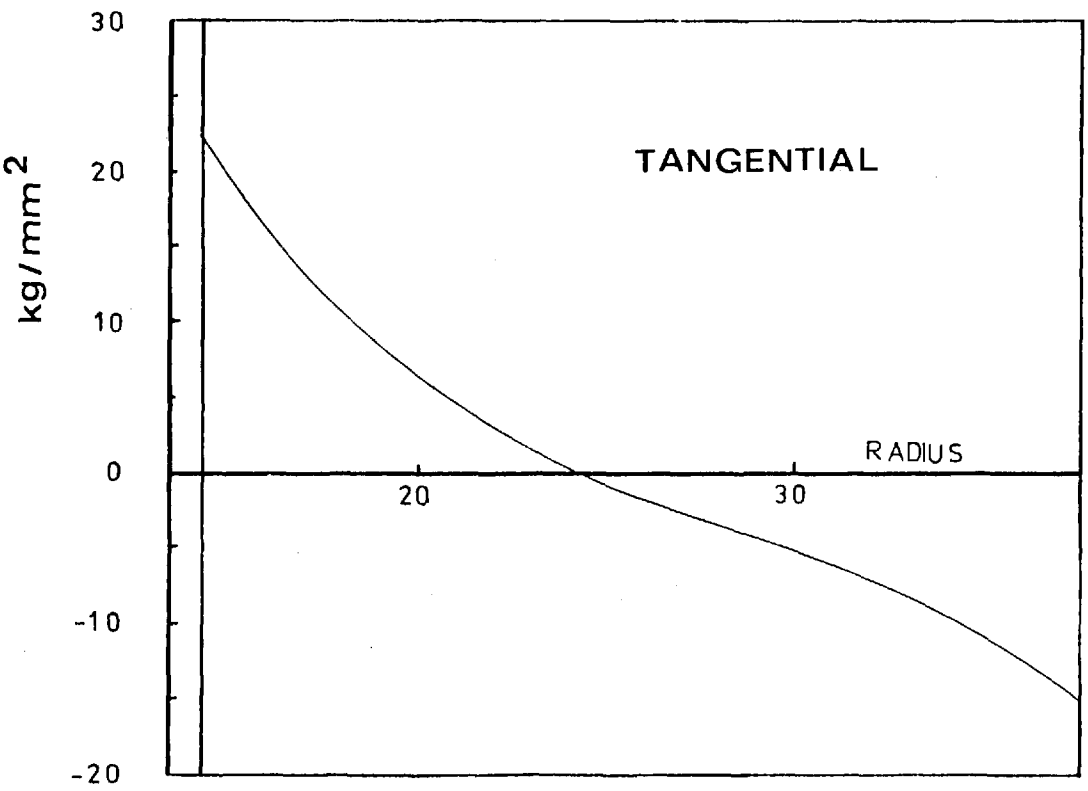
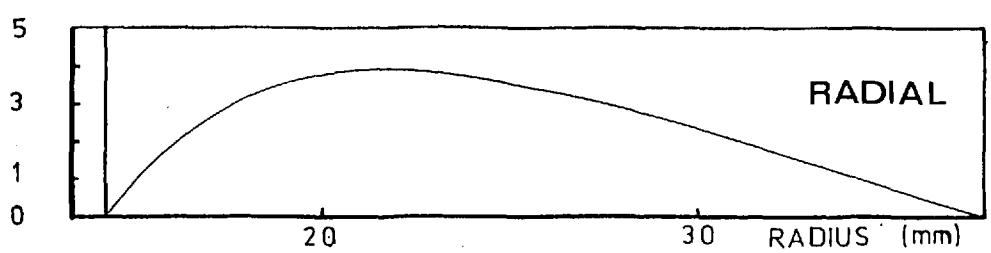
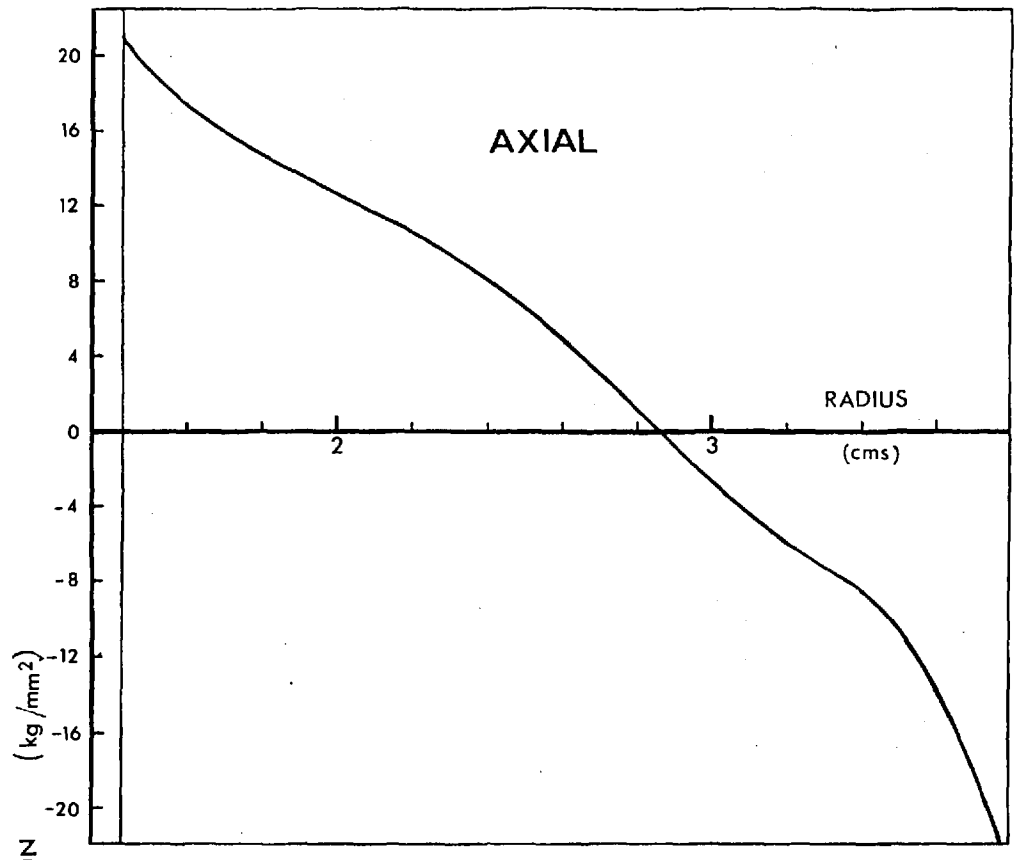


Figure 13



RESIDUAL STRESS



Specimen 4

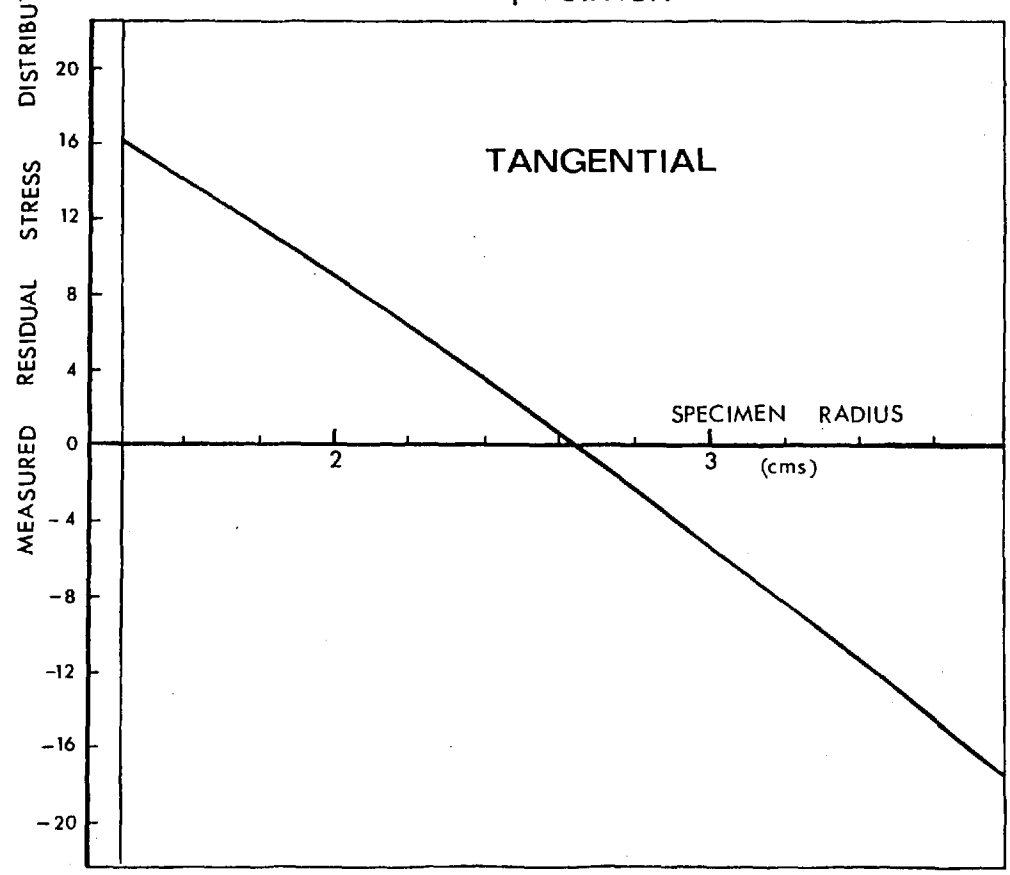
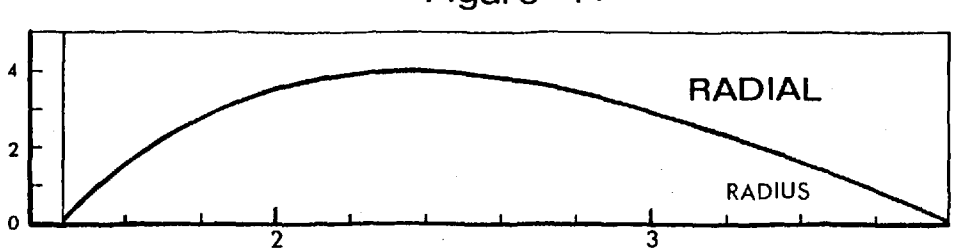
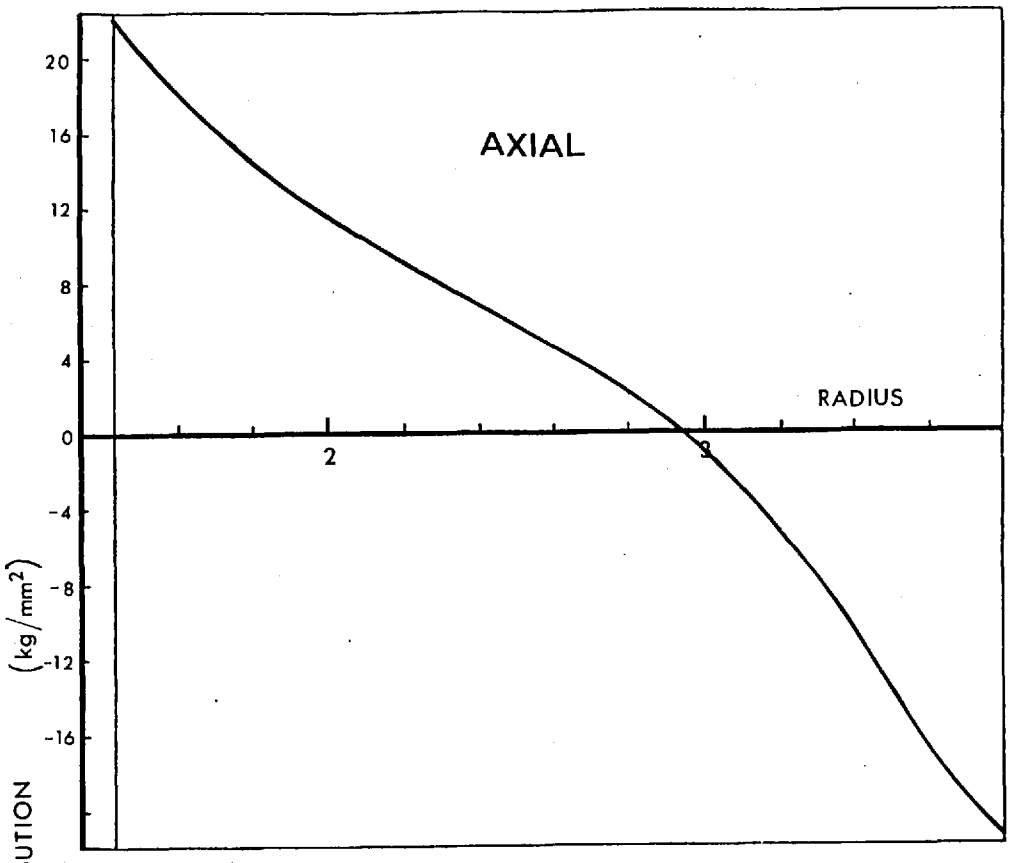


Figure 14





Specimen 5

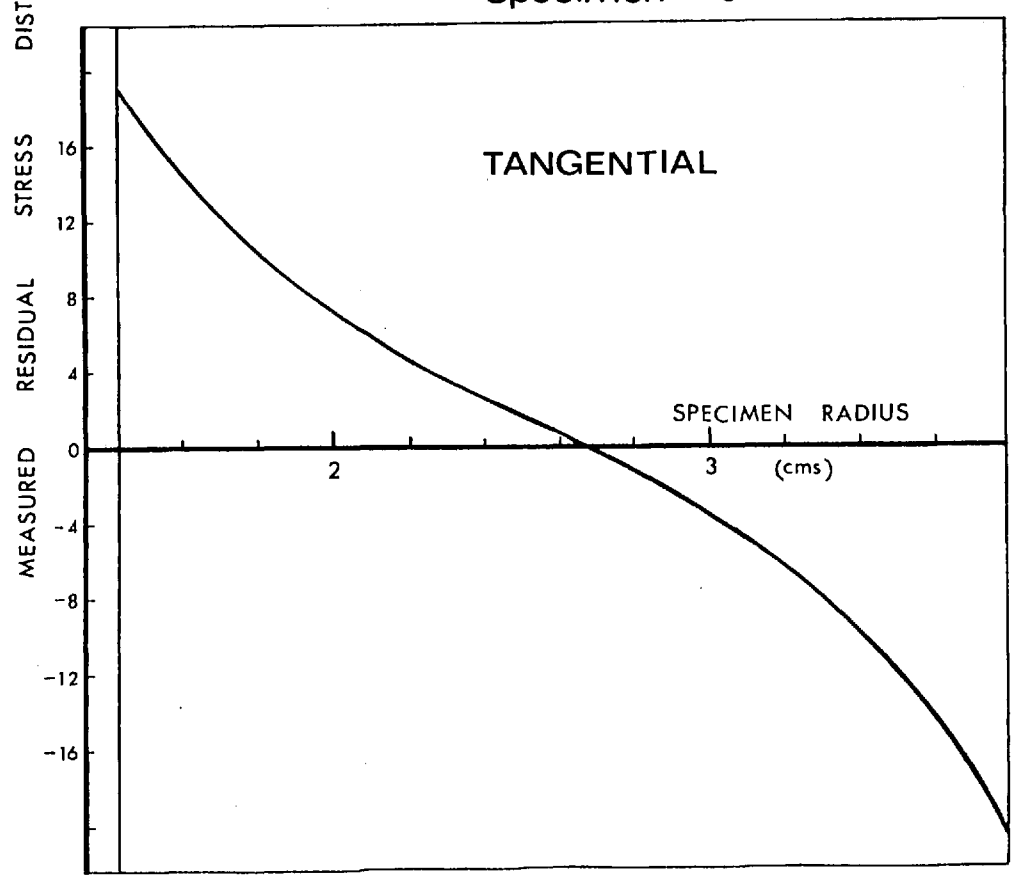
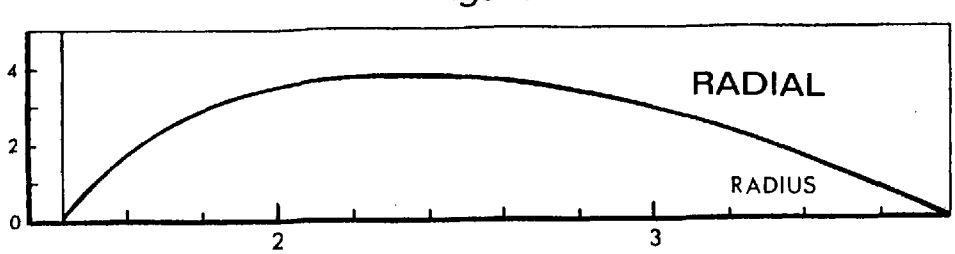
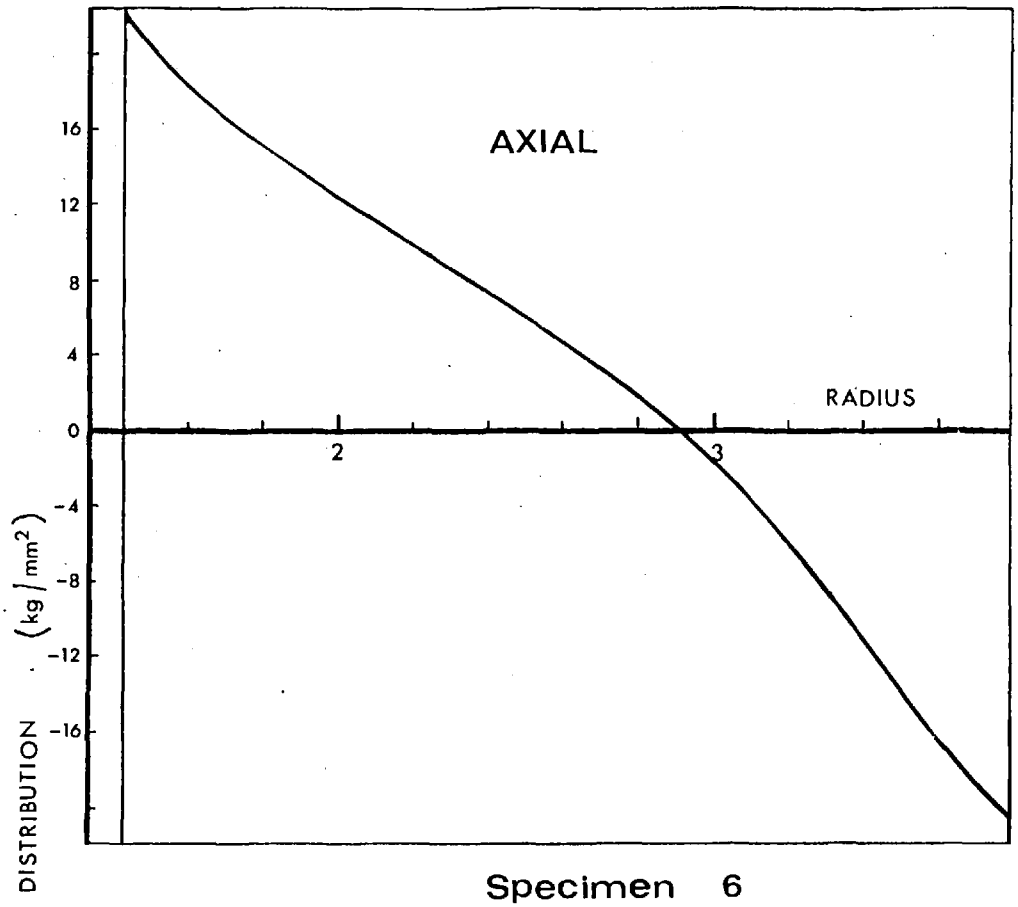


Figure 15





Specimen 6

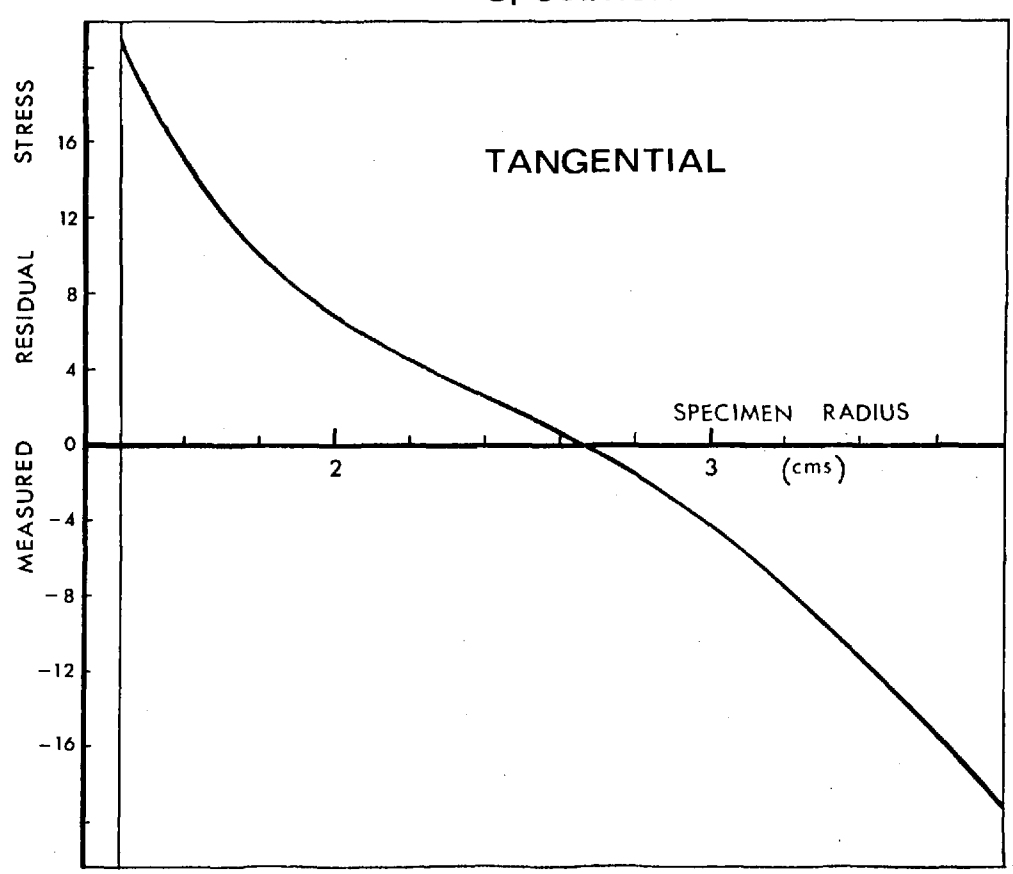
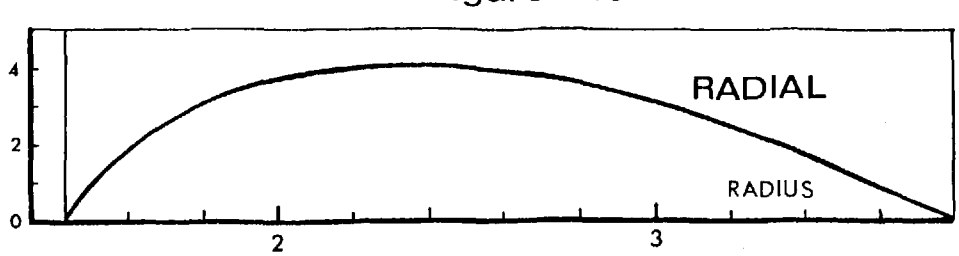
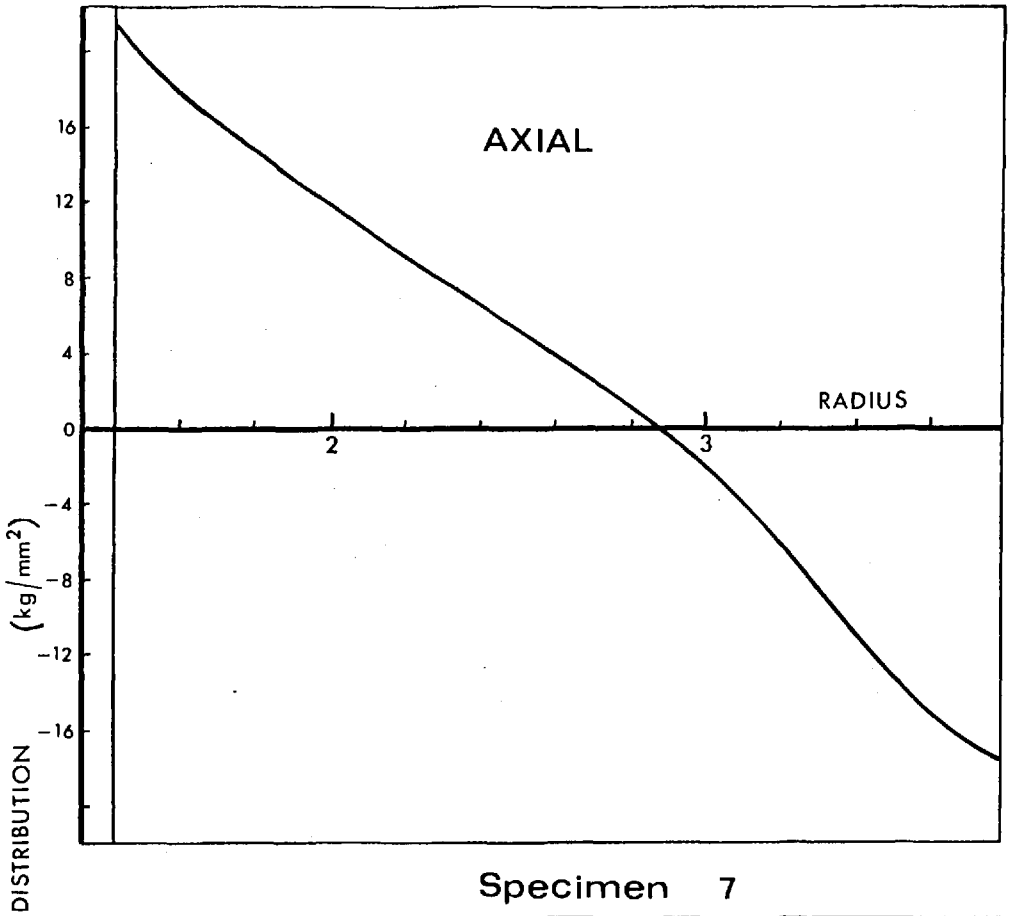


Figure 16





Specimen 7

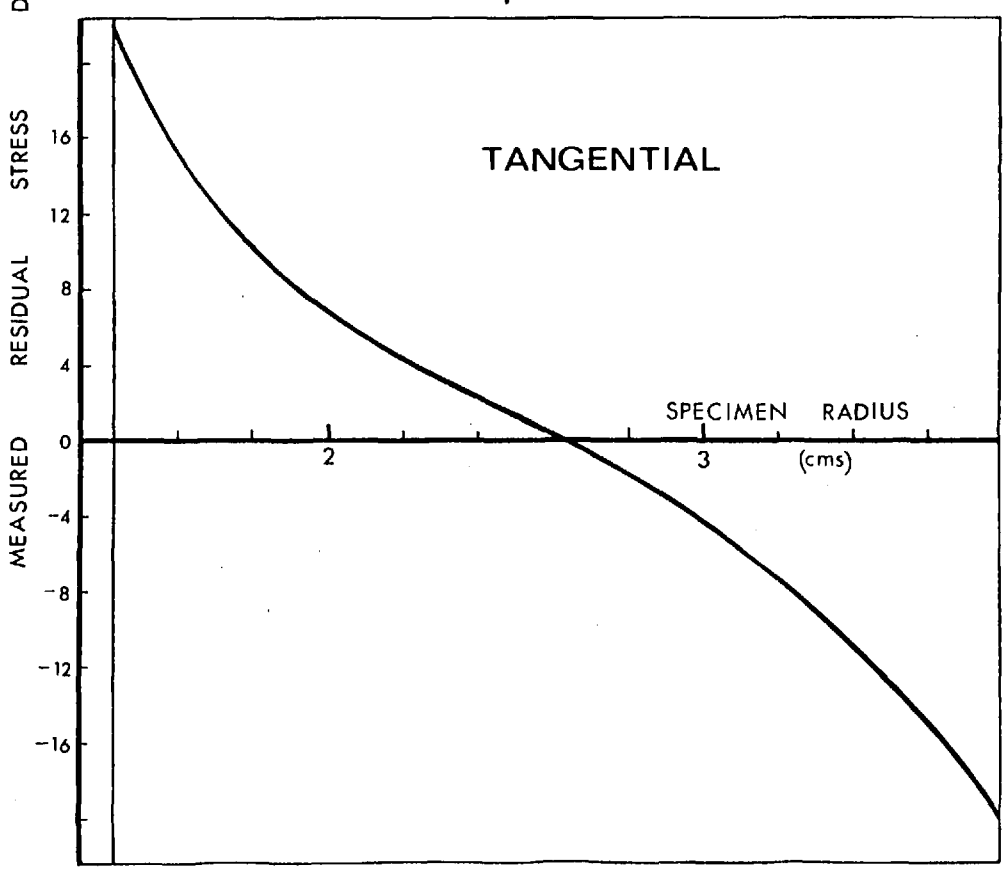
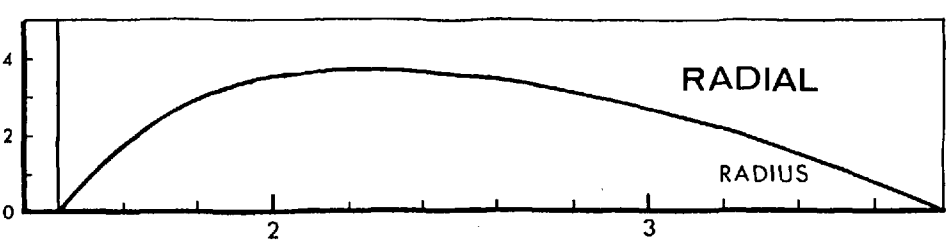
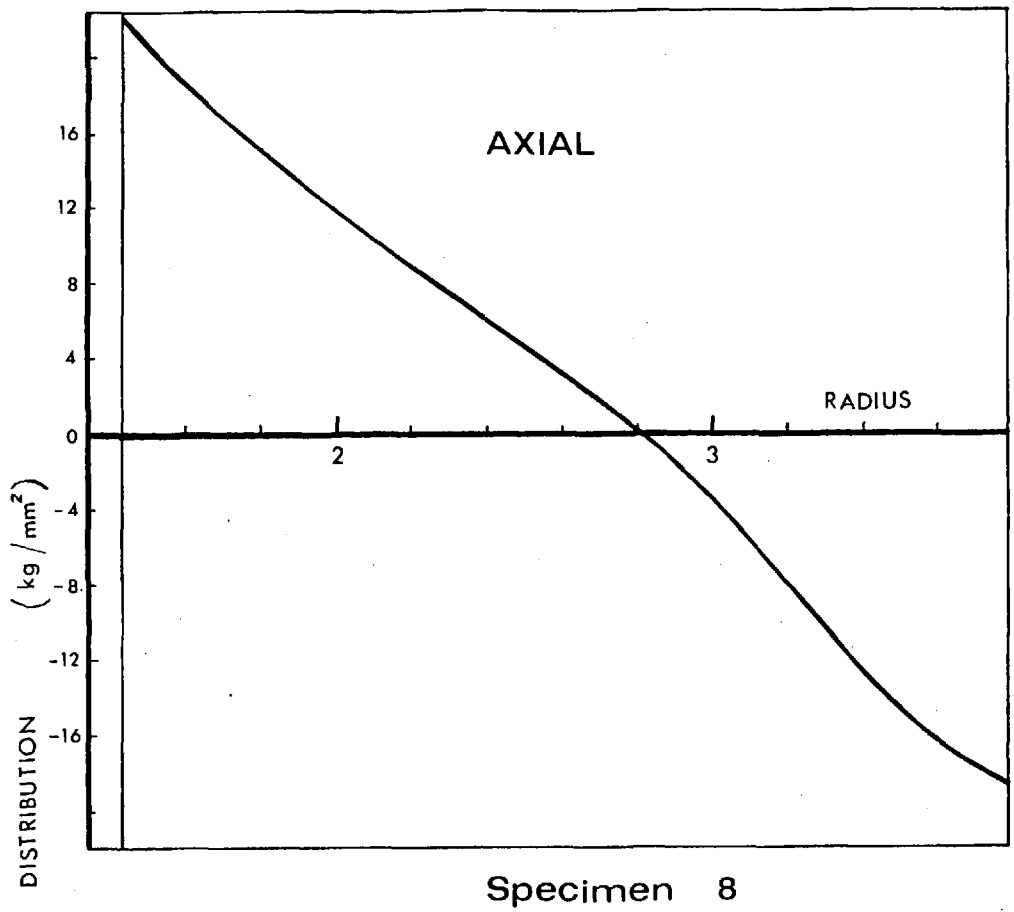


Figure 17





Specimen 8

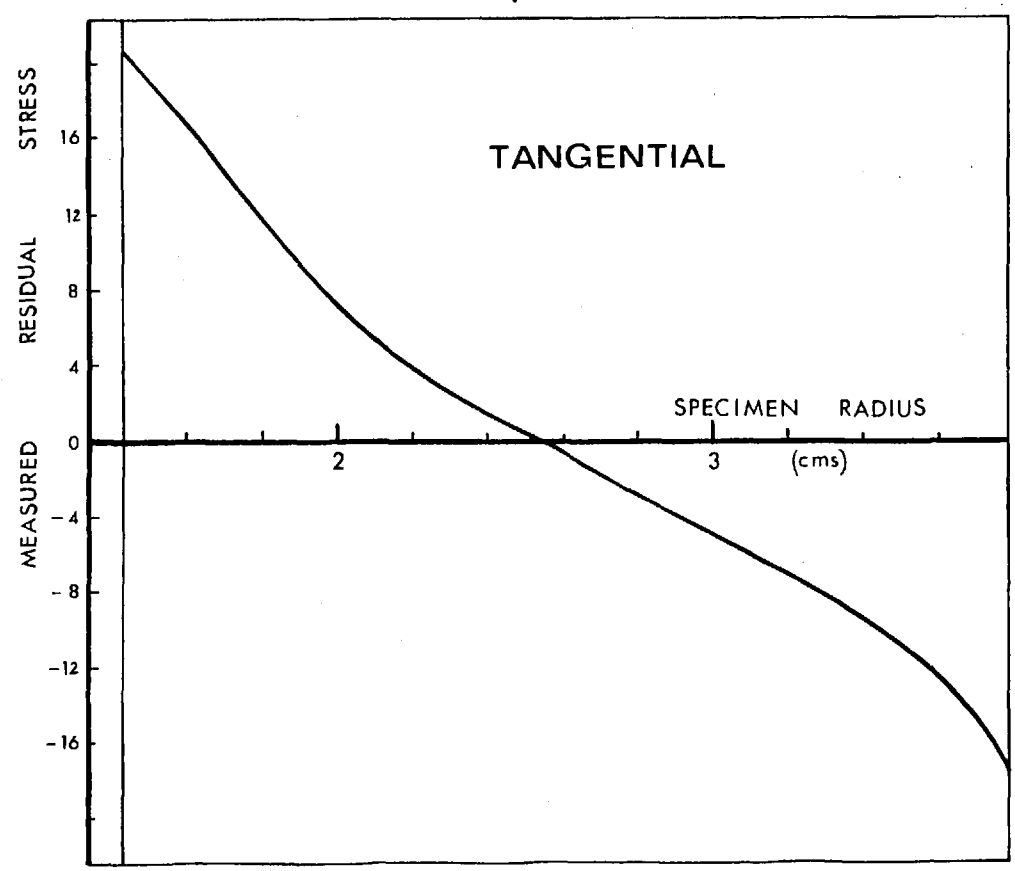
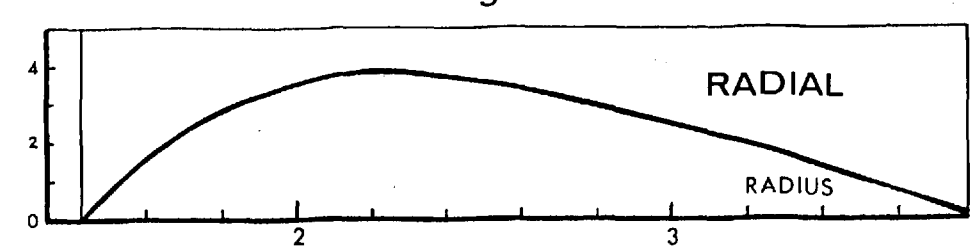
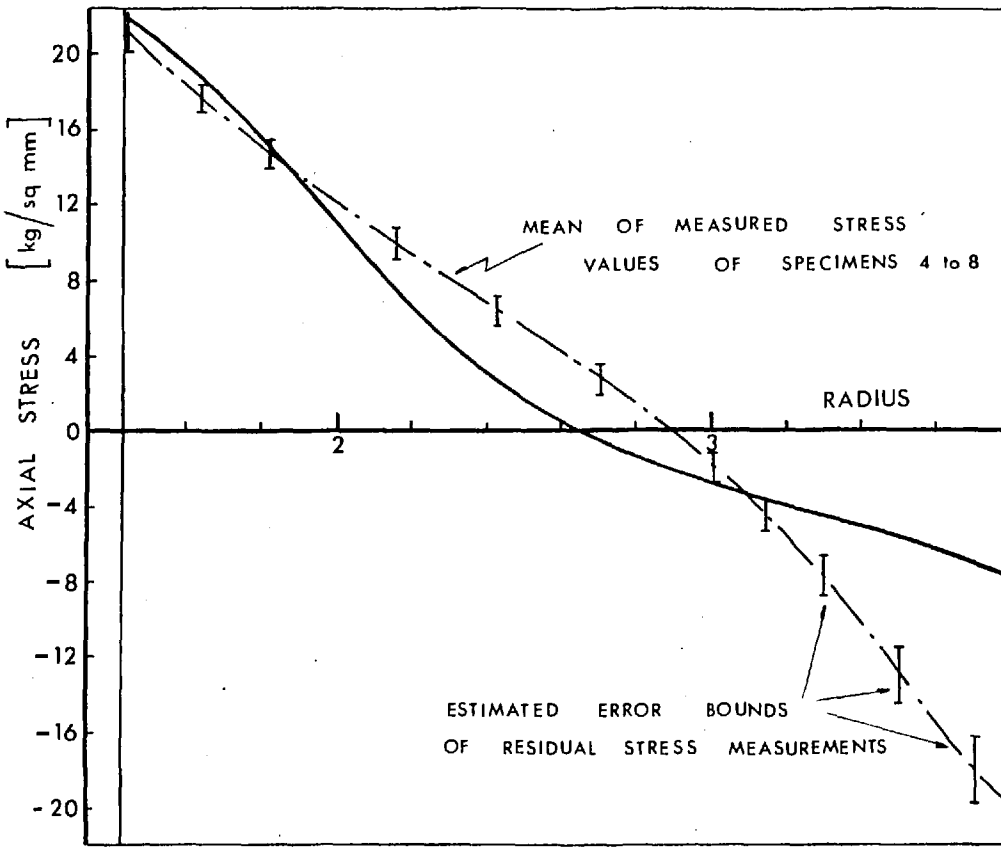


Figure 18





Comparison of Measured and Computed Stresses

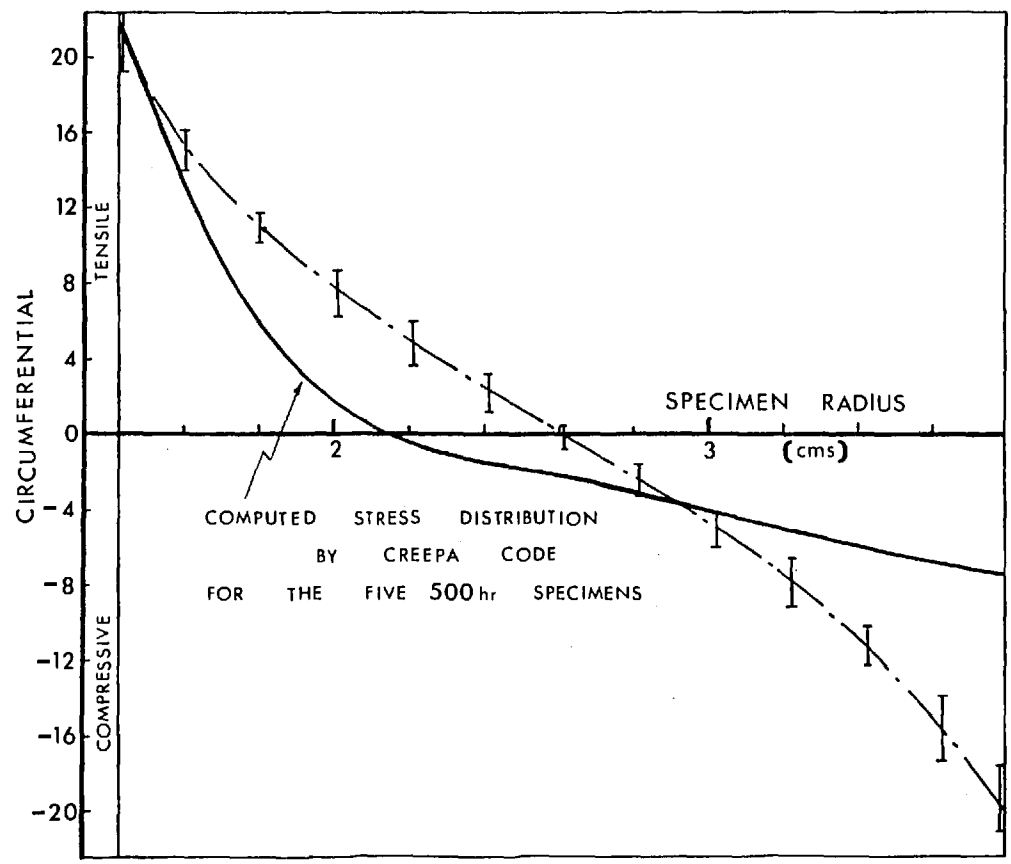
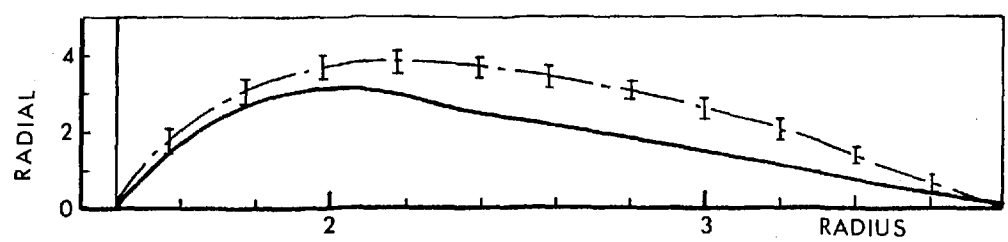


Figure 19



CHAPTER 6

DISCUSSION AND CONCLUSIONS

As illustrated in the previous chapter, agreement between experiment and theory was found to be poor. This is particularly noticeable at the outer surface of the cylinder. It might be argued that despite this discrepancy on the outer surface, the prediction is close enough in the region of greatest importance - i.e. where the stresses are highest. It is nevertheless necessary to examine possible causes of this apparent difference between experimental and analytical stress fields. There is some doubt as to whether the fault lies with the analytical method or the experimental measurements and with the benefit of hind-sight, it is regretted that the stress at the outer surface of at least one specimen was not verified experimentally. This could have been achieved by the method of Rimrott and Weikinger[32] in which strain gauges are bonded to the outer surface and two thin grooves are cut into the surface at the ends of the strain gauge by chemical milling. The grooves are not required to penetrate very far below the surface in order to achieve complete relaxation of the surface stresses beneath the strain gauges and therefore this process could have been combined with the Sachs process, at least on one specimen. Alternatively the simpler hole drilling technique of surface residual stress determination could have been employed.

It might be contended that the error lies entirely in the experimentally obtained stress field, arising from measurement errors or systematic errors in the Sachs theory,

or both. By the arguments already put forward in Chapter 5, the systematic errors in the surface strain readings are claimed to have been maintained at an insignificant level. Scatter due to random variations in the measurement showed an increase as layer removal progressed, hence giving greater significance to the strain readings corresponding to the outermost layers - i.e. the first layers removed in the chemical milling. The discrepancy between the measured and calculated stresses is greater in these outer layers and therefore is not likely to be due to errors in the actual surface strain measurement.

The Sachs equations used to calculate the residual stress pattern from the surface strain readings are described in Chapter 4. This method has been well tested and has been used successfully for a wide variety of axisymmetric cylindrical components. However, it is clear that if the inherent assumptions in the method are violated, the Sachs equations will fail to produce a reliable evaluation of the component residual stress pattern. This is well illustrated, for example, in the work of Olsen and Bert[33] in which a modified version of Sach's equations (for the boring out process) was derived to make allowance for several cylindrically anisotropic cases. It was found in a residual stress study of ZTA grade graphite based on Sach's equations, that an error of approximately 80 per cent in the tangential stress could result, and between 25 and 35 per cent error in the radial stress, depending on the surface strain ratios encountered. With an orthotropic ratio $E_z/E_r = 0.275$, this is perhaps an extreme example, but it serves to indicate the magnitude of error that can arise due to anisotropy. In the case of the Nimonic cylinders examined in this project, such a high degree of anisotropy

would not be expected. Any anisotropy present in the material would originate from the manufacturing process and the overageing during the loading cycle. The former has been discussed in Chapter 2 with respect to creep behaviour, and the same arguments might be applied to the case of the elastic moduli, namely, that the extrusion process is completed at a temperature high enough for recrystalization to take place and so, at least partially, the effect of preferred crystal orientation from the extrusion is nullified.

Anisotropy from the extrusion process would be manifest in a microscopic examination of the grain structure but in the material used for the cylindrical specimens, no such evidence was observed. It is unfortunate that tests on the tensile specimens cut from the longitudinal and transverse directions of extrusion could not be completed in time for inclusion here. This would have permitted a more definite conclusion in this regard. On the strength of the available evidence,it appears that any anisotropy resulting from the manufacturing process was not likely to be significant.

The other source of anisotropic elastic moduli is metallurgical, rather than physical. It has been observed by Cox[34] and others[35] that overageing at high temperatures in Nimonic 80A can result in a change in the value of Young's Modulus at that temperature. In one case, a 20% decrease in Young's Modulus at 800^{o}C was observed after 800 hours. However, the room temperature value of Young's Modulus is hardly affected and in the same case, it was only approximately 7% lower after the 800 hours. The reason for this change is not readily explicable and indeed the effect has hardly been

investigated beyond mere observation. The room temperature value of Young's Modulus obtained from some of the 500 hour remnant shells, as described in Chapter 5, was similar to the values quoted by the manufactureres for the standard heat-treated material.

If this change in elastic properties with overaging at high temperatures is a characteristic of this material, then it goes some way toward explaining the discrepancy between analysis and experiment. The thermal elastic stress distribution in the cylinder could alter significantly with a non-uniform change in the elastic constants across the wall, but this process would have to be quite sensitive to the ageing temperature to produce a noticeable affect, in this particular application. The room temperature residual stress pattern would be further altered with any subsequent relative change in the elastic moduli on cooling. It is regretted that metallographic examinations of the cylindrical specimens were not performed before commencing the layer removal procedure, as these may have thrown some light on the problem.

A hardness survey on a cylinder used in preliminary tests showed a definite decrease in hardness across the wall from the outer surface inwards. This may not be a direct indication of the variation in the elastic moduli, but it does confirm a change in the metallurgical condition observed in over-ageing.

From the foregoing it might be reasonably concluded that the error does not lie entirely with the experimental results. It is accepted that the experimentally obtained residual

stress patterns are subject to some error, but at the same time, the short-comings of the computational model will also contribute to the discrepancy. The inability of the model to accomodate time-varying property changes such as strain ageing and recovery can result in unrealistic predictions at elevated temperatures, as might also the effect of negative creep on reduction of the load, although in this particular case it would tend to accentuate the discrepancy. The simple time- and strain-hardening theories led to similar predictions in this case, but the observed deviation from experiment seems to warrant some sceptecism as to the range of application of the computational model.

Conclusions and Recommendations for Further Work.

A satisfactory procedure for applying a chemical milling process for layer removal in the Sachs method of residual stress determination has been developed. Replication of the test conditions indicated that the random errors in the measurement of the surface strain changes had been reduced to an acceptable level. The systematic errors cannot be checked absolutely, but a reasonable degree of confidence has been placed in the readings from the checks that could be made in this regard.

The predicted stress redistribution in the cylindrical component after a single complex loading cycle differs appreciably from that obtained experimentally, especially near the outer surface of the cylinder wall. Further tests necessary to evaluate the accuracy of the experimental values in this region could not be completed in the allotted time.

Neither was it possible to verify the possible explanations for this difference.

In view of the importance of the effects of cyclic loading at high temperatures and the lack of related experimentation, it is thought worthwhile to persist in this line of research. The scope of the investigation ought now to be extended by building a second rig in which additional forms of loading may be applied to the component, for example, an internal pressure. The possibility of using convective heat transfer ought to be considered as this will allow a high radial flux to be obtained with a lower surface temperature. (A thinner wall in the specimen might also be considered.) This would enable studies to be made of other component materials - type 316 Stainless Steel, which has potential application in Fast Reactor structures, has been suggested. The complex metallurgical nature of Nimonic 80A strongly favours the adoption of another component material.

Agreement between theoretically and experimentally obtained stresses after a series of load cycles would be a great encouragement to design engineers.

ACKNOWLEDGEMENTS

The author is indebted to the Atomic Energy Board of South Africa for their sponsorship during most of this project, and to the Science Research Council for providing financial assistance toward the cost of materials.

Thanks are due to Dr. J.L. Head for his interest and guidance in supervising the project, to the members of the technical staff in the Nuclear Power section for their help and advice, and to my cousin, Maureen Isted, for typing the manuscript.

Finally, thanks are due to my wife for her patience, understanding and encouragement throughout the duration of the project.

REFERENCES

1. Proceedings of Group Sessions C,D,F,G,L and M; 2nd International Conference on Structural Mechanics in Reactor Technology, Berlin, Sept 1973.

2. Ratcliff B.J., Brit. J. Non-Destr. Testing Sept 1963 11(3) pp 48 - 58.

3. Taira S., and Ohtani R., 'Creep of Tubular Specimens under Combined Stress', Advances in Creep Design, Applied Science, 1971.

4. Betteridge W., The Nimonic Alloys, Edward Arnold 1959.

5. Clarke J.M., 1966, NGTE Report No. R284.

6. Finnie I., and Heller W., Creep of Engineering Materials, McGraw Hill, 1959.

7. Penny R.K., and Marriott D.L., Design for Creep, McGraw-Hill, 1971, p41.

8. Spoelstra J.L., MSc Dissertation, University of London, 1969.

9. Frederick C.O., Chubb E.J., and Bromley W.P., 'Cyclic Loading of a Tube with Creep, Plasticity and Thermal Effects', Paper 15, Applied Mechanics Convention, 1966.

10. Smith E.M., 'Primary Creep Behaviour of Thick Tubes' Paper 20, Converence on Thermal Loading and Creep in Structures and Components, 1964.

11. Bailey R.W., Proc Inst Mech Eng., 1951, Vol 164, (4), p425.

12. Sully A.H., Brandes E.A., and Waterhouse R.B., Brit J. Appl Physics, 1952, 3, p97.

13. Betteridge W., and Franklin A.W., J. Inst. Metals, 1957, 85, p473.

14. Pheil L.B., Allen N.P., and Conway C.G., Special Report 43, Iron and Steel Inst.

15. Fell E.A., Mitchell W.I., and Wakeman D.W., 'The Metallography of Creep Resistant Alloys', Special Report 70, Iron and Steel Inst., 1961.

16. Weaver C.W., J. Inst. Metals, 1959 - 60, 88, p462.

17. Denton A.A., Review 101, J Inst Metals 1966 Vol 94.

18. Sachs G., Z. Metallkunde, 1927, 19, p352.

19. Bühler H., 'Residual Stresses in Metals and Metal Construction' (ed W.R. Osgood), Reinhold Clarendon Press, 1954.

20. Barker A., and Hardy E.H., Proc Instn Mech Eng, 1957, 171, (17), p581.

21. Hanke E., and Tiemann E., Hart - Tech. Mitteilungen, 1970, 25 (2) p81.

22. Kawagoe H., Bull. J.S.M.E., 1967, 10,(40), p588

23. Denton A.A., PhD Thesis, University of London, 1966.

24. Sachs G., Trans Am. Inst. Min. Eng., 1942, 147, p348.

25. Bloomfield B.S., (R.A.R.D.E., Fort Halstead) Private Communication.

26. Sweet H.J., and Weiner P.D., Experimental Mechanics, 1968, 8, (9), p19N.

27. Micro Measurements Strain Gauge Techniques, Instruction Bulletin B - 137.

28. Andrea G., Materialprüfung,12, (3) March 1970, p87.

29. Bergqvist B., Memorandum No. 69, Aeronautical Research Institute of Sweden, 1970.

30. Cadwell J., and Hudson D., 'Least Squares Fit of Polynomial, with Statistical Analysis', E202, CERN 7090 Programme Library, 1963.

31. Chatfield C., Statistics for Technology, Penguin, 1970, p182.

32. Rimrott F.P.J., and Weikinger H.K., Materialprüfung 1963, 5, No 10 p365.

33. Olsen W.A., and Bert C.W., Experimental Mechanics, 1966, Vol 6 No 9, p451.

34. Cox P., (Rolls-Royce, Leavesdon) Private Communication.

35. Myatt A., (Henry Wiggin Ltd) Private Communication.

36. Rimrott F.P.J., J Appl Mech 1959 26 (2) 271-275.

37. Clarke J.M. and Barnes J. F., 'Stress redistributions caused by creep in a thick-walled circular cylinder under axial and thermal loading' Advances in Creep Design, Applied Science, 1971.

38. Smith A.I. and Henderson J., 'The contribution of Dr A.E. Johnson to the development of engineering design for

Creep', Advances in Creep Design, Applied Science,1971.

39. The Nimonic Alloys - Physical and Mechanical properties. Henry Wiggin Publication 3270.

40. Walles K.F.A., N.G.T.E. Note number N.T. 386, 1959.

Appendix I

TABLE 1

SPECIMEN 1

Radial Temperature Distribution (^{o}C)

Time at Load Change (hrs)	Radius (cms)				
	3.51	2.56	2.09	1.67	1.42
12	760	785	800	817	830
88	748	770	785	802	815
96	672	695	711	729	741
118	681	705	720	739	751
142	704	729	745	763	775
154	690	718	732	750	762
167	575	588	599	610	617
178	658	675	690	704	714
190	756	777	792	810	822
213	760	785	800	817	830
236	744	797	781	766	809
263	716	736	751	768	779
345	698	716	728	742	752
392	656	673	686	700	708
422*	747	770	780	797	811
557	721	745	758	773	789
656	713	739	751	768	781
845	726	752	768	784	798
902	723	751	766	782	795
940	584	600	610	618	629
941	20	20	20	20	20

*First Platinum Heater Installed.

TABLE 2

SPECIMEN 2

Radial Temperature Distribution (°C)

Time at Load Change (hrs)	Radius (cms)				
	3.55	2.56	2.09	1.67	1.42
224	738	756	775	798	807
672	750	772	790	812	820
675*	738	759	778	799	806
1025	750	772	790	812	820
1026	20	20	20	20	20

*Vacuum Pump Failure.

SPECIMEN 3

Radial Temperature Distribution (°C)

Time at Load Change (hrs)	Radius (cms)				
	3.55	2.56	2.09	1.67	1.42
172**	731	757	777	794	803
222	740	748	770	787	798
1005	767	777	800	812	831
1006	20	20	20	20	20

** Heater Terminal Failure.

SPECIMENS 4 - 8

Radial Temperature Distribution (°C)

Loading Period (hrs)	Radius (cms)					
	3.55	2.56	2.09	1.67	1.42	
500	752†	774†	788†	807†	810†	Specimen 4
500	728	770†	768	782	810†	Specimen 5
500	732	772†	775	788	808†	Specimen 6
500	728	770†	780	792	813†	Specimen 7
500	737	774†	782	798	813†	Specimen 8

† Termocouples extended into top of Specimen.

TABLE 3

SPECIMEN 1

Cylinder Diameter (cms.)	Hoop Gauges (microstrain) Gauge 2	Gauge 4	Gauge 6	Axial Gauges (microstrain) Gauge 1	Gauge 3	Gauge 5
7.62	0	0	0	0	0	0
7.21	-29	-40	-31	-40	-41	-14
	-30	-39	-33	-42	-40	-15
7.23	-39	-47	-40	-50	-47	-12
	-40	-48	-40	-50	-47	-13
7.09	-52	-60	-51	-60	-49	-3
	-51	-61	-56	-62	-52	-8
6.97	-66	-74	-71	-76	-68	-1
	-65	-78	-70	-74	-62	-8
6.91	-69	-82	-73	-80	-61	-2
	-70	-83	-75	-80	-62	-2
6.81	-82	-99	-86	-91	-72	†
	-83	-99	-88	-91	-73	
6.71	-91	-110	-103	-101	-83	
	-92	-111	-103	-101	-85	
6.63	-100	-126	-119	-112	-96	
	-103	-121	-120	-112	-97	
3.55	-112	-131	-129	-121	-101	
	-113	-133	-131	-120	-100	
6.47	-117	-141	-140	-127	-102	
	-118	-141	-141	-127	-101	
6.44*	-112*	-139*	-138*	-135*	-112*	
	-113*	-139*	-133*	-136*	-110*	
6.28	-134	-170	-161	-142	-102	
	-135	-169	-167	-143	-103	
6.01	-160	-205	-196	-160	-101	
	-161	-204	-201	-159	-101	
5.97*	-160*	-207*	-198*	-173*	-110*	
	-160*	-205*	-200*	-174*	-110*	
5.84	-184	-233	-225	-181	-120	
	-188	-234	-228	-180	-120	
5.55	-208	-262	-249	-201	-130	
	-210	-263	-253	-200	-132	
5.51	-219	-283	-261	-210	-141	
	-220	-284	-265	-210	-143	
5.36	-240	-308	-291	-227	-151	
	-240	-309	-292	-225	-152	
5.24	-260	-328	-322	-239	-166	
	-260	-329	-325	-240	-168	
5.18*	-260*	-329*	-322*	-253*	-179*	
	-259*	-327*	-321*	-252*	-173*	

† Gauge defective. * Readings taken after machining.

SPECIMEN 1 (contd)

Cylinder Diameter (cms.)	Hoop Gauges (microstrain)			Axial Gauges (microstrain)		
	Gauge 2	Gauge 4	Gauge 6	Gauge 1	Gauge 3	Gauge 5
5.04	-281 -281	-362 -363	-368 -372	-262 -261	-177 -175	
4.91	-299 -298	-383 -480	-385 -386	-280 -280	-195 -197	
4.74	-315 -319	-408 -410	-407 -408	-298 -298	-212 -202	
4.46	-333 -333	-440 -441	-432 -438	-308 -310	-249 -260	
4.13	-385 -383	-502 -503	-484 -487	-360 -360	-276 -270	
3.99*	-394* -396*	-518* -516*	-498* -500*	-416* -415*	-338* -430*	
3.74	-469 -470	-592 -590	-566 -568	-447 -449	-360 -359	
3.38	-526 -528	-676 -670	-640 -644	-520 -518	-404 -415	
3.29*	-498* -500*	-658* -650*	-628* -626*	-582* -480*	-431* -435*	
3.18	-498 -498	-644 -644	-628 -630	-566 -566	-444 -546	
3.00	-528 -522	-702 -702	-680 -685	-556 -556	-450 -455	
2.80	-540 -540	-746 -750	-726 -724	-574 -578	-490 -500	

* Readings taken after machining.

TABLE 4

SPECIMEN 2

Cylinder Diameter (cms.)	Hoop Gauges Gauge 1 (microstrain)	Gauge 3	Gauge 5	Gauge 8	Axial Gauges Gauge 2 (microstrain)	Gauge 4	Gauge 6	Gauge 7
7.62	0	0	0	0	0	0	0	0
7.40	-52	-40	-52	-51	-73	-38	-44	-32
	-52	-41	-52	-52	-69	-39	-44	-35
7.29	-72	-80	-76	-73	-57	-55	-60	-60
	-74	-82	-78	-72	-58	-56	-61	-61
7.13	-105	-100	-110	-102	-86	-85	-90	-83
	-105	-100	-111	-103	-85	-86	-91	-84
6.92	-140	-151	-150	-132	-126	-117	-125	-119
	-140	-150	-151	-132	-126	-118	-126	-119
6.75	-170	-158	-184	-162	-157	-150	-159	-150
	-170	-158	-183	-161	-157	-149	-159	-150
6.65	-188	-172	-200	-181	-171	-164	-173	-172
	-188	-171	-198	-179	-170	-162	-170	-169
6.54	-202	-189	-210	-199	-197	-178	-190	-182
	-201	-188	-219	-191	-205	-185	-193	-183
6.45	-219	-201	-243	-209	-197	-197	-211	-197
	-220	-200	-241	-207	-194	-197	-209	-195
6.23	-264	-253	-267	-239	-257	-223	-244	-237
	-260	-257	-264	-241	-257	-227	-246	-239
6.02	-287	-280	-290	-270	-295	-255	-284	-279
	-289	-279	-291	-270	-295	-254	-285	-279
5.77	-313	-313	-326	-298	-325	-287	-328	-305
	-308	-314	-328	-296	-327	-291	-330	-309
5.63	-335	-350	-352	-328	-347	-313	-358	-335
	-335	-350	-355	-328	-349	-315	-360	-331
5.21	-410	-368	-400	-407	-435	-418	-429	-413
	-408	-367	-298	-405	-435	-422	-430	-409
5.14 *	-433*	-386*	-423*	-428*	-425*	-410*	-418*	-404*
	-433*	-387*	-422*	-427*	-425*	-412*	-418*	-401*
4.91	-470	-437	-459	-455	-478	-472	-483	-476
	-465	-426	-463	-453	-480	-475	-488	-481
4.61	-503	-486	-507	-493	-530	-527	-535	-527
	-504	-483	-510	-492	-531	-526	-540	-534
4.34	-540	-530	-546	-544	-563	-567	-583	-575
	-541	-530	-548	-535	-565	-568	-583	-574
4.10	-570	-564	-581	-555	-606	-607	-624	-610
	-570	-558	-583	-553	-608	-608	-624	-609
3.89	-602	-598	-615	-593	-644	-633	-658	-646
	-600	-614	-612	-592	-644	-632	-660	-646
3.61	-650	-662	-655	-640	-697	-672	-708	-691
	-649	-666	-663	-637	-697	-673	-710	-698
3.43	-675	-686	-690	-665	-715	-706	-734	-712
	-676	-688	-692	-665	-717	-718	-734	-710
3.16	-650	-680	-683	-680	-696	-696	-740	-696
	-652	-698	-685	-680	-694	-698	-744	-702

* Readings taken after machining

TABLE 5

SPECIMEN 3

Cylinder Diameter (cms.)	Hoop Gauges (microstrain) Gauge 2	Gauge 4	Gauge 5	Gauge 7	Axial Gauges (microstrain) Gauge 1	Gauge 3	Gauge 6	Gauge 8
7.51	0	0	0	0	0	0	0	0
7.34	-27	-24	-36	-34	-39	-35	-30	-36
	-29	-23	-36	-31	-40	-31	-40	-36
7.19	-47	-48	-50	-39	-68	-52	-64	-49
	-51	-50	-53	-40	-65	-49	-61	-50
7.05	-60	-60	-63	-61	-68	-73	-74	-74
	-59	-57	-60	-58	-68	-73	-74	-71
6.87	-81	-79	-86	-80	-101	-106	-105	-104
	-80	-78	-84	-80	-100	-104	-105	-105
6.73	-91	-92	-107	-91	-119	-92	-124	-118
	-90	-91	-107	-90	-118	-91	-124	-118
6.60*	-108*	-107*	-109*	-111*	-127*	-97*	-128*	-125*
	-106*	-106*	-110*	-108*	-125*	-96*	-129*	-127*
6.58	-109	-107	-121	-115	-151	-156	-148	-148
	-109	-108	-118	-110	-147	-150	-147	-145
6.50	-123	-127	-128	-125	-160	-166	-164	-165
	-121	-125	-128	-124	-158	-165	-165	-165
6.21	-150	-148	-156	-146	-198	-201	-202	-199
	-156	-151	-161	-155	-201	-206	-204	-205
6.04	-172	-170	-181	-166	-221	-226	-222	-219
	-173	-169	-181	-169	-226	-228	-221	-219
5.87	-192	-188	-206	-187	-246	-247	-247	-237
	-193	-188	-201	-186	-244	-246	-245	-238
5.72	-211	-207	-228	-205	-271	-278	-275	-258
	-213	-209	-227	-206	-269	-276	-269	-257
5.45	-244	-243	-260	-240	-320	-320	-326	-320
	-242	-242	-260	-242	-318	-321	-326	-319
5.21	-273	-260	-291	-259	-358	-343	-382	-358
	-273	-260	-291	-259	-353	-340	-378	-353
4.97	-303	-288	-322	-283	-392	-381	-413	-389
	-306	-291	-324	-288	-394	-387	-417	-390
4.72	-331	-322	-340	-325	-420	-422	-444	-440
	-330	-325	-339	-325	-421	-427	-441	-440
4.60*	-385*	-378*	-397*	-376*	-434*	-423*	-458*	-444*
	-381*	-377*	-395*	-376*	-435*	427*	-455*	-444*
4.32	-374	-382	-400	-379	-498	-498	-514	-482
	-377	-382	-402	-380	-499	-471	-513	-482
4.04	-438	-433	-467	-423	-558	-547	-580	-536
	-437	-432	-468	-424	-558	-536	-581	-537

SPECIMEN 3 (contd)

Cylinder Diameter (cms.)	Hoop Gauges (microstrain)				Axial Gauges (microstrain)			
	Gauge 2	Gauge 4	Gauge 5	Gauge 7	Gauge 1	Gauge 3	Gauge 6	Gauge 8
3.83	-480	-475	-522	-463	-602	-584	-638	-575
	-482	-475	-522	-463	-603	-586	-636	-577
3.59	-518	-512	-580	-503	-650	-640	-684	-617
	-520	-512	-578	-505	-652	-644	-684	-617
2.70	-558	-551	-612	-540	-692	-690	-730	-649
	-561	-553	-622	-543	-694	-690	-736	-649
2.52	-594	-585	-658	-574	-730	-732	-770	-685
	-593	-586	-670	-577	-734	-738	-770	-685

*Readings taken after machining.

TABLE 6

SPECIMEN 4

Cylinder Diameter (cms.)	Hoop Gauges (microstrain) Gauge 2	Gauge 4	Gauge 5	Gauge 7	Axial Gauges (microstrain) Gauge 1	Gauge 3	Gauge 6	Gauge 8
7.51	0	0	0	0	0	0	0	0
7.28	-30	-33	-47	-46	-45	-47	-55	-60
	-30	-32	-48	-47	-47	-49	-57	-62
7.12	-35	-64	-68	-69	-70	-80	-82	-92
	-36	-59	-71	-72	-70	-80	-82	-91
7.02	-59	-69	-82	-88	-69	-133	-102	-114
	-59	-69	-81	-88	-70	-130	-102	-116
6.78	-70	-91	-102	-100	-112	-117	-136	-142
	-70	-90	-101	-100	-112	-118	-137	-142
6.64	-89	-107	-119	-116	-131	-139	-160	-161
	-89	-107	-119	-116	-131	-140	-161	-161
6.54	-100	-120	-132	-127	-147	-158	-179	-173
	-111	-120	-131	-128	-148	-160	-181	-178
6.46	-99	-82	-140	-160	-149	-149	-189	-194
	-98	-89	-139	-159	-150	-152	-190	-195
6.18	†	†	-195	-180	†	†	-255	-247
			-207	-183			-257	-248
5.90			-218	-202			-292	-269
			-218	-195			-288	-268
5.72			-243	-252			-314	-293
			-242	-251			-314	-291
5.69*			-259*	-270*			-312*	-290*
			-257*	-269*			-313*	-289*
5.51			-262	-261			-337	-322
			-264	-265			-335	-325
5.10			-300	-314			-369	-385
			-300	-312			-370	-383
4.74			-320	-328			-406	-430
			-323	-327			-405	-429
4.54			-349	-361			-437	-455
			-340	-365			-438	-455
4.20			-389	-404			-485	-496
			-390	-402			-487	-497
3.96			-421	-438			-521	-525
			-424	-441			-522	-527
3.72			-453	-460			-539	-531
			-453	-463			-540	-533
3.58			-480	-490			-560	-555
			-479	-491			-561	-555
3.42			-497	-509			-580	-567
			-501	-509			-580	-566
3.28			-494	-510			-573	-565
			-510	-521			-572	-565

† Gauge defective. *Readings taken after machining.

TABLE 7

SPECIMEN 5

Cylinder Diameter (cms.)	Hoop Gauges (microstrain)				Axial Gauges (microstrain)			
	Gauge 2	Gauge 4	Gauge 5	Gauge 7	Gauge 1	Gauge 3	Gauge 6	Gauge 8
7.51	0	0	0	0	0	0	0	0
7.25	-42	-40	-46	-42	-49	-44	-60	-54
	-44	-43	-48	-44	-51	-48	-60	-59
7.04	-74	-67	-72	-71	-92	-88	-100	-97
	-68	-69	-76	-80	-97	-91	-102	-101
6.88	-96	-92	-96	-101	-128	-120	-127	-128
	-98	-95	-102	-101	-128	-121	-128	-132
6.73	-118	-112	-126	-121	-162	-148	-152	-155
	-117	-115	-126	-122	-158	-147	-152	-155
6.55	-139	-133	-148	-143	-188	-177	-185	-188
	-142	-135	-146	-146	-190	-178	-186	-188
6.32	-168	-153	-166	-170	-224	-203	-220	-225
	-169	-155	-169	-172	-225	-207	-221	-226
6.12	-195	-177	-192	-197	-257	-237	-250	-255
	-195	-178	-195	-199	-256	-237	-250	-255
5.91	-223	-202	-219	-222	-286	-265	-278	-285
	-224	-204	-220	-223	-286	-263	-279	-288
5.65	-233	-234	-239	-246	-306	-281	-310	-317
	-236	-234	-241	-245	-306	-282	-311	-318
5.38	-262	-275	-278	-279	-323	-325	-342	-347
	-266	-278	-280	-282	-323	-328	-347	-357
5.21	-280	-293	-291	-292	-368	-355	-368	-374
	-281	-293	-292	-292	-348	-354	-369	-374
5.04	-290	-301	-302	-304	-371	-379	-390	-397
	-290	-301	-302	-303	-371	-378	-391	-403
4.81	-316	-322	-323	-326	-404	-411	-424	-429
	-317	-323	-324	-328	-406	-411	-422	-432
4.55	-342	-343	-352	-352	-439	-448	-461	-470
	-344	-343	-352	-352	-437	-445	-461	-472
4.28	-378	-373	-389	-391	-474	-480	-500	-504
	-378	-372	-389	-389	-479	-496	-501	-505
4.00	-408	-402	-428	-427	-510	-522	-538	-544
	-408	-402	-424	-425	-517	-526	-540	-545
3.78	-430	-423	-453	-455	-541	-550	-570	-572
	-429	-422	-450	-453	-538	-550	-570	-571
3.51	-468	-454	-499	-499	-570	-576	-608	-612
	-468	-453	-499	-428	-570	-576	-610	-616
3.24	-496	-487	-533	-538	-587	-588	-639	-632
	-498	-487	-531	-538	-598	-592	-638	-637

TABLE 8

SPECIMEN 6

Cylinder Diameter (cms.)	Hoop Gauges Gauge 2 (microstrain)	Gauge 4	Gauge 5	Gauge 7	Axial Gauges Gauge 1 (microstrain)	Gauge 3	Gauge 6	Gauge 8
7.51	0	0	0	0	0	0	0	0
7.21	-55	-50	-47	-45	-56	-59	-54	-65
	-55	-50	-44	-51	-56	-60	-55	-65
7.00	-95	-84	-80	-79	-102	-103	-98	-104
	-90	-87	-83	-75	-100	-101	-100	-103
6.87	-120	-104	-98	-94	-126	-125	-121	-129
	-110	-105	-101	-95	-124	-124	-123	-130
6.71	-135	-126	-119	-115	-150	-154	-151	-159
	-140	-130	-120	-118	-152	-153	-151	-160
6.62	-150	-140	-132	-129	-169	-169	-168	-176
	-145	-141	-138	-130	-169	-171	-169	-177
6.35	-185	-178	-170	-161	-215	-215	-215	-219
	-185	-177	-170	-160	-215	-214	-216	-219
6.14	-220	-203	-194	-183	-248	-245	-248	-250
	-210	-203	-194	-184	-248	-247	-247	-250
5.89	-240	-235	-220	-210	-286	-283	-279	-284
	-240	-235	-228	-212	-289	-283	-283	-287
5.66	-270	-257	-252	-235	-316	-309	-312	-316
	-275	-263	-260	-239	-317	-314	-318	-319
5.30	-315	-304	-294	-274	-354	-354	-350	-358
	-315	-304	-298	-273	-351	-353	-354	-367
5.14	-320	-322	-314	-285	-370	-374	-438	-379
	-325	-324	-314	-286	-375	-375	-379	-382
4.89	-360	-334	-340	-307	-421	-388	-407	-414
	-355	-332	-342	-311	-417	-388	-408	-415
4.66	-390	-358	-362	-331	-439	-419	-441	-447
	-390	-356	-362	-331	-448	-423	-441	-447
4.44	-410	-380	-394	-359	-475	-454	-463	-473
	-420	-372	-394	-355	-490	-454	-472	-475
4.11	-450	-424	-434	-395	-513	-501	-520	-521
	-455	-408	-434	-396	-525	-505	-518	-523
3.82	-485	-444	-466	-431	-613	-543	-552	-553
	-485	-470	-476	-431	-615	-552	-554	-553
3.59	-520	-522	-536	-482	-596	-552	-604	-595
	-510	-520	-536	-479	-618	-556	-606	-595
3.33	-575	-542	-578	-513	-605	-582	-636	-629
	-575	-540	-574	-511	-606	-577	-636	-625

TABLE 9

SPECIMEN 7

Cylinder Diameter (cms.)	Hoop Gauges (microstrain)				Axial Gauges (microstrain)			
	Gauge 2	Gauge 4	Gauge 5	Gauge 7	Gauge 1	Gauge 3	Gauge 6	Gauge 8
7.51	0	0	0	0	0	0	0	0
7.24	-45 -49	-52 -53	-53 -57	-47 -48	-40 -45	-36 -44	-43 -48	-57 -50
7.03	-76 -78	-81 -86	-80 -81	-81 -82	-79 -79	-76 -78	-82 -82	-84 -86
6.80	-110 -108	-118 -118	-115 -113	-116 -115	-121 -114	-118 -116	-124 -124	-127 -129
6.62	-137 -140	-144 -143	-140 -142	-144 -144	-146 -147	-154 -154	-156 -160	-161 -163
6.37	-161 -164	-174 -176	-165 -171	-170 -170	-175 -177	-188 -188	-193 -194	-199 -201
6.14	-188 -188	-204 -206	-194 -200	-196 -198	-213 -212	-226 -226	-229 -232	-232 -239
5.92	-215 -217	-236 -238	-224 -225	-226 -224	-243 -242	-262 -267	-261 -263	-269 -268
5.63	-246 -244	-266 -272	-256 -256	-256 -256	-277 -276	-297 -297	-294 -298	-303 -305
5.35	-274 -276	-300 -304	-285 -286	-286 -285	-314 -314	-337 -337	-333 -334	-339 -341
4 .96	-308 -302	-342 -346	-327 -330	-326 -326	-369 -365	-387 -387	-385 -394	-393 -391
4.67	-335 -337	-370 -378	-356 -357	-355 -353	-401 -401	-432 -432	-432 -437	-435 -435
4.44	-364 -363	-402 -404	-388 -383	-378 -373	-437 -437	-472 -472	-472 -470	-471 -471
4.21	-386 -383	-448 -444	-414 -414	-404 -404	-465 -467	-497 -497	-504 -504	-499 -499
3.91	-425 -425	-488 -494	-457 -461	-448 -448	-501 -499	-547 -542	-542 -546	-541 -539
3.65	-478 -480	-527 -527	-497 -496	-492 -489	-534 -534	-582 -582	-580 -581	-578 -574
3.49	-498 -501	-569 -571	-514 -519	-517 -516	-552 -554	-612 -607	-607 -611	-602 -604
3.24	-426 -428	-625 -623	-554 -556	-559 -557	-574 -576	-637 -637	-643 -643	-634 -636

TABLE 10

SPECIMEN 8

Cylinder Diameter (cms.)	Hoop Gauges Gauge 2	Gauge 4	Gauge 5	Gauge 7	Axial Gauges Gauge 1	Gauge 3	Gauge 6	Gauge 8
	(microstrain)				(microstrain)			
7.51	0	0	0	0	0	0	0	0
7.18	-53	-42	-52	-50	-67	-59	-40	-22
	-54	-57	-52	-50	-47	-42	-35	-24
6.93	-75	-73	-83	-85	-87	-83	-80	-64
	-79	-76	-85	-85	-91	-85	-81	-70
6.72	-117	-111	-114	-120	-132	-131	-128	-110
	-118	-112	-117	-120	-136	-129	-124	-108
6.53	-142	-139	-141	-143	-164	-159	-153	-144
	-150	-146	-141	-143	-165	-163	-155	-142
6.32	-169	-170	-160	-168	-199	-196	-187	-182
	-172	-170	-163	-170	-200	-199	-190	-180
6.12	-196	-202	-184	-192	-229	-227	-217	-208
	-191	-200	-185	-192	-230	-228	-217	-208
5.96	-216	-220	-202	-210	-250	-252	-242	-238
	-218	-226	-204	-211	-254	-254	-242	-240
5.68	-246	-255	-232	-240	-295	-296	-278	-276
	-251	-262	-232	-241	-291	-296	-278	-278
5.29	-290	-302	-274	-285	-346	-342	-332	-332
	-287	-297	-274	-283	-349	-344	-332	-332
5.04	-306	-322	-294	-310	-377	-380	-366	-372
	-308	-322	-296	-310	-381	-378	-366	-372
4.83	-329	-348	-314	-334	-409	-412	-396	-397
	-332	-350	-314	-335	-411	-412	-396	-397
4.54	-367	-391	-351	-372	-457	-460	-444	-442
	-366	-391	-350	-372	-463	-460	-444	-447
4.34	-391	-415	-371	-400	-493	-490	-472	-477
	-391	-413	-373	-400	-495	-490	-476	-482
4.03	-429	-465	-417	-448	-537	-536	-516	-527
	-436	-462	-417	-448	-537	-534	-516	-527
3.77	-471	-505	-457	-487	-577	-580	-558	-567
	-467	-517	-457	-486	-573	-580	-558	-567
3.59	-507	-544	-489	-516	-605	-614	-588	-592
	-505	-542	-489	-517	-601	-614	-588	-592
3.37	-546	-596	-533	-557	-641	-656	-626	-632
	-544	-592	-531	-553	-641	-654	-624	-632
3.23	-564	-616	-551	-570	-653	-678	-644	-647
	-564	-618	-553	-571	-653	-674	-642	-647
3.06	-564	-626	-587	-598	-643	-670	-630	-632
	-564	-622	-589	-598	-653	-674	-632	-637